

**SIGNATURES OF CP VIOLATION AND
PHYSICS BEYOND THE STANDARD MODEL**

POULOSE POULOSE

Ph. D. THESIS

June, 1997

PHYSICAL RESEARCH LABORATORY

NAVRANGPURA

AHMEDABAD - 380 009, INDIA

**SIGNATURES OF CP VIOLATION AND
PHYSICS BEYOND THE STANDARD MODEL**

A THESIS SUBMITTED
TO
GUJARAT UNIVERSITY
FOR
THE DEGREE OF DOCTOR OF PHILOSOPHY
IN PHYSICS

by
Poulose Poulose

PHYSICAL RESEARCH LABORATORY,
NAVRANGPURA,
AHMEDABAD - 380 009, INDIA

June, 1997

CERTIFICATE

I hereby declare that the work presented in this thesis is original and has not formed the basis for the award of any degree or diploma by any University or Institution.




P. Poulse

(Author)

Theory Group

Physical Research Laboratory

Ahmedabad.



Prof. Saurabh D. Rindani

(Thesis Supervisor)

Theory Group

Physical Research Laboratory

Ahmedabad

To

Appan, Amma,
Vellechhi, Kochhechhi, Annie and Davis.

Contents

Acknowledgements	v
1 Introduction	1
1.1 The Standard Model	3
1.2 P and C Symmetries	10
1.2.1 Space Inversion or Parity (P)	10
1.2.2 Charge Conjugation (C)	11
1.3 CP Violation Phenomenology	12
1.4 CP Violation and Extensions of SM	15
1.5 Effective Lagrangian Method	16
1.6 Sensitivity of the measurements	17
1.7 Plan of the Thesis	19

2	<i>CP</i>-violating Asymmetries in $e^+e^- \rightarrow t\bar{t}$	21
2.1	<i>CP</i> -Odd Asymmetries	22
2.2	Calculation of Asymmetries	26
2.3	Numerical Results	32
3	The Leptonic Charge Asymmetries in $e^+e^- \rightarrow t\bar{t}$	42
3.1	Expressions for the Asymmetries	43
3.2	Discussion of Numerical Results	47
4	Effects Due to Helicity-Flip Initial State Radiation	54
4.1	Calculation of the Background Contribution	56
4.2	Numerical Results	62
5	<i>CP</i>-Violating Asymmetries in $\gamma\gamma \rightarrow t\bar{t}$	64
5.1	Features of a $\gamma\gamma$ Collider	65
5.2	Charge Asymmetries in $\gamma\gamma \rightarrow t\bar{t}$	69
5.3	Results	77
6	<i>CP</i>-violating Effective Vertex in a Leptoquark Model	82

6.1	Scalar Leptoquark Couplings in $SU(2)_L \times U(1) \times SU(3)_C$ Theory	85
6.2	Expressions for Electric and Weak Dipole Form Factors	87
6.2.1	EDFF and WDFP of the Top Quark	87
6.2.2	EDFF and WDFP of the τ Lepton	90
6.3	Discussion of Numerical Results	91
7	Conclusions	100
	Appendix A	104
A.1	QCD Lagrangian	104
A.2	Dirac Field Bilinears Under Space Inversion	104
A.3	Dirac Spinors Under Charge Conjugation	105
A.4	Dirac Field Bilinears Under Charge Conjugation	106
	Appendix B	108
B.1	Expressions for A_i , B_i , C_i and D_i	108
B.2	Expressions for A_i , etc. in Chapter 4	110
B.3	T_i in Chapter 4	111

B.4	Expression for $d\sigma_{ij}$ in Chapter 5	112
-----	--	-----

B.5	Production Density Matrix Elements Corresponding to Different $d\sigma_{ij}$	113
-----	--	-----

Appendix C		117
------------	--	-----

C.1	$t\bar{t}\gamma(Z)$ Vertex at One-Loop Level	117
-----	--	-----

Acknowledgements

I express my sincere and deep gratitude to Prof. Saurabh D. Rindani for suggesting a thesis topic of current interest and for his consistent supervision over the project. All the work done in this thesis is in collaboration with him. He taught me various aspects of high energy physics with patience. I thank him for that. I also thank him for critically going through the manuscript and suggesting changes.

I would like to thank Prof. Anjan S. Joshipura, Prof. Utpal Sarkar and Dr. Subhendra Mohanty whose presence in the group itself was inspiring. Thanks are also due to Prof. J. C. Parikh, Prof. A. R. Prasanna, Prof. V. K. B. Kota and Dr. Sai Iyer for helping me learn different aspects of physics.

I sincerely thank Ravindran for the discussions and also for going through the manuscript of the thesis. I also thank him for discussions on the work described in Chapter 5 of the thesis. More than all these I thank him for being a good friend. I thank Torsten Arens for the collaboration on the work described in Chapter 6 of this thesis.

I thank Mr. Viswanathan, Mr. Joseph and Mr. Murali of the Theory Group Office, PRL, for helping me in administrative matters. I also take this opportunity to thank the staff of Computer Services, PRL, the staff of Library, PRL and the staff of Administrative Section, PRL for all the help they have extended to me.

Friends have always been an important part of my life and that is very much so at PRL. They have helped me live an easy life in all these years I spent here. Without venturing into mentioning them individually I sincerely thank all my friends at PRL for the happy moments we had together.

Clement, Watson, Biju, Shibu John and Shibu Mathew have been very good friends to me. I thank them for the love and care they have given me; for all the heated arguments, lively discussions and the joyful moments together, the memory of which will always be there with me.

I will always remember the pleasant company of Aparna. She is among them, whom I consider closest and feel most comfortable with. I thank her for the friendship.

Thanks to Sandeep, Anshu and Prashant for being good friends to me and for the discussions we had on various topics. I thank Abhijit and Debu for the happy times we had together. Kunu has been a friend ever ready to help whenever I needed it. I thank her for all that.

I thank Madhu for the long and friendly association. His encouraging letters have

helped me during my stay at PRL. I also thank Kashmira for the nice company.

My thanks to Manoj for all the useful discussions we had on physics and otherwise.

I express my gratitude to Jose and Delia for their friendship and for all those fabulous dinners. My thanks to Clement's family for their generous hospitality. I also thank Pauline and her family for the pleasant evenings.

I thank my parents, sisters and brother for providing me everything I needed. I would not have been what I am without the love and care they have shown to me. Their consistent encouragement right from my school days and all the sacrifices they have made for my sake are the sources of my energy.

I also remember with gratitude my teachers who directed me to physics.

Lastly I would like to thank Physical Research Laboratory, Ahmedabad, and DoS, India for providing me with all the facilities I required during this thesis work.

Chapter 1

Introduction

The Standard Model (SM) of High Energy Physics is a highly successful theoretical model describing the dynamics of fundamental particles under the basic forces. It has been tested to a very high accuracy in various experiments for the past two and a half decades. Even then there are certain issues like understanding CP violation in nature which need greater attention. Different models considering effects outside the regime of SM have been proposed to study the behaviour of nature at the level of fundamental particles. Predictions of such models have to be tested in experiments which can be carried out at proposed colliders which will be running at higher energies.

Electron-positron colliders have been used in the past to obtain a number of important results. They have an advantage over hadron colliders because leptons are more nearly pointlike than hadrons. Consequently, their interactions are better understood than those of hadrons. Moreover, hadronic backgrounds are larger in hadronic colliders. Thus e^+e^- colliders provide a much cleaner environment.

Circular e^+e^- colliders cannot go beyond a certain centre-of-mass energy because

of the synchrotron radiation losses and hence future colliders must be linear colliders. The proposed electron-positron linear colliders, for example SLAC's Next Linear Collider (NLC), will be running at centre of mass energies of several hundred GeV's. A large number of top-antitop quark pairs are expected to be produced in such colliders. The top quark being very massive [1] is considered to be a good place to test many of the new physics effects. Studying CP violation in such systems is very promising. In this thesis we have studied CP -violating asymmetries arising due to electric and weak dipole form factors (DFF) of the top quark, which might be observable at NLC ¹

A high degree of longitudinal beam polarization can be achieved for an electron in linear colliders as confirmed in, *e.g.*, experiments at SLC [2] and KEK [3]. The effect of electron beam polarization on CP -violating signals is therefore also included in this work.

Apart from electron-positron colliders, the possibility of a $\gamma\gamma$ collider has also been considered in the literature [4]. The idea is that high-energy photon beams could be obtained by the Compton backscattering of an intense laser beam off a high-energy electron (or positron) beam. The $\gamma\gamma \rightarrow t\bar{t}$ system is studied in this thesis for CP -violating signals in the presence of the top quark DFF's.

In an attempt to investigate whether any new models can lead to large DFF's, we consider a scenario where third-generation leptoquarks are present. These leptoquarks couple top quarks with τ leptons. One-loop correction to the $\tau\bar{\tau}\gamma(Z)$ vertex arising from the above coupling is studied for CP violation. From the existing lim-

¹Various proposals for building a high-energy linear e^+e^- collider are being examined. Notable of these are for SLC (Stanford), TESLA (DESY), JLC (KEK) and CLIC (CERN). While the term NLC was first used for the proposed collider at Stanford, we will use this term to denote any of the future linear colliders

<u>Leptons</u>		<u>Quarks</u>		
$l_L^i \equiv \begin{pmatrix} \nu_i \\ e_i \end{pmatrix}_L$	e_R^i	$q_L^i \equiv \begin{pmatrix} u_i \\ d_i \end{pmatrix}_L$	u_R^i	d_R^i
(1,2,1)	(1,1,2)	(3,2,- $\frac{1}{3}$)	(3,1,- $\frac{4}{3}$)	(3,1, $\frac{2}{3}$)

Table 1.1: Fermion content of the Standard Model

its on DFF's we are able to put bounds on the mass and coupling constant of the leptoquarks. A similar study is done in case of $t\bar{t}$ as well.

In the following four sections we shall review the relevant aspects of SM and then discuss the phenomenology of CP violation. In sections 1.5 and 1.6 we shall introduce the method used in our studies.

Throughout the thesis, Bjorken and Drell conventions are used for the metric and Dirac gamma matrices.

1.1 The Standard Model

Particle interactions in high energy physics are studied using field theory techniques and are currently believed to arise from gauge theories. In a gauge theory, a certain local gauge symmetry is assigned to the Lagrangian of the system studied. The standard model of Particle Physics assumes a gauge group $SU(3)_C \times SU(2)_L \times U(1)_Y$ to study particle dynamics. Fundamental fields are classified in SM in the following way.

Table 1.1 summarizes the fermion content of SM. In the table the subscripts L and R denote the chiralities of the particles. In the case of a particle represented by the Dirac spinor ψ , chiralities are defined by the following projections:

$$\psi_{R,L} = \frac{1}{2} (1 \pm \gamma^5) \psi. \quad (1.1)$$

In SM left-chirality particles are doublets under $SU(2)_L$ whereas right-chirality particles are singlets. Notice that SM does not have right-helicity neutrinos in it. In Table 1.1, colour $SU(3)_c$ indices are suppressed. All the quarks are colour triplets while leptons are colour neutral. Last row in Table 1.1 indicates to which multiplet of $SU(3)_c$ and $SU(2)_L$ the particles belong and what their $U(1)_Y$ hypercharges are. $i = 1, 2, 3$ correspond to three families. Charges of the particles are related to the hypercharge(Y) and the third component of the $SU(2)_L$ quantum number, (T_3) by the Gell-Mann–Nishijima relation, $Q = T_3 - \frac{Y}{2}$. Apart from these particles SM has two charged gauge bosons in it, the W^\pm and two neutral gauge bosons, Z and photon, which are the mediators of the electroweak interactions, and eight gluons, which mediate the strong interactions. To generate masses for the particles SM uses a technique known as the Higgs mechanism. For this purpose, scalar fields, the Higgs fields (ϕ), are introduced into the theory. They are colour neutral and are $SU(2)_L$ doublets with hypercharge -1 in the minimal version of SM.

The Lagrangian describing the fundamental particles and their behaviour under the basic forces (except gravity) is invariant under the above group transformations, apart from being Lorentz invariant. This thesis discusses the phenomenon of CP violation in the electroweak sector of high energy physics. Rest of this section will therefore discuss only the electroweak part of SM.

The general form of an electroweak Lagrangian (see Appendix A, Equation A.1 for

the QCD part of the Lagrangian) is

$$\mathcal{L} = \mathcal{L}_G + \mathcal{L}_F + \mathcal{L}_Y + \mathcal{L}_H, \quad (1.2)$$

where

$$\begin{aligned} \mathcal{L}_G &= -\frac{1}{4} B_{\mu\nu} B^{\mu\nu} - \frac{1}{4} \vec{W}_{\mu\nu} \cdot \vec{W}^{\mu\nu}, \\ \mathcal{L}_F &= \sum \bar{\psi}_L i \not{D}_L \psi_L + \sum \bar{\psi}_R i \not{D}_R \psi_R, \\ \mathcal{L}_Y &= h_{ij}^u \bar{q}_L^i \tilde{\phi} u_R^j + h_{ij}^d \bar{q}_L^i \phi d_R^j + h_{ij}^e \bar{l}_L^i \phi e_R^j + h.c., \\ \mathcal{L}_H &= (D_L^\mu \phi)^\dagger (D_{L\mu} \phi) - V(\phi). \end{aligned}$$

In \mathcal{L}_F the summation is over all left-handed doublets ψ_L in the first term and over all right-handed singlets ψ_R in the second term.

Here $\tilde{\phi} = i\tau_2 \phi^*$, and the covariant derivatives are given by

$$\begin{aligned} D_L^\mu &= \partial^\mu + i g \frac{\vec{\tau}}{2} \cdot \vec{W}^\mu + i g' \frac{Y}{2} B^\mu, \\ D_R^\mu &= \partial^\mu + i g' \frac{Y}{2} B^\mu, \end{aligned}$$

where g and g' are coupling constants corresponding to $SU(2)_L$ and $U(1)_Y$ gauge groups, and \vec{W}^μ , B^μ are vector gauge fields corresponding to these groups. \vec{W}^μ is an $SU(2)_L$ triplet with $Y = 0$ and B^μ is neutral under $SU(2)_L \times U(1)_Y$.

$$V(\phi) = \mu^2 \phi^\dagger \phi + \lambda (\phi^\dagger \phi)^2 \quad (1.3)$$

is the scalar potential, where μ and λ are the two coupling constants. The gauge field strengths are

$$B_{\mu\nu} = \partial_\mu B_\nu - \partial_\nu B_\mu \quad (1.4)$$

and

$$\vec{W}_{\mu\nu} = \partial_\mu \vec{W}_\nu - \partial_\nu \vec{W}_\mu + g \vec{W}_\mu \times \vec{W}_\nu.$$

The Lagrangian \mathcal{L} is invariant under local $SU(2)$ gauge transformations.

Under $SU(2)_L$, ψ_L transforms like a doublet and ψ_R transforms like a singlet, and hence a typical fermionic mass term, $m \bar{\psi}_L \psi_R$ is not gauge invariant. The gauge boson mass terms ($m^2 A_\mu^a A_\mu^a$) are also not gauge invariant. Since we demand the gauge invariance of the SM Lagrangian it cannot accommodate these mass terms. At the same time we know that the real particles are massive. To save the situation, SM generates masses for particles by breaking the gauge symmetry using the Higgs mechanism in which the Higgs field is introduced in such a way that the field has a non-zero expectation value (v) in the true vacuum state. This is done by choosing $\mu^2 < 0$ and λ positive. In that case for smaller values of ϕ , where the quadratic term dominates the scalar potential will be negative while at larger values of ϕ the quartic term dominates giving positive values to the potential. This results in having a minimum for the potential at a non-zero value of the electrically neutral component of ϕ ($\langle \phi_0 \rangle = v = -\frac{\mu^2}{\lambda}$). This phenomenon where the vacuum does not respect the symmetry, while the Lagrangian is still gauge invariant, is known as spontaneous symmetry breaking.

Out of the four components (the real and the imaginary parts of the upper and the

lower components of the doublet) of the Higgs field ϕ , three can be rotated away by using the gauge transformation. Since we want to retain the electromagnetic gauge invariance, we give vacuum expectation value to the neutral component of the Higgs field. A convenient choice of Higgs field is $\phi = \frac{1}{\sqrt{2}} \begin{pmatrix} 0 \\ v + \eta(x) \end{pmatrix}$ and $\tilde{\phi} = i\tau_2 \phi^*$. Here η corresponds to the only Higgs particle remaining out of the four. When this Higgs field is used in the Lagrangian 1.2 we get the following mass terms for the fermions:

$$\mathcal{L}_{mass} = \bar{u}_L^i M_{ij}^u u_R^j + \bar{d}_L^i M_{ij}^d d_R^j + \bar{e}_L^i M_{ij}^e e_R^j,$$

where $M_{ij}^f = \frac{v}{\sqrt{2}} h_{ij}^f$ with $f = u, d, e$. There are no mass terms for neutrinos because SM does not have a right-handed neutrino.

Here the mass matrices M^u , M^d and M^e are not necessarily diagonal. Physical particles should correspond to definite mass states and the corresponding fields will be the eigenvectors of these mass matrices. Diagonalization of mass matrices is done by a biunitary transformation, with a separate unitary transformation on the left-handed and the right-handed fermions. In this process “flavour” fields introduced in the original Lagrangian are transformed to physical fields. The transformations are given below:

$$\begin{aligned} u_L &\rightarrow u'_L \equiv U_L u_L, & d_L &\rightarrow d'_L \equiv D_L d_L, & e_L &\rightarrow e'_L \equiv E_L e_L, \\ u_R &\rightarrow u'_R \equiv U_R u_R, & d_R &\rightarrow d'_R \equiv D_R d_R, & e_R &\rightarrow e'_R \equiv E_R e_R, \\ M^u &\rightarrow M^{u'} \equiv U_L M^u U_R^\dagger, & M^d &\rightarrow M^{d'} \equiv D_L M^d D_R^\dagger, & M^e &\rightarrow M^{e'} \equiv E_L M^e E_R^\dagger. \end{aligned}$$

Going back to the Lagrangian given in Equation 1.2, now written in terms of the physical fields (the primed ones), the fermionic part includes a kinetic energy term,

a charged current interaction term and a neutral current interaction term:

$$\mathcal{L}_F = \mathcal{L}_{KE} + \mathcal{L}_{CC} + \mathcal{L}_{NC}.$$

Here

$$\mathcal{L}_{KE} = \sum \bar{\psi}' i \not{\partial} \psi',$$

$$\mathcal{L}_{CC} = -\frac{g}{2} \bar{u}'_L \gamma^\mu V d'_L (W_\mu^1 + i W_\mu^2) - \frac{g}{2} \bar{\nu}'_L \gamma^\mu e'_L (W_\mu^1 + i W_\mu^2) + h.c.$$

and

$$\mathcal{L}_{NC} = -g \sum \bar{\psi}'_L \gamma^\mu \frac{\tau_3}{2} \psi'_L W_\mu^3 - g' \sum \frac{Y}{2} \bar{\psi}' \gamma^\mu \psi' B_\mu.$$

$W^\pm = \frac{1}{\sqrt{2}} (W_\mu^1 \pm i W_\mu^2)$ are the two charged gauge bosons. The neutral current is written in terms of the photon and the Z-boson fields as

$$\mathcal{L}_{NC} = e \sum Q \bar{\psi}' \gamma^\mu \psi' A_\mu + \sum g_R \bar{\psi}'_R \gamma^\mu \psi'_R Z_\mu + \sum g_L \bar{\psi}'_L \gamma^\mu \psi'_L Z_\mu,$$

where

$$A_\mu = g' W_\mu^3 + g B_\mu \tag{1.5}$$

and

$$Z_\mu = g W_\mu^3 - g' B_\mu \tag{1.6}$$

are the gauge boson corresponding to the electromagnetic force and the weak neutral gauge boson respectively, obtained by diagonalization of the 2×2 mass matrix of W^3 and B . This diagonalization gives a mass $m_Z = \frac{v}{2} \sqrt{g^2 + g'^2}$ for Z , while the photon is massless. The Higgs mechanism also leads to a mass $M_W = \frac{gv}{2}$ for the W^\pm .

The neutral current couplings of various fermions are written in terms of their respective T_3 and Q values by

$$g_L = \frac{e}{\sin \theta_W \cos \theta_W} \left(\frac{T_3}{2} - Q \sin^2 \theta_W \right)$$

and

$$g_R = \frac{e}{\sin \theta_W \cos \theta_W} (-Q \sin^2 \theta_W)$$

are the left- and right-handed couplings.

Family indices are suppressed in the above expression. e is the electric charge of positron and is related to the $SU(2)_L$ and $U(1)_Y$ couplings by $e = \sqrt{g^2 + g'^2}$. T_3 is the third component of the weak isospin and Y , the hypercharge. Note that the neutral current terms continue to be diagonal.

$V = U_L D_L^\dagger$ is a 3×3 unitary matrix (called CKM matrix, named after Cabbibo, Kobayashi and Maskawa.) Out of the 9 independent parameters of V , 3 are angles (an orthogonal matrix of dimension three has 3 independent parameters) and the rest are phases. 5 of these phases can be rotated away by redefining the quark fields leaving one phase which makes the matrix V complex. No such matrix appears in the charge current coupling of the leptons because with massless neutrinos, such a

unitary matrix can be absorbed in the redefinition of the neutrino fields.

Thus, couplings of charged bosons to the quarks are complex and cause CP violation. We will first discuss in brief the P and the C symmetries before going on to CP violation.

1.2 P and C Symmetries

Dynamical equations of a physical system are invariant under Lorentz transformations. Transformation properties under other discrete symmetries are also important to understand a physical system. In this section we shall look at the space inversion and the charge conjugation transformations.

1.2.1 Space Inversion or Parity (P)

Under this transformation all space coordinates change sign. i.e., $(\vec{x}, t) \rightarrow (-\vec{x}, t)$. Invariance of the Dirac equation under a spatial transformation $x'^\mu = \Lambda^\mu_\nu x^\nu$ requires a matrix S satisfying

$$S^{-1} \gamma^\mu S = \Lambda^\mu_\nu \gamma^\nu.$$

Fermion fields transform under this transformation as

$$\psi(x) \rightarrow \psi'(x') = S \psi(x).$$

For space inversion $\Lambda = \text{diag}(1, -1, -1, -1)$, implying $S^{-1} \gamma_\mu S = \gamma^\mu$. $S = \gamma^0$ satisfies this condition.

See A.2 for transformation properties of Dirac field bilinears under P .

1.2.2 Charge Conjugation (C)

Under charge conjugation all the additive quantum numbers of a particle change sign. For a free particle this amounts to changing the particle creation (annihilation) operator to an antiparticle creation (annihilation) operator and vice versa. Demanding that the particle and its charge conjugated counterpart under an external electromagnetic field obey the same Dirac equation, we get the transformation property of a spinor under charge conjugation as

$$\psi \rightarrow C \bar{\psi}^T,$$

where C is a 4×4 matrix satisfying the condition (see Section A.3 in Appendix A.)

$$C^{-1} \gamma^\mu C = -(\gamma^\mu)^T.$$

Section A.4 gives the transformation properties of bilinears under C .

From the experimental data available till then, especially, looking at the two different decay modes of K^+ , viz., $K^+ \rightarrow 2\pi$ and $K^+ \rightarrow 3\pi$, Lee and Yang in 1956 [5] observed that parity was violated in weak interactions. A year later Wu *et al.* [6] confirmed P violation in the ^{60}Co to ^{60}Ni transition. Also, neutrinos in β decay are found to be left-handed and never right-handed while antineutrinos from the conjugate process is always right-handed. This clearly violates charge conjugation invariance.

In SM maximal violation of P and C are explicitly brought in by choosing a (V-A) form for the weak interactions and by assuming the non-existence of right-handed neutrino. It was believed till 1964 that the combined symmetry CP is not violated even though C and P are broken maximally when taken individually. Christenson *et al.* [7] provided experimental evidence for CP violation in the K -meson system. Later on this small violation of CP was explained successfully by SM using the CKM phase.

1.3 CP Violation Phenomenology

Christenson *et al.*'s [7] discovery of the 2π decay of the long lived neutral kaon, K_L , implying that it is not a CP eigenstate, was the first experimental evidence for CP violation. They measured a branching ratio, $R = \frac{K_L \rightarrow \pi^+ \pi^-}{K_L \rightarrow (All)} = (2.0 \pm 0.4) \times 10^{-3}$. This gives $|\epsilon| \sim 2.3 \times 10^{-3}$, where, ϵ is the mixing parameter in expressing the long-lived, physical K-meson, K_L in terms of the weak eigenstates, K_0 and \bar{K}_0 ;

$$K_L = \frac{1}{\sqrt{2}} [(K_0 - \bar{K}_0) + \epsilon(K_0 + \bar{K}_0)].$$

ϵ is given in terms of the experimentally measurable quantities

$$\eta_{+-} = \frac{K_L^0 \rightarrow \pi^+ \pi^-}{K_S^0 \rightarrow \pi^+ \pi^-} \quad \text{and} \quad \eta_{00} = \frac{K_L^0 \rightarrow \pi^0 \pi^0}{K_S^0 \rightarrow \pi^0 \pi^0}$$

as

$$\eta_{+-} = \epsilon + \epsilon' \quad \text{and} \quad \eta_{00} = \epsilon - 2\epsilon'.$$

ϵ' is the ratio of transition amplitude of K^0 decay to isospin two state to the amplitude of K^0 decay to an isospin zero state.

Present experimental values of the parameters are [8]:

$$|\eta_{+-}| = (2.285 \pm 0.019) \times 10^{-3},$$

$$|\eta_{00}| = (2.275 \pm 0.019) \times 10^{-3}$$

and

$$\frac{\epsilon'}{\epsilon} = (1.5 \pm 0.8) \times 10^{-3}.$$

CP violation needs complex coupling, which is supplied in SM by the CKM matrix, which has complex elements arising from a single phase.

Experimental results are compatible with the SM predictions. But SM does not say anything about the value of CKM phase and it has to be fixed from experiments. An independent test of the CKM picture of CP violation could be done in the proposed B-factories. Until then, alternative CP violation scenarios cannot be ruled out. To understand the phenomenon better, it is required to look for other CP -violating effects in nature. It can be seen that presence of electric dipole moment (EDM) indicates CP violation. The electric dipole interaction with electromagnetic field is given by the term $d_\psi^E \bar{\psi} \sigma_{\mu\nu} \gamma^5 \psi F^{\mu\nu}$ which is odd under CP transformation. An analogous term can be written for the weak neutral current interaction, $d_\psi^Z \bar{\psi} \sigma_{\mu\nu} \gamma^5 \psi (\partial^\mu Z^\nu - \partial^\nu Z^\mu)$, which is also CP -violating. d_ψ^Z is referred to as the weak dipole moment. Interference of this term with CP -even terms in the Lagrangian causes observable CP violation. It is a dimension 5 term and thus

$d_e^\gamma = (-0.3 \pm 0.8) \times 10^{-26}$
$d_\mu^\gamma = (3.7 \pm 3.4) \times 10^{-19}$
$d_\tau^\gamma < 5 \times 10^{-17}$
$d_n^\gamma < 1.1 \times 10^{-17}$
$\text{Red}_\tau^Z < 5.6 \times 10^{-18}$
$\text{Im}d_\tau^Z < 1.5 \times 10^{-17}$

Table 1.2: Experimental limits on particle dipole moments in units of $e \text{ cm}$.

cannot be included as a fundamental interaction in a renormalizable theory. It has to come from higher order terms in the perturbation expansion. In SM there is no dipole term up to two-loop level and so particle dipole moments are predicted to be very small. Experimental bounds on particle dipole moments ($d_f^{\gamma,Z}$ correspond respectively to electromagnetic and weak dipole couplings) are given in the Table 1.2 [8, 9]

In SM dipole moments come as higher order corrections in the perturbation theory. There are no dipole moment at one-loop level as the diagrams in these cases are self-conjugate. The contribution from two-loop diagrams is also zero [10]. Since the only CP violating phase that is available in SM is the CKM phase which comes in the quark sector, leptons acquire dipole moments through the dipole couplings of quarks and/or gauge-boson fields. SM predicts electric dipole moment of electron to be $\sim 10^{-38}$ while for neutron it is $\sim 10^{-31}$.

From the table it is clear that SM predictions are far too small compared to the experimental bounds. There are many extensions of SM which give dipole moments of particles close to the experimental values. In the next section we shall have a look at some of the models trying to explain CP violation.

1.4 CP Violation and Extensions of SM

There were many models prior to the Glashow-Weinberg-Salam model of particle physics (the Standard Model) trying to explain CP violation, among which are the superweak hypothesis of Wolfenstein [11] (strength $\sim 10^{-7} G_F$), semi-strong interaction theory of Prentki and Veltman [12] and the milliweak theory of Wu and Yang [13]. Kobayashi and Maskawa [14] explained how CP violation can be brought into SM through quark mixing by extending the fermions to three generations. Later on, Weinberg's [15] two Higgs doublet model treating CP violation as a spontaneously broken symmetry proposed CP violation in the quark sector through Higgs exchange. The strength of CP violation in this case is milliweak. Mohapatra and Pati [16] have discussed the possibility of CP violation in a left-right symmetric model. Here CP violation comes through the inequality of the masses of the two gauge bosons, W_L and W_R , which interact with the left and right chiral currents. The strength of CP -violating interactions, in this case, is milliweak or weaker than milliweak.

Coming to the recent models investigating CP violation, multi-Higgs models [17, 18] have been discussed extensively. These models have been used in constructing CP -odd correlations and asymmetries in hadronic and e^+e^- reactions. CP violation effects generated in supersymmetric models [19] are also studied in the context of both hadronic and e^+e^- colliders. There are also investigations of CP violation effects in left-right symmetric models [20].

The effective Lagrangian method, which is made use of in the studies we have carried out in this thesis is described in the next section.

1.5 Effective Lagrangian Method

As seen in the previous section, CP violation has been studied in a large number of models. A model independent way of looking at the whole scenario is the effective Lagrangian method. In this approach, an effective Lagrangian, having electric and weak dipole terms in addition to the SM terms, is considered. Dipole moments are parameters in this approach and are fixed from experimental measurements of CP -violating observables. We have chosen this approach in our studies.

We consider the effective Lagrangian;

$$\mathcal{L}_{eff} = \mathcal{L}_{SM} + \mathcal{L}_{CP}, \quad (1.7)$$

where

$$\mathcal{L}_{CP} = \frac{ic_d^\gamma}{2m_t} \bar{\psi}_t \sigma^{\mu\nu} \gamma_5 \psi_t F_{\mu\nu} + \frac{ic_d^Z}{2m_t} \bar{\psi}_t \sigma^{\mu\nu} \gamma_5 \psi_t Z_{\mu\nu},$$

with

$$F_{\mu\nu} = \partial_\mu A_\nu - \partial_\nu A_\mu. \quad (1.8)$$

and

$$Z_{\mu\nu} = \partial_\mu Z_\nu - \partial_\nu Z_\mu$$

c_d^j ($j = \gamma, Z$) are the electric and the weak dipole form factors and are, in general, complex and momentum dependent. This modifies the Standard Model $t\bar{t}\gamma(Z)$

coupling to $ie\Gamma_\mu$, where

$$\Gamma_\mu^j = c_v^j \gamma_\mu + c_a^j \gamma_\mu \gamma_5 + \frac{c_d^j}{2m_t} \sigma_{\mu\nu} \gamma_5 (p_t + p_{\bar{t}})^\nu, \quad j = \gamma, Z. \quad (1.9)$$

The dipole moments are related to c_d^j by $d^j = c_d^j/(2m_t)$. We have considered the top quark system because it is confirmed now that top quark is heavy with mass, $m_t = 180 \pm 12 \text{ GeV}$ [1] and therefore decays very fast. Its life time, $\tau \sim 10^{-24} \text{ sec}$, is less than the time it requires to hadronize ($R_{conf} = \Lambda_{QCD}^{-1} \sim 10^{-23} \text{ sec}$) [21]. Thus the top quark produced in a collider decays before hadronization, and the decay products preserve the spin information, which then can be used to study CP properties of the interaction.

We study CP violation using CP -odd asymmetries constructed with Lagrangian in Equation 1.7. How the asymmetries are used to determine allowed regions in the parameter space and the sensitivity of the experiment are discussed in the next section. In our work we consider the top quark decay to be the standard one. For discussions which include CP violation effects in the decay, see [22, 23].

1.6 Sensitivity of the measurements

CP -odd asymmetries are studied in the following chapters of this thesis as signatures of CP violation. Experimental measurements of these asymmetries can determine the dipole form factors, or if the asymmetries are found consistent with zero, they can put bounds on the dipole form factors of the top quark. Sensitivity of an experiment depends on the statistics. The number of asymmetric events must be greater than the statistical fluctuation by a certain factor for it to be observed. This factor determines the confidence level (C.L.) of the measurement. For a sys-

tem with one degree of freedom the number of asymmetric events, N_A ($= N A$, where A is the asymmetry and N is the total number of events.) should then be greater than $1.64\sqrt{N}$ for observing it at 90% C.L., where \sqrt{N} corresponds to the standard deviation. Using this we can get limits on the dipole form factors. They are given by

$$\delta c_d^j = \frac{1.64\sqrt{N}c_d^j}{N_A}, \quad (1.10)$$

where c_d^j is the value of either electric or weak dipole form factor (DFF) at which A is calculated. The other c_d^j is fixed in this case.

To get simultaneous limits on two DFF's one should do the following. For two degrees of freedom 90% C.L. corresponds to 2.15σ and therefore to observe an asymmetry we must have an asymmetric number of events satisfying the condition

$$N_A > 2.15\sqrt{N}.$$

A is a function of c_d^γ and c_d^Z (either the real or the imaginary parts). The minimum number of events for the asymmetry to be observable is given by

$$N_A(c_d^\gamma, c_d^Z) = 2.15\sqrt{N}. \quad (1.11)$$

This gives a linear equation in c_d^γ and c_d^Z . Since the number of events is the absolute value of $N A$, and A could be either positive or negative, we get a band of allowed values in the $c_d^\gamma - c_d^Z$ plane. This does not really fix the DFF's as we can choose any value of c_d^γ and get the corresponding value of c_d^Z from the graph. Use of another asymmetry will give a different band restricting the values of DFF's. The

intersecting region of the two bands helps getting the range of allowed values of DFF's independently.

The other possibility in the study of CP violation is the investigation using correlations of CP -odd kinematic variables. Of particular importance are variables known as optimal variables [23, 24], whose correlations are minimized compared to the error in their measurement. Realizing that the statistical significance of the non-zero value of the correlation increases with the resolving power, R , we can say that the optimal variable is the correlation with maximum R . Correlations of optimal variables have an advantage over asymmetries mainly in case of distributions with several kinematic variables. We restrict ourselves to asymmetries which are conceptually simpler than correlations of optimal variables, and also allow us to obtain analytic expressions.

1.7 Plan of the Thesis

The plan of the thesis is as follows. In Chapter 2, CP violation studies in $e^+e^- \rightarrow t\bar{t}$ and the subsequent decay of t and \bar{t} are made by constructing CP -violating asymmetries. Some other asymmetries, which may be simpler from the experimental point of view are discussed in Chapter 3. In the case when only electron beam is polarized a collinear helicity-flip photon emission from the initial state can in principle give rise to a background to the asymmetries considered. Here CP non-invariant helicity combination in the initial state may lead to the same asymmetries that are considered even in the absence of dipole form factors (or any other genuine CP breaking parameter.) Chapter 4 discusses this background to the asymmetries considered in Chapters 2 & 3.

CP -violating effects in the top quark production in $\gamma\gamma$ -collider is discussed in Chapter 5. Chapter 6 describes CP violation studies made in a leptoquark model. Finally, conclusions of the studies are given in Chapter 7.

Chapter 2

CP-violating Asymmetries in $e^+e^- \rightarrow t\bar{t}$

This chapter discusses some *CP*-violating asymmetries arising due to electric and weak dipole moments of the top quark in top-antitop pair production in an e^+e^- collider. We make use of an effective Lagrangian (Equation 1.7), which includes dipole interaction terms in addition to the SM terms. As mentioned in Section 1.5, the top quark system is chosen because heaviness of the top quark implies that it decays before hadronization takes place [21] and the decay products preserve top quark spin information which can be used to study *CP* properties of the interaction. In the following we have defined *CP*-odd asymmetries which signal *CP* violation when the initial state is a *CP* eigenstate. These asymmetries are used to determine the dipole moments, which are the parameters of the theory. We have four parameters altogether, viz., the real and the imaginary parts of the electric and the weak dipole form factors and hence we require at least four asymmetries to fix them.

Rest of the chapter discusses some *CP*-odd asymmetries which may be constructed

out of final state momenta. Section 2.1 will introduce the asymmetries. Expressions for the asymmetries and details of the calculations are given in Section 2.2. In the last section we shall discuss the results and possible conclusions drawn from it.

2.1 CP -Odd Asymmetries

In the process $e^+e^- \rightarrow t\bar{t}$ spins and momenta of the top quark and the antitop quark and the momentum of the electron are the variables we would be able to use to construct the asymmetries with. It is essential to consider spins as it is not possible to construct CP -odd asymmetries (or correlations) only using the momenta [25].

CP violation effects in e^+e^- colliders ¹ using CP -odd correlations and CP -odd asymmetries have been studied by various groups [27, 28]. One of the asymmetries which directly depends on the top quark polarization is the following.

Among the different helicity combinations of $t\bar{t}$ pair produced, $t_L\bar{t}_L$ and $t_R\bar{t}_R$ are CP conjugates of each other, while $t_L\bar{t}_R$ and $t_R\bar{t}_L$ are CP self-conjugates. Thus any asymmetry in the production rates of $t_L\bar{t}_L$ and $t_R\bar{t}_R$ will signal CP violation. This possibility is discussed by Schmidt and Peskin [29] in the context of hadron colliders and in a supersymmetric model, and in the case of an e^+e^- collider by Chang *et al.* [30]. This number asymmetry can be converted into a lepton energy asymmetry in the limit of bottom quark mass going to zero as explained below [29].

Top quark being heavy, decays mostly into longitudinally polarized W^+ and b and the W^+ in turn decays into leptons or hadronic jets. Antitop quark also follows a

¹For studies on hadron colliders see, *e.g.*, Ref. [26].

similar decay process.

$$\begin{aligned} t &\rightarrow W^+ b & \bar{t} &\rightarrow W^- \bar{b} \\ W^+ &\rightarrow l^+ \nu X & W^- &\rightarrow l^- \bar{\nu} \bar{X} \end{aligned}$$

In the limit $m_b \rightarrow 0$, the b quark is left-handed and hence will move opposite to the top quark spin direction. Thus t_R decay will have a W moving in the top quark momentum direction while t_L will produce a W which moves against the top momentum direction. Hence the antilepton produced in the decay of W from t_R will be more energetic than the one produced in the decay of W from t_L . On the other hand leptons produced in the decay of \bar{t}_L will be more energetic than that from \bar{t}_R . Therefore $t_R \bar{t}_R$ will have more energetic antileptons than leptons and $t_L \bar{t}_L$ will have more energetic leptons than antileptons. Thus the number asymmetry in the $t_R \bar{t}_R$ and $t_L \bar{t}_L$ becomes an asymmetry in the energy of leptons and antileptons produced. Energy asymmetry between distributions of l^+ and l^- at the same value of $x = x(l^+) = x(l^-) = 4 E(l^\pm)/\sqrt{s}$ is given by

$$A_E(x) = \frac{1}{\sigma} \left[\frac{d\sigma}{dx(l^+)} - \frac{d\sigma}{dx(l^-)} \right]. \quad (2.1)$$

Extending the work of [30], we have discussed this energy asymmetry in the presence of longitudinal beam polarization.

The other asymmetry discussed in [30] is the so called up-down asymmetry. Asymmetry in the number of leptons and antileptons taken together between the two hemispheres separated by the $t\bar{t}$ production plane is a CP -odd quantity. Here up/down refers to $(p_{l^\pm})_y \gtrless 0$, $(p_{l^\pm})_y$ being the y component of \vec{p}_{l^\pm} , with respect to a coordinate system chosen in the $e^+ e^-$ center-of-mass (c.m.) frame so that the z -axis is along \vec{p}_t , and the y -axis is along $\vec{p}_e \times \vec{p}_t$. The $t\bar{t}$ production plane is thus

the xz plane.

Schematically the up-down asymmetry [30] is

$$A_{ud} = \int_{-1}^{+1} A_{ud}(\theta) d \cos \theta, \quad (2.2)$$

where

$$A_{ud}(\theta) = \frac{1}{2\sigma} \left[\frac{d\sigma(l^+, \text{up})}{d \cos \theta} - \frac{d\sigma(l^+, \text{down})}{d \cos \theta} + \frac{d\sigma(l^-, \text{up})}{d \cos \theta} - \frac{d\sigma(l^-, \text{down})}{d \cos \theta} \right]. \quad (2.3)$$

Here θ refers to the scattering angle, i.e., the angle between \vec{p}_t and \vec{p}_e in the c.m. frame.

As already mentioned we have four parameters here: real and imaginary parts of the electric and the weak dipole form factors. Depending on the CPT property (here T is the naive time reversal with only the momenta and spins reversed) of the asymmetry it will be proportional to either the real or the imaginary part of DFF's. That is because a CPT -odd observable must be proportional to the absorptive part. (For details see, e.g., Rindani [31].) The up-down asymmetry defined above is CPT -even and hence proportional to the real parts of DFF's. To disentangle the electric and weak dipole form factors we need at least one more CP -odd asymmetry which is CPT -even, and to fix the imaginary parts we need another two CP and CPT -odd asymmetries. We therefore propose the following new asymmetries [32].

A combination of the up-down and forward-backward asymmetry A_{ud}^{fb} is again CPT even which could be used together with A_{ud} to disentangle the real parts of

DFF's. Given the definition of $A_{ud}(\theta)$ (Eqn. 2.3), A_{ud}^{fb} is defined as

$$A_{ud}^{fb} = \int_0^1 A_{ud}(\theta) d \cos \theta - \int_{-1}^0 A_{ud}(\theta) d \cos \theta. \quad (2.4)$$

Next we define a left-right asymmetry along the lines of the up-down asymmetry, but now with the hemispheres separated by the yz plane in the same coordinate system described earlier. *i.e.*, left/right refers to $(p_{l\pm})_x \gtrless 0$. This asymmetry along with the forward-backward combined left-right asymmetry helps to fix the imaginary parts of DFF's, as they are CPT odd. The following equations define these asymmetries:

The left-right asymmetry is

$$A_{lr} = \int_{-1}^{+1} A_{lr}(\theta) d \cos \theta, \quad (2.5)$$

where

$$A_{lr}(\theta) = \frac{1}{2\sigma} \left[\frac{d\sigma(l^+, \text{left})}{d \cos \theta} - \frac{d\sigma(l^+, \text{right})}{d \cos \theta} + \frac{d\sigma(l^-, \text{left})}{d \cos \theta} - \frac{d\sigma(l^-, \text{right})}{d \cos \theta} \right], \quad (2.6)$$

and the combined left-right and forward-backward asymmetry is

$$A_{lr}^{fb} = \int_0^1 A_{lr}(\theta) d \cos \theta - \int_{-1}^0 A_{lr}(\theta) d \cos \theta. \quad (2.7)$$

In case of e^+e^- colliders with longitudinal beam polarization we need to have only one asymmetry in each category (CPT -odd or CPT -even) to disentangle the four parameters. These asymmetries measured at different beam polarizations – either differing in magnitudes or simply differing in sign – will help to disentangle the parameters. As we will see later, using polarized beams also improves

the sensitivity of the measurement of asymmetries. (A similar thing happens in the case of CP -violating asymmetries in $\tau\bar{\tau}$ production [33].) Presently more than 80% electron beam polarization is available at SLAC [2], where they use strained GaAs as photocathode. KEK/Nayoga/NEC collaboration has achieved 71% polarization [3] using a GaAs-AlGaAs superlattice photocathodes. NLC is expected to have similar degree of polarization. However, we use the conservative value of 50% for the polarization expected at NLC.

Next section discusses these asymmetries in detail.

2.2 Calculation of Asymmetries

The cross section for the process $e^+e^- \rightarrow t\bar{t}$ and subsequent decay of the quarks is calculated treating top quark and antitop quark as produced on shell in the narrow width approximation. In that case it is possible to split the production and decay parts at the amplitude level [34, 35]. Spinor techniques developed by Gastman and Wu [36] can be used to compute helicity amplitudes of processes involving massless fermions. This technique was later on extended to include massive fermions by Kleiss and Stirling [37]. We use this technique to calculate the helicity amplitudes. Furthermore we assume on-shell production of W 's in t and \bar{t} decay, again in the narrow width approximation.

To the first order in c_d^γ and c_d^Z the production helicity amplitudes $e^2 M_p(\lambda_e, \lambda_{\bar{e}}, \lambda_t, \lambda_{\bar{t}})$, where $\lambda_e, \lambda_{\bar{e}}, \lambda_t$ and $\lambda_{\bar{t}}$ are twice the electron, positron, top quark and antitop quark helicities respectively, are given by

$$M_p(-+ -+) = \left[(c_v^\gamma + r_L c_v^Z - \beta r_L c_a^Z) \right] (1 + \cos \theta), \quad (2.8)$$

$$\begin{aligned}
M_p(-+ + -) &= - \left[(c_v^\gamma + r_L c_v^Z + \beta r_L c_a^Z) \right] (1 - \cos \theta), \\
M_p(-+ - -) &= i \left[2t (c_v^\gamma + r_L c_v^Z) - \frac{i}{2} \frac{\beta}{t} (c_d^\gamma + r_L c_d^Z) \right] \sin \theta, \\
M_p(-+ + +) &= i \left[2t (c_v^\gamma + r_L c_v^Z) + \frac{i}{2} \frac{\beta}{t} (c_d^\gamma + r_L c_d^Z) \right] \sin \theta.
\end{aligned}$$

Here c_v^γ , c_v^Z , c_a^Z are the vector and axial vector couplings of the top quark to photon and Z-boson whose values are

$$\begin{aligned}
c_v^\gamma &= \frac{2}{3}, \quad c_a^\gamma = 0, \\
c_v^Z &= \frac{\left(\frac{1}{4} - \frac{2}{3} x_w\right)}{\sqrt{x_w(1-x_w)}}, \\
c_a^Z &= -\frac{1}{4\sqrt{x_w(1-x_w)}},
\end{aligned} \tag{2.9}$$

with $x_w = \sin^2 \theta_w$, θ_w being the weak mixing angle. $t = \frac{m_t}{\sqrt{s}}$, where m_t is the top quark mass and \sqrt{s} is the c.m. energy. $\beta = \sqrt{1-4t^2}$ is the top quark velocity. c_d^j ($j = \gamma, Z$) are the electric and the weak dipole form factors and θ is the scattering angle. r_L , the product of the Z propagator and the electron coupling with the Z boson is given by

$$r_L = \frac{\left(\frac{1}{2} - x_w\right)}{\left(1 - \frac{m_Z^2}{s}\right) \sqrt{x_w(1-x_w)}}. \tag{2.10}$$

The above amplitudes are of the helicity combination $e_L \bar{e}_R$. For the other combination, $e_R \bar{e}_L$ we have helicity amplitudes

$$M_p(+ - - +) = - \left[(c_v^\gamma + r_L c_v^Z - \beta r_L c_a^Z) \right] (1 - \cos \theta), \tag{2.11}$$

$$\begin{aligned}
M_p(+ - + -) &= \left[(c_v^\gamma + r_L c_v^Z + \beta r_L c_a^Z) \right] (1 + \cos \theta), \\
M_p(+ - - -) &= i \left[2t (c_v^\gamma + r_L c_v^Z) - \frac{i\beta}{2t} (c_d^\gamma + r_L c_d^Z) \right] \sin \theta, \\
M_p(+ - + +) &= i \left[2t (c_v^\gamma + r_L c_v^Z) + \frac{\beta}{t} (c_d^\gamma + r_L c_d^Z) \right] \sin \theta,
\end{aligned}$$

where

$$r_R = \frac{-x_w}{\left(1 - \frac{m_Z^2}{s}\right) \sqrt{x_w (1 - x_w)}}. \quad (2.12)$$

These amplitudes agree with those given in [30] upto a phase. The main decay channel of heavy top quark is $t \rightarrow bW^+$ with on shell W^+ . We consider the case where these W 's further decay into leptons. The decay density matrix elements are given by

$$\begin{aligned}
\Gamma_d(++) &= \left[\frac{m_t^2}{2} - m_t E_{l+} \right] 8m_t E_{l+} (1 + \cos \theta_l), \\
\Gamma_d(--) &= \left[\frac{m_t^2}{2} - m_t E_{l+} \right] 8m_t E_{l+} (1 - \cos \theta_l), \\
\Gamma_d(+-) &= \left[\frac{m_t^2}{2} - m_t E_{l+} \right] (-8i) m_t E_{l+} \sin \theta_l e^{i\phi_l}.
\end{aligned} \quad (2.13)$$

Here \pm in the l.h.s. denote the helicity of the top quark and θ_l and ϕ_l are the polar and the azimuthal angles of the top quark. A common constant of $\left(\frac{2\pi\alpha}{x_w}\right)^2 \frac{\pi \delta(p_W^2 - m_W^2)}{\Gamma_W M_W}$ has been factored out.

Corresponding density matrix elements for \bar{t} decay are given by

$$\bar{\Gamma}_d(++) = \left[\frac{m_t^2}{2} - m_t E_{l-} \right] 8m_t E_{l-} (1 - \cos \theta_l), \quad (2.14)$$

$$\begin{aligned}\bar{\Gamma}_d(--) &= \left[\frac{m_t^2}{2} - m_t E_{l-} \right] 8m_t E_{l-} (1 + \cos \theta_l), \\ \bar{\Gamma}_d(+-) &= \left[\frac{m_t^2}{2} - m_t E_{l-} \right] (-8i)m_t E_{l-} \sin \theta_l e^{-i\phi_l}.\end{aligned}$$

With these the differential cross section for $t\bar{t}$ production followed by t decay will be

$$\begin{aligned}d\sigma^+ &= \frac{(4\pi\alpha)^4}{4x_W^2} \frac{\pi^2}{\Gamma_t m_t \Gamma_W m_W} \delta(p_{W^+}^2 - m_W^2) \delta(p_t^2 - m_t^2) \\ &\times \{ \rho(++) \Gamma_d(++) + \rho(--) \Gamma_d(--) \\ &+ 2\text{Re} [\rho(+-) \Gamma_d(+-)] \} dLips,\end{aligned}\tag{2.15}$$

where $\rho(\lambda_t, \lambda'_t)$ are production density matrices with top quark spin state shown explicitly;

$$\rho(\lambda_t, \lambda'_t) = \frac{1}{4} \sum_{\lambda_e, \lambda_{\bar{e}}, \lambda_{\bar{t}}} \left[M_p(\lambda_e, \lambda_{\bar{e}}, \lambda_t, \lambda_{\bar{t}}) M_p^*(\lambda_e, \lambda_{\bar{e}}, \lambda'_t, \lambda_{\bar{t}}) \right] (1 + \lambda_e P_e) (1 + \lambda_{\bar{e}} P_{\bar{e}})$$

and $dLips$ is the Lorentz invariant phase space element. The differential cross section for $t\bar{t}$ production followed by \bar{t} decaying into $\bar{b}l^-\bar{\nu}$ through W^- is given by

$$\begin{aligned}d\sigma^- &= \frac{(4\pi\alpha)^4}{4x_W^2} \frac{\pi^2}{\Gamma_t m_t \Gamma_W m_W} \delta(p_{W^-}^2 - m_W^2) \delta(p_{\bar{t}}^2 - m_t^2) \\ &\times \{ \bar{\rho}(++) \bar{\Gamma}_d(++) + \bar{\rho}(--) \bar{\Gamma}_d(--) \\ &+ 2\text{Re} [\bar{\rho}(+-) \bar{\Gamma}_d(+-)] \} \overline{dLips},\end{aligned}\tag{2.16}$$

with

$$\bar{\rho}(\lambda_{\bar{t}}, \lambda'_{\bar{t}}) = \frac{1}{4} \sum_{\lambda_e, \lambda_{\bar{e}}, \lambda_t} \left[\bar{M}_p(\lambda_e, \lambda_{\bar{e}}, \lambda_t, \lambda'_{\bar{t}}) \bar{M}_p^*(\lambda_e, \lambda_{\bar{e}}, \lambda_t, \lambda_{\bar{t}}) \right] (1 + \lambda_e P_e) (1 + \lambda_{\bar{e}} P_{\bar{e}}).$$

Substituting expressions for the helicity amplitudes given in Equations 2.8–2.14, we get expression for the cross section as

$$\begin{aligned}
\frac{d\sigma^\pm}{d\cos\theta_t dE_l d\cos\theta_l d\phi_l} = & \frac{3\alpha^4\beta}{16x_w^2\sqrt{s}} \frac{E_l}{\Gamma_t\Gamma_W m_W} \left(\frac{1}{1-\beta\cos\theta_{tl}} - \frac{4E_l}{\sqrt{s}(1-\beta^2)} \right) \\
& \times \left\{ \left(A_0 + A_1 \cos\theta_t + A_2 \cos^2\theta_t \right) (1-\beta\cos\theta_{tl}) \right. \\
& + \left(B_0^\pm + B_1 \cos\theta_t + B_2^\pm \cos^2\theta_t \right) (\cos\theta_{tl} - \beta) \\
& + \left(C_0^\pm + C_1^\pm \cos\theta_t \right) (1-\beta^2) \sin\theta_t \sin\theta_l (\cos\theta_t \cos\phi_l - \sin\theta_t \cot\theta_l) \\
& \left. + \left(D_0^\pm + D_1^\pm \cos\theta_t \right) (1-\beta^2) \sin\theta_t \sin\theta_l \sin\phi_l \right\}. \tag{2.17}
\end{aligned}$$

Here \pm refers to the l^+ and l^- distributions. Expressions for A , B , C and D are given in Section B.1. Asymmetries defined in the previous section (Equations 2.2-2.7) are given by the following expressions [30, 32]:

$$\begin{aligned}
A_E(x) = & \frac{2\beta}{C} \{ f_L(x, \beta) - f_R(x, \beta) \} \\
& \times \left\{ \text{Im } c_d^\gamma \left[(1 - P_e P_{\bar{e}}) \left(2c_v^\gamma + (r_L + r_R) c_v^Z \right) \right. \right. \\
& + (P_{\bar{e}} - P_e) (r_L - r_R) c_v^Z \left. \right] \\
& + \text{Im } c_d^Z \left[(1 - P_e P_{\bar{e}}) \left((r_L + r_R) c_v^\gamma + (r_L^2 + r_R^2) c_v^Z \right) \right. \\
& \left. \left. + (P_{\bar{e}} - P_e) \left((r_L - r_R) c_v^\gamma + (r_L^2 - r_R^2) c_v^Z \right) \right] \right\}, \tag{2.18}
\end{aligned}$$

where

$$\begin{aligned}
C = & (1 - P_e P_{\bar{e}}) \left\{ (3 - \beta^2) \left[(c_v^\gamma + r_L c_v^Z)^2 + (c_v^\gamma + r_R c_v^Z)^2 \right] \right. \\
& + 2\beta^2 (c_a^Z)^2 (r_L^2 + r_R^2) \left. \right\} \\
& + (P_{\bar{e}} - P_e) \left\{ (3 - \beta^2) \left[(c_v^\gamma + r_L c_v^Z)^2 - (c_v^\gamma + r_R c_v^Z)^2 \right] \right.
\end{aligned}$$

$$+ 2\beta^2(c_a^Z)^2 (r_L^2 - r_R^2)\}, \quad (2.19)$$

and the lepton energy distribution in t decay is given for left and right top helicities by [38]

$$f_{L,R}(x, \beta) = \int_{\frac{x}{1+\beta}}^{\frac{x}{1-\beta}} f(x_0) \frac{\beta x_0 \mp (x - x_0)}{2 x_0^2 \beta^2} dx_0, \quad (2.20)$$

$f(x_0)$ being the distribution in the t rest frame,

$$f(x_0) = \frac{x_0(1 - x_0)}{\frac{1}{6} - \frac{1}{2} \left(\frac{m_W}{m_t}\right)^4 + \frac{1}{3} \left(\frac{m_W}{m_t}\right)^6} \theta(1 - x_0) \theta(x_0 - \frac{m_W^2}{m_t^2}). \quad (2.21)$$

$\beta = (1 - 4m_t^2/s)^{\frac{1}{2}}$ is the top velocity in the c.m. frame.

$$\begin{aligned} A_{ud} = & -\frac{3\pi\beta\sqrt{s}}{16m_t C} \left\{ \text{Re } c_d^\gamma \left[(1 - P_e P_{\bar{e}})(r_L - r_R)c_v^Z \right. \right. \\ & + (P_{\bar{e}} - P_e)(2c_v^\gamma + (r_L + r_R)c_v^Z) \\ & + \text{Re } c_d^Z \left[(1 - P_e P_{\bar{e}}) \left((r_L - r_R)c_v^\gamma + (r_L^2 - r_R^2)c_v^Z \right) \right. \\ & \left. \left. + (P_{\bar{e}} - P_e) \left((r_L + r_R)c_v^\gamma + (r_L^2 + r_R^2)c_v^Z \right) \right] \right\}, \quad (2.22) \end{aligned}$$

$$\begin{aligned} A_{ud}^{fb} = & \frac{\beta^2\sqrt{s}}{4m_t C} c_a^Z \left\{ \text{Re } c_d^\gamma \left[(1 - P_e P_{\bar{e}})(r_L + r_R) \right. \right. \\ & + (P_{\bar{e}} - P_e)(r_L - r_R) \\ & \left. \left. + \text{Re } c_d^Z \left[(1 - P_e P_{\bar{e}})(r_L^2 + r_R^2) + (P_{\bar{e}} - P_e)(r_L^2 - r_R^2) \right] \right] \right\}, \quad (2.23) \end{aligned}$$

$$\begin{aligned} A_{lr} = & -\frac{3\pi\beta^2\sqrt{s}}{16m_t C} c_a^Z \left\{ \text{Im } c_d^\gamma \left[(1 - P_e P_{\bar{e}})(r_L - r_R) \right. \right. \\ & + (P_{\bar{e}} - P_e)(r_L + r_R) \\ & \left. \left. + \text{Im } c_d^Z \left[(1 - P_e P_{\bar{e}})(r_L^2 - r_R^2) + (P_{\bar{e}} - P_e)(r_L^2 + r_R^2) \right] \right] \right\}, \quad (2.24) \end{aligned}$$

$$\begin{aligned}
A_{lr}^{fb} = & \frac{\beta\sqrt{s}}{4m_t C} \left\{ \text{Im } c_d^\gamma \left[(1 - P_e P_{\bar{e}})(2c_v^\gamma + (r_L + r_R)c_v^Z) \right. \right. \\
& + (P_{\bar{e}} - P_e)(r_L - r_R)c_v^Z \left. \right] \\
& + \text{Re } c_d^Z \left[(1 - P_e P_{\bar{e}}) \left((r_L + r_R)c_v^\gamma + (r_L^2 + r_R^2)c_v^Z \right) \right. \\
& + (P_{\bar{e}} - P_e) \left. \left. \left((r_L - r_R)c_v^\gamma + (r_L^2 - r_R^2)c_v^Z \right) \right] \right\}, \tag{2.25}
\end{aligned}$$

As mentioned earlier these asymmetries depend linearly on either the real or the imaginary part of DFF's.

These asymmetries can be measured at a future e^+e^- collider. The next linear collider (NLC) with an integrated luminosity of 10fb^{-1} is assumed in our calculations. A higher luminosity, if available, will improve the limits which can be obtained.

The next section discusses the numerical results we obtained.

2.3 Numerical Results

In our calculations we have assumed the NLC with c.m. energy, $\sqrt{s} = 500 \text{ GeV}$ and an integrated luminosity $\int \mathcal{L} = 10\text{fb}^{-1}$. We look at only semi-leptonic events, *viz.*, either of t or \bar{t} decays leptonically, while the other decays hadronically. Furthermore, we do not consider the top quark decaying into tau leptons as the experimental detection is difficult in that case.

The cross section for a top mass of 174 GeV is plotted as a function of \sqrt{s} in Figure 2.1.

Figure 2.2 shows the asymmetries plotted against the centre of mass energy of the

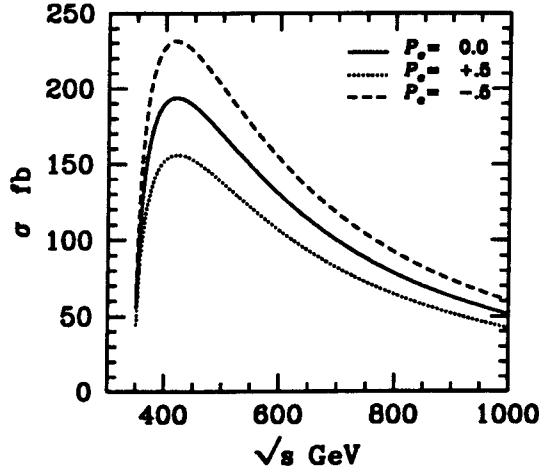


Figure 2.1: Cross section for $t\bar{t}$ production is plotted against c.m. energy. The top mass is taken to be 174 GeV. Curves are plotted for different beam polarizations.

collider for typical values of the real and the imaginary parts of DFF's.

Procedure to obtain limits on the values of DFF's from the experimental measurements of asymmetries and the sensitivities of the experiments is already described in section 1.6. Equations 1.10 and 1.11 in case of the asymmetries described in this chapter become

$$\delta c_d^j = \frac{1.64 c_d^j}{2\sqrt{N}A}$$

and

$$A(c_d^\gamma, c_d^Z) = \frac{2.15}{2\sqrt{N}}, \quad (2.26)$$

where A stands for any one of A_{ud} , A_{ud}^{fb} , A_{lr} or A_{lr}^{fb} . We plot contours obtained using Equation 2.26 showing the allowed region at 90% C.L., if no signal for CP violation is seen experimentally.

Figure 2.3 shows bands in the $|\text{Re } c_d^\gamma| - |\text{Re } c_d^Z|$ plane which correspond to 90 % C.L.

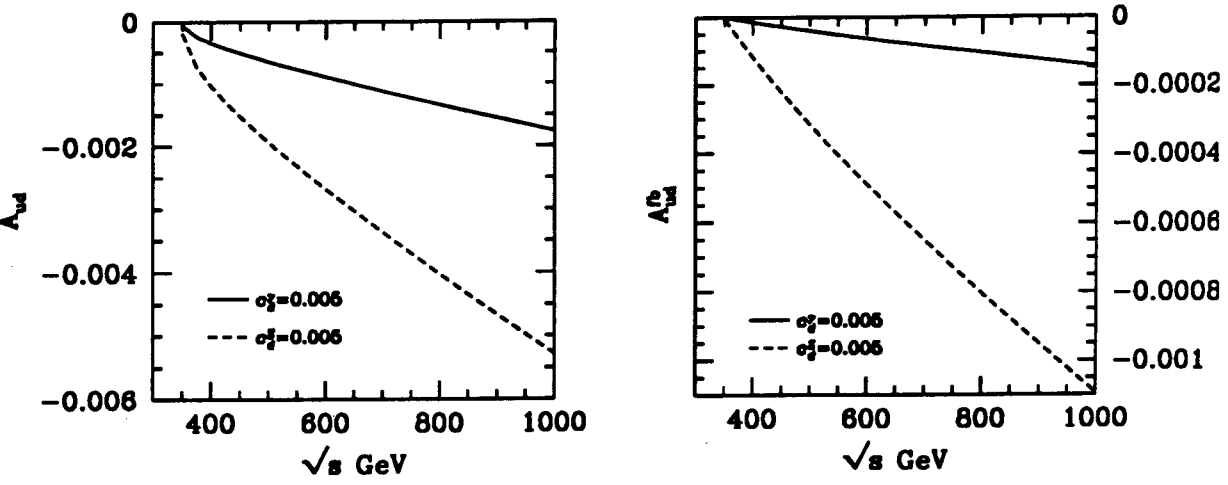


Figure 2.2: A_{ud} (left) and A_{ud}^{fb} (right) are plotted against c.m. energy at a top mass of 174 GeV for the case of unpolarized electron beams. Solid lines correspond to $c_d^\gamma = 0.005$ and dashed lines corresponds to $c_d^Z = 0.005$ with the other dipole form factor taken to be zero in each case.

limits obtained from A_{ud} and A_{ud}^{fb} , with and without longitudinal beam polarization. In case of unpolarized beams, while A_{ud} or A_{ud}^{fb} taken singly can limit one of $|\text{Re } c_d^\gamma|$ or $|\text{Re } c_d^Z|$ when the other is known, both the asymmetries put together can provide independent limits on $|\text{Re } c_d^\gamma|$ and $|\text{Re } c_d^Z|$, of the order of 5 and 1.5 respectively. Figure 2.3 also shows bands from A_{ud} for e^- polarization $P_e = \pm 0.5$ (with $P_e = 0$). The limits obtainable are improved by an order of magnitude. The top quark mass is taken to be 174 GeV in these cases. A similar analysis is done for top quark masses of 180 GeV and 200 GeV the plots of which are shown in Figures 2.4-2.5.

Figures 2.6-2.8 show contours obtained from A_{lr} and A_{lr}^{fb} for different top quark masses. This puts 90% C.L. limits on $|\text{Im } c_d^\gamma|$ and $|\text{Im } c_d^Z|$. Again, for $P_e = 0$, only a simultaneous search for both these asymmetries can put independent limits on $|\text{Im } c_d^\gamma|$ and $|\text{Im } c_d^Z|$, of the order of 0.7 and 6, respectively. Limits on A_{lr} with $P_e = \pm 0.5$, also shown in these figures, can improve these numbers by a factor of about 4 – 7.

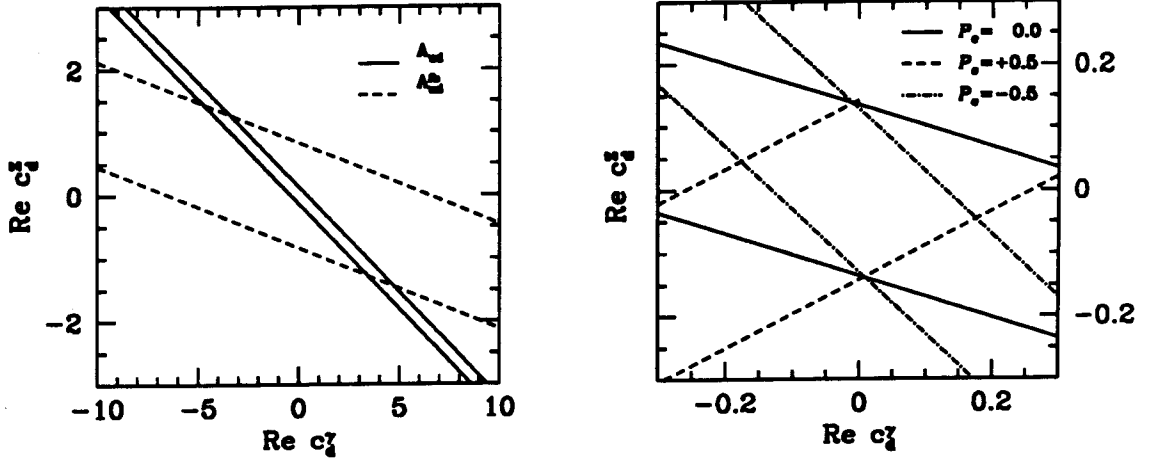


Figure 2.3: Contours showing the allowed region of $\text{Re } c_d^\gamma$ – $\text{Re } c_d^Z$ plane. Top mass is taken to be 174 GeV. Unpolarized beam is considered in case of figure on the left where contours are obtained from the asymmetries A_{ud} and A_{ud}^{fb} , while only A_{ud} is considered with different beam polarizations in the other figure. A c.m. energy of 500 GeV and a luminosity of 10 fb^{-1} are assumed.

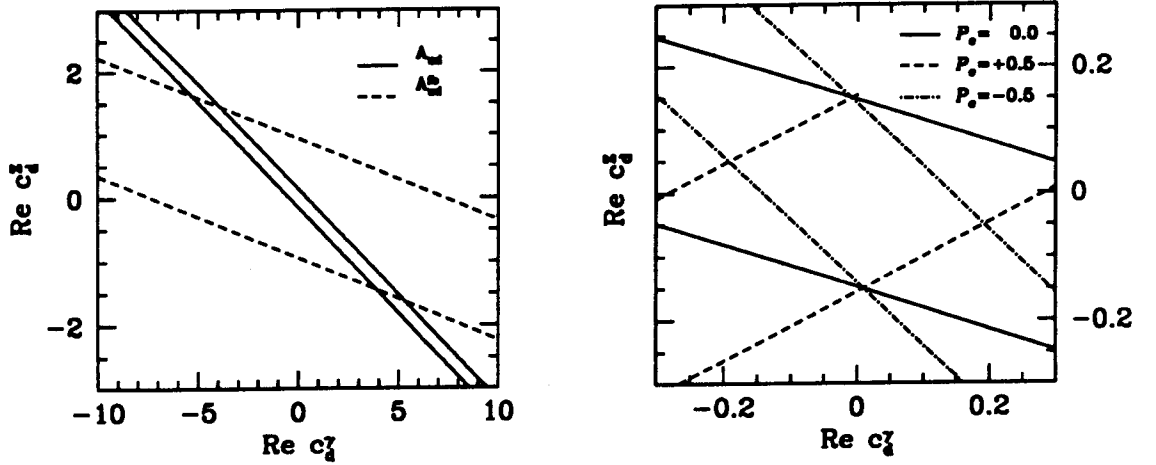


Figure 2.4: Contours similar to those of Figure 2.3 but with top quark mass of 180 GeV.

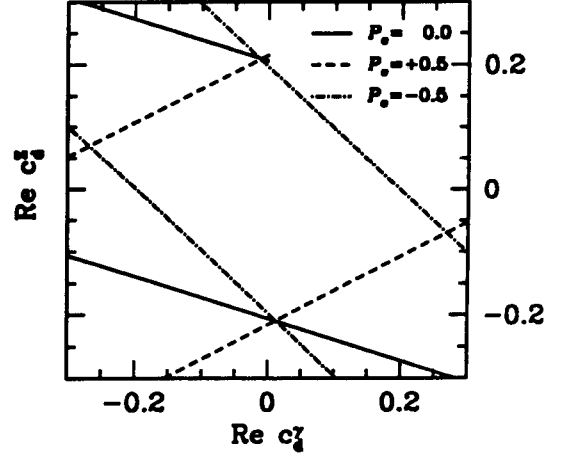
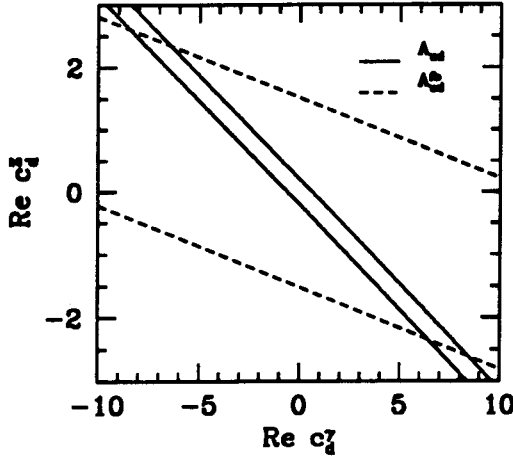


Figure 2.5: Contours similar to those of Figures 2.3 and 2.4 but with top quark mass of 200 GeV.

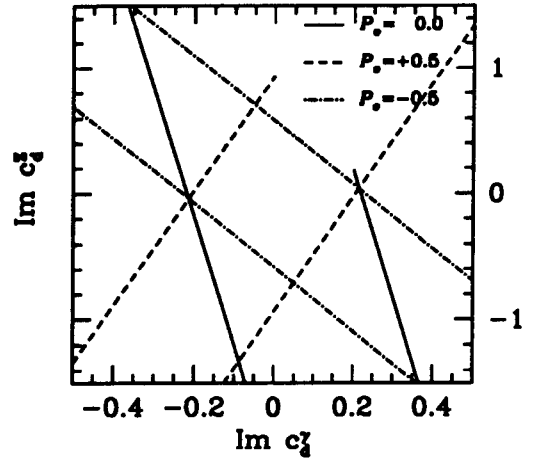
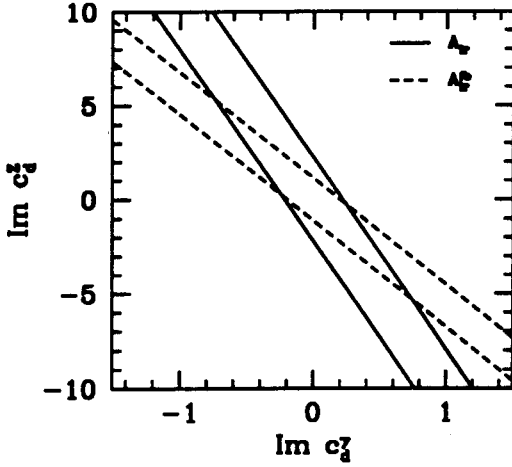


Figure 2.6: Contours showing the allowed region of $|\text{Im}c_d^\gamma| - |\text{Im}c_d^Z|$ plane. Top mass is taken to be 174 GeV. Unpolarized beam is considered in case of figure on the left where contours are obtained from the asymmetries A_{Lr} and A_{Lr}^{fb} , while only A_{Lr} is considered at different beam polarizations in the other figure. A c.m. energy of 500 GeV and a luminosity of 10 fb^{-1} are assumed.

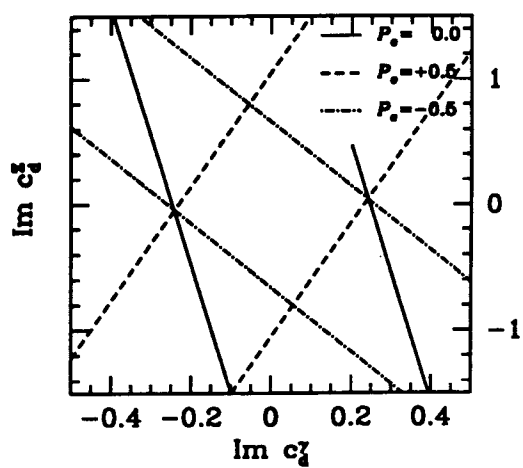
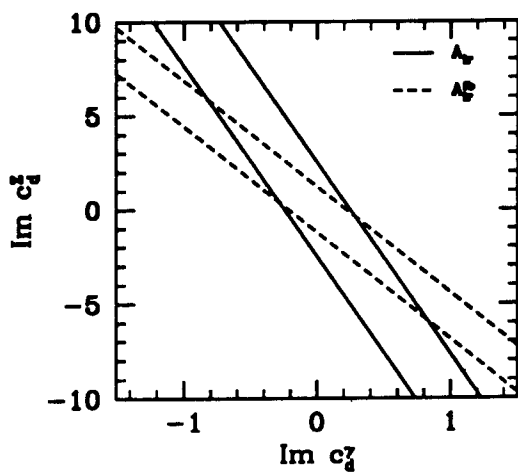


Figure 2.7: Contours similar to Figure 2.6. Top quark mass here is 180 GeV.

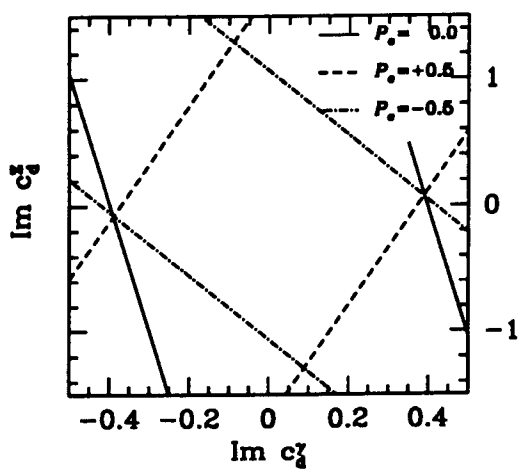
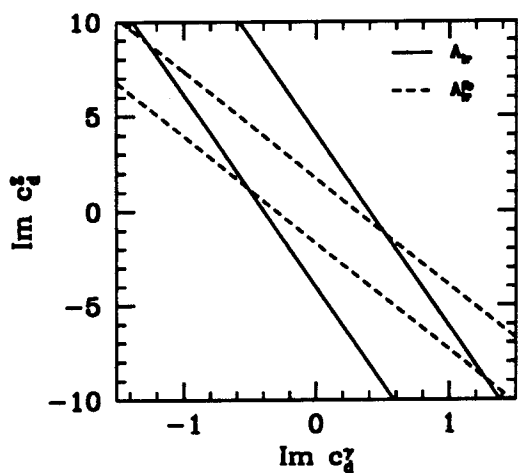


Figure 2.8: Contours similar to Figures 2.6 and 2.7. Top quark mass here is 200 GeV.

		90 % C.L. limits on			
		$ Re\ c_d^\gamma $	$ Re\ c_d^Z $	$ Im\ c_d^\gamma $	$ Im\ c_d^Z $
Unpolarized beam		4.8	1.4	0.7	5.5
Polarized case ($P_e = \pm 0.5$)	(a)	0.2	0.2	0.2	0.8
	(b)	1.1	0.8	0.2	0.7

Table 2.1: Limits on the dipole couplings obtained from different asymmetries. In the unpolarized case the asymmetries A_{ud} and A_{ud}^{fb} are together used to get the limits on the real parts of $c_d^{\gamma,Z}$ and A_{lr} and A_{lr}^{fb} to obtain the limits on the imaginary parts. In the case of polarization, the limits obtained from A_{ud} and A_{lr} are denoted by (a) and the ones from A_{ud}^{fb} and A_{lr}^{fb} are denoted by (b).

The effect of polarization in the case of combined up-down (left-right) and forward-backward asymmetries for non-zero polarization is similar.

Thus, by using polarization, one can obtain independent limits of the order of 0.2-0.25 on three of the four dipole coupling parameters. The remaining parameter, $Im\ c_d^Z$ can be constrained to about 0.8.

The various independent limits that can be obtained with and without beam polarization are collected in Table 2.1.

Having considered independent limits, we now consider limits obtained from the energy asymmetry on either the electric or the weak dipole moment, assuming the other dipole moment to be zero.

For the energy asymmetry, we have estimated limits in the following fashion. The

asymmetries corresponding to x values in a range of 0.1 to 1.5 at definite intervals are obtained. Limit on the DFF is obtained in each bin using the formula

$$\delta(c_d^j)_x = \frac{1.65}{\sqrt{N_x}} \frac{c_d^j}{A_E(x)},$$

where N_x is the number of events in that particular bin and $A_E(x)$ is the asymmetry at x with DFF value, c_d^j , the other c_d^j being kept zero. An average obtained using the formula

$$\delta c_d^j = \frac{1}{N_b} \frac{1}{\sqrt{\sum_x (1/\delta(c_d^j)_x)^2}},$$

where N_b is the number of bins, gives the actual limit on the DFF. We have considered a bin size of .1 with x value in a range of .1 to 1.5. The improvement in sensitivity is about a factor of 3 for $P_e = -0.5$ as compared to $P_e = 0$ for $|\text{Im } c_d^Z|$, whereas measurement of $|\text{Im } c_d^\gamma|$ is insensitive to polarization. We also find that in some cases the sensitivity is greatly enhanced by isolating the polarization-dependent part of the distribution. Thus, if we take a polarization asymmetrized sample, corresponding to $|d\sigma(P_e, P_\epsilon) - d\sigma(-P_e, -P_\epsilon)|$, and evaluate all asymmetries with respect to this new sample, we get a different set of asymmetries with different sensitivities. The sensitivity from this sample for $|\text{Im } c_d^Z|$ is improved by a factor of about 12 as compared to the unpolarized case, giving the best attainable 90% C.L. limit as 0.06. The limits are given in Table 2.2.

The polarization asymmetrized distributions for $P_e = 0.5$ leads to an improvement in the sensitivities from the measurement of A_{ud} and A_{ud}^{fb} , whereas the sensitivity is worse in the case of A_{lr} and A_{lr}^{fb} . For example, A_{ud} can give a limit on $\text{Re } c_d^\gamma$ of 0.04 as compared to 0.10 obtained without the asymmetrization procedure.

		$m_t = 174 \text{ GeV}$		$m_t = 180 \text{ GeV}$	
		$ \text{Im } c_d^\gamma $	$ \text{Im } c_d^Z $	$ \text{Im } c_d^\gamma $	$ \text{Im } c_d^Z $
$P_e =$	0.0	0.097	0.0002	0.075	0.042
	+ .5	0.099	0.07	0.077	0.051
	- .5	0.093	0.21	0.072	0.16
Pol. asymmetrized		0.34	0.11	0.36	0.12

Table 2.2: Limits on the dipole couplings obtained from energy asymmetry at 90% C. L. at a c. m. energy of 500 GeV .

One can also consider combinations of the different procedures mentioned above to maximize the sensitivity available.

We end the chapter with the following conclusions. We have calculated several CP-violating asymmetries which can arise in the process $e^+ e^- \rightarrow t \bar{t}$, with subsequent t, \bar{t} decay, in the presence of electric and weak dipole couplings of the top quark. In order to disentangle the CP-violating dipole couplings from each other, at least two T-odd asymmetries are needed for the real parts and two T-even asymmetries are needed for the imaginary parts, and we calculated possible asymmetries which could be used for the purpose. It was shown that longitudinal polarization of the electron can help in separating the various parameters, and in addition, leads to higher sensitivity. At the NLC with $\sqrt{s} = 500 \text{ GeV}$ and polarized electron beams with $\pm 50\%$ polarization, 90% C.L. sensitivities of the order of 0.25 are obtainable on independent determinations $|\text{Re } c_d^\gamma|$, $|\text{Re } c_d^Z|$, and $|\text{Im } c_d^\gamma|$, respectively, and a sensitivity of about 0.8 for $|\text{Im } c_d^Z|$.

Of these, the measurements of the real parts of $c_d^{\gamma,Z}$ are free from CP-invariant back-

ground contributions. As for the T-even asymmetries depending on the imaginary parts of $c_d^{\gamma,Z}$, the backgrounds from order- α collinear initial-state photon emission have to be calculated and subtracted. This will be treated in Chapter 4.

Chapter 3

The Leptonic Charge Asymmetries in $e^+e^- \rightarrow t\bar{t}$

In Chapter 2 we have discussed some of the CP -odd asymmetries that could be constructed out of the final state momenta of the process $e^+e^- \rightarrow t\bar{t}$ with the subsequent decay of the quark pairs into a semileptonic channel, whose non-zero values will signal CP violation. These asymmetries and other similar asymmetries in the literature [22, 27, 30, 32] need reconstruction of the top quark momentum (with the exception of lepton energy asymmetry [23, 29, 30, 32, 35]). Experimentally it is desirable to have asymmetries which do not depend on the top quark momentum. The charge asymmetry defined as the net charge of leptons produced, in the presence of a cut in the polar angle, is a simple asymmetry in this category [39, 40]. In the absence of a cut on the angle this asymmetry becomes just the difference in the number of t and \bar{t} produced and is zero because of charge conservation. The leptonic forward-backward asymmetry combined with charge asymmetry, again with a cut-off, is another CP -odd asymmetry which does not depend on the top quark momentum direction.

The next section discusses these asymmetries in detail in the presence of longitudinal electron beam polarization and Section 3.2 contains the results obtained.

3.1 Expressions for the Asymmetries

We first describe the asymmetries defined above in terms of the electric and weak dipole couplings of the top quarks. These CP -violating electric and weak dipole couplings of the top quark give rise to polarization asymmetries in $e^+e^- \rightarrow t\bar{t}$ and these in turn give rise to angular asymmetries in the subsequent decay $t \rightarrow b\nu_l l^+$ ($\bar{t} \rightarrow \bar{b}\bar{\nu}_l l^-$). As in the case of A_{ud} , A_{lr} , etc. discussed in Chapter 2, here also we adopt the narrow-width approximation for t and \bar{t} , as well as for W^\pm produced in t, \bar{t} decay (see Section 2.2).

We assume the top quark couplings to γ and Z to be given by the vertex factor $ie\Gamma_\mu^j$, where

$$\Gamma_\mu^j = c_v^j \gamma_\mu + c_a^j \gamma_\mu \gamma_5 + \frac{c_d^j}{2m_t} i\gamma_5 (p_t - p_{\bar{t}})_\mu, \quad j = \gamma, Z, \quad (3.1)$$

coming from the effective Lagrangian given by Equation 1.7 with the vector and axial vector coupling given by Equation 2.9.

The helicity amplitudes for the process $e^+e^- \rightarrow t\bar{t}$ in the c.m. frame, including the dipole couplings, are given in Equations 2.8 and 2.11 and the density matrix elements for the $t\bar{t}$ decay are given by Equations 2.13 and 2.14.

Combining the production and the decay amplitudes in the narrow-width approximation for t, \bar{t} and W^\pm , and using appropriate Lorentz boosts to calculate ev-

everything in the e^+e^- c.m. frame, we obtained the l^+ and l^- distributions for the case of e^- , e^+ with polarization P_e , $P_{\bar{e}}$, expressions for which are given by Equation 2.17. We further carry out the necessary integrations to obtain the polar angle distributions for the leptons [40],

$$\begin{aligned}
\frac{d\sigma^\pm}{d\cos\theta_l} = & \frac{3\pi\alpha^2}{32s} B_t B_{\bar{t}} \left\{ 4A_0 - 2A_1 \left(\frac{1-\beta^2}{\beta^2} \log \frac{1+\beta}{1-\beta} - \frac{2}{\beta} \right) \cos\theta_l \right. \\
& + 2A_2 \left(\frac{1-\beta^2}{\beta^3} \log \frac{1+\beta}{1-\beta} (1-3\cos^2\theta_l) \right. \\
& \left. \left. - \frac{2}{\beta^2} (1-3\cos^2\theta_l - \beta^2 + 2\beta^2 \cos^2\theta_l) \right) \right. \\
& + 2B_1 \frac{1-\beta^2}{\beta^2} \left(\frac{1}{\beta} \log \frac{1-\beta}{1+\beta} - 2 \right) \cos\theta_l \\
& + B_2^\pm \frac{1}{\beta^3} \left(\frac{\beta^2-2}{\beta} \log \frac{1+\beta}{1-\beta} + 6 \right) (1-3\cos^2\theta_l) \\
& + 2C_0^\pm \frac{1-\beta^2}{\beta^2} \left(\frac{1}{\beta} \log \frac{1+\beta}{1-\beta} - 2 \right) \cos\theta_l \\
& \left. \left. - C_1^\pm \frac{1}{\beta^3} \left(\frac{3(1-\beta^2)}{\beta} \log \frac{1+\beta}{1-\beta} - 2(3-2\beta^2) \right) (1-3\cos^2\theta_l) \right\}. \quad (3.2)
\end{aligned}$$

A , B and C are given in Appendix B (B.1). Here β is the velocity of the top quark and θ_l is the polar angle of either l^+ or l^- , with z axis chosen along the e^- momentum direction. The above expression for angular distribution agrees with that given by Arens and Sehgal in the limit of exact CP symmetry [35].

We use this to write down expressions for the CP -violating asymmetries, the lepton-charge asymmetry, A_{ch} and the charge asymmetry combined with the leptonic forward-backward asymmetry, A_{fb} . This forward-backward asymmetry is different from the one described in Chapter 2. In that case we had forward and backward directions relative to the top direction whereas here it is the forward and

backward directions with respect to the electron beam which are considered.

These asymmetries depend on different linear combinations of $\text{Im } c_d^\gamma$ and $\text{Im } c_d^Z$. It is not possible to define CP -odd quantities which determine $\text{Re } c_d^{\gamma, Z}$ using single-lepton distributions, as can be seen from the expression for the CP -odd combination

$$\frac{d\sigma^+}{d\cos\theta_l}(\theta_l) - \frac{d\sigma^-}{d\cos\theta_l}(\pi - \theta_l).$$

The two asymmetries are written in terms of differential cross section as follows.

$$A_{ch}(\theta_0) = \frac{\int_{\theta_0}^{\pi-\theta_0} d\theta_l \left(\frac{d\sigma^+}{d\theta_l} - \frac{d\sigma^-}{d\theta_l} \right)}{\int_{\theta_0}^{\pi-\theta_0} d\theta_l \left(\frac{d\sigma^+}{d\theta_l} + \frac{d\sigma^-}{d\theta_l} \right)} \quad (3.3)$$

and

$$A_{fb}(\theta_0) = \frac{\int_{\theta_0}^{\frac{\pi}{2}} d\theta_l \left(\frac{d\sigma^+}{d\theta_l} - \frac{d\sigma^-}{d\theta_l} \right) - \int_{\frac{\pi}{2}}^{\pi-\theta_0} d\theta_l \left(\frac{d\sigma^+}{d\theta_l} - \frac{d\sigma^-}{d\theta_l} \right)}{\int_{\theta_0}^{\pi-\theta_0} d\theta_l \left(\frac{d\sigma^+}{d\theta_l} + \frac{d\sigma^-}{d\theta_l} \right)} \quad (3.4)$$

In the above equations, σ^+ and σ^- refer respectively to the l^+ and l^- distributions in the c.m. frame and θ_0 is the cut-off.

These asymmetries are a measure of CP violation in the unpolarized case and in the case when electron and positron beam polarizations are equal and opposite ($P_e = -P_{\bar{e}}$). When $P_e \neq -P_{\bar{e}}$, the initial state is not invariant under CP , and therefore CP -invariant interactions can contribute to the asymmetries. However, to the leading order in α , these CP -invariant contributions vanish in the limit $m_e =$

0. Order- α collinear helicity-flip photon emission can give a CP -even contribution. An explicit calculation of this background contribution, described in Chapter 4, shows that it is negligible for luminosities under consideration.

The expressions for $A_{ch}(\theta_0)$ and $A_{fb}(\theta_0)$ are given below.

$$\begin{aligned}
A_{ch}(\theta_0) &= \frac{1}{2\sigma(\theta_0)} \frac{3\pi\alpha^2}{4s} B_t B_{\bar{t}} 2 \cos \theta_0 \sin^2 \theta_0 \left((1 - \beta^2) \log \frac{1 + \beta}{1 - \beta} - 2\beta \right) \\
&\times \left(\text{Im} c_d^\gamma \left\{ \left[2c_v^\gamma + (r_L + r_R) c_v^Z \right] (1 - P_e P_{\bar{e}}) + (r_L - r_R) c_v^Z (P_{\bar{e}} - P_e) \right\} \right. \\
&+ \text{Im} c_d^Z \left\{ \left[(r_L + r_R) c_v^\gamma + (r_L^2 + r_R^2) c_v^Z \right] (1 - P_e P_{\bar{e}}) + [(r_L - r_R) c_v^\gamma \right. \\
&\left. \left. + (r_L^2 - r_R^2) c_v^Z \right] (P_{\bar{e}} - P_e) \right\} \right), \\
A_{fb}(\theta_0) &= \frac{1}{2\sigma(\theta_0)} \frac{3\pi\alpha^2}{2s} B_t B_{\bar{t}} \cos^2 \theta_0 \left((1 - \beta^2) \log \frac{1 + \beta}{1 - \beta} - 2\beta \right) c_a^Z \\
&\times \left\{ \text{Im} c_d^\gamma [(r_L - r_R)(1 - P_e P_{\bar{e}}) + (r_L + r_R)(P_{\bar{e}} - P_e)] \right. \\
&\left. + \text{Im} c_d^Z [(r_L^2 - r_R^2)(1 - P_e P_{\bar{e}}) + (r_L^2 + r_R^2)(P_{\bar{e}} - P_e)] \right\}. \quad (3.5)
\end{aligned}$$

Here $\sigma(\theta_0)$ is the cross section for l^+ or l^- production with a cut-off θ_0 , and is given by

$$\begin{aligned}
\sigma(\theta_0) &= \frac{3\pi\alpha^2}{8s} B_t B_{\bar{t}} 2 \cos \theta_0 \left\{ \left((1 - \beta^2) \log \frac{1 + \beta}{1 - \beta} \sin^2 \theta_0 \right. \right. \\
&\left. \left. + 2\beta \left[1 + \left(1 - \frac{2}{3} \beta^2 \right) \cos^2 \theta_0 \right] \right\} \right. \\
&\times \left\{ \left[2c_v^{\gamma^2} + 2c_v^\gamma c_v^Z (r_L + r_R) + c_v^{Z^2} (r_L^2 + r_R^2) \right] (1 - P_e P_{\bar{e}}) \right. \\
&\left. + c_v^Z [(r_L - r_R) c_v^\gamma + (r_L^2 - r_R^2) c_v^Z] (P_{\bar{e}} - P_e) \right\} \\
&+ \left\{ (1 - \beta^2) \log \frac{1 + \beta}{1 - \beta} \sin^2 \theta_0 + 2\beta \left[2\beta^2 - 1 + \left(1 - \frac{2}{3} \beta^2 \right) \cos^2 \theta_0 \right] \right\} \\
&\times c_a^{Z^2} \left\{ (r_L^2 + r_R^2)(1 - P_e P_{\bar{e}}) + (r_L^2 - r_R^2)(P_{\bar{e}} - P_e) \right\} - 2(1 - \beta^2)
\end{aligned}$$

$$\begin{aligned}
& \times \left(\log \frac{1+\beta}{1-\beta} - 2 \right) \sin^2 \theta_0 c_a^Z \left\{ \left[(r_L + r_R) c_v^\gamma + (r_L^2 + r_R^2) c_v^Z \right] \right. \\
& \times \left. \left(1 - P_e P_{\bar{e}} \right) + \left[(r_L - r_R) c_v^\gamma + (r_L^2 - r_R^2) c_v^Z \right] (P_{\bar{e}} - P_e) \right\}. \quad (3.6)
\end{aligned}$$

In these equations, β is the t (or \bar{t}) velocity: $\beta = \sqrt{1 - 4m_t^2/s}$, $\gamma = 1/\sqrt{1 - \beta^2}$, and B_t and $B_{\bar{t}}$ are respectively the branching ratios of t and \bar{t} into the final states being considered. $-er_{L,R}/s$ is the product of the Z -propagator and left-handed (right-handed) electron couplings to Z (Equation 2.10 and 2.12).

Note that $A_{ch}(\theta_0)$ vanishes for $\theta_0 = 0$ as it is just the difference in t and \bar{t} production rates. $A_{fb}(\theta_0)$, however, is nonzero even at $\theta_0 = 0$.

The next section discusses the numerical results.

3.2 Discussion of Numerical Results

In this section we shall describe the numerical results for the calculation of 90% confidence level (C.L.) limits that could be put on $\text{Im}c_d^{\gamma,Z}$ using the asymmetries described in the previous section, as well as the full CP -odd angular distribution in Equation 3.3.

We consider only semileptonic final states. That is to say, when t decays leptonically, we assume \bar{t} decays hadronically, and *vice versa*. We sum over the electron and muon decay channels leaving the tau channel which is difficult to detect experimentally. Thus, $B_t B_{\bar{t}}$ is taken to be $2/3 \times 2/9$.

Figure 3.1 shows variation of cross section with c.m. energy for a top mass of 174 GeV .

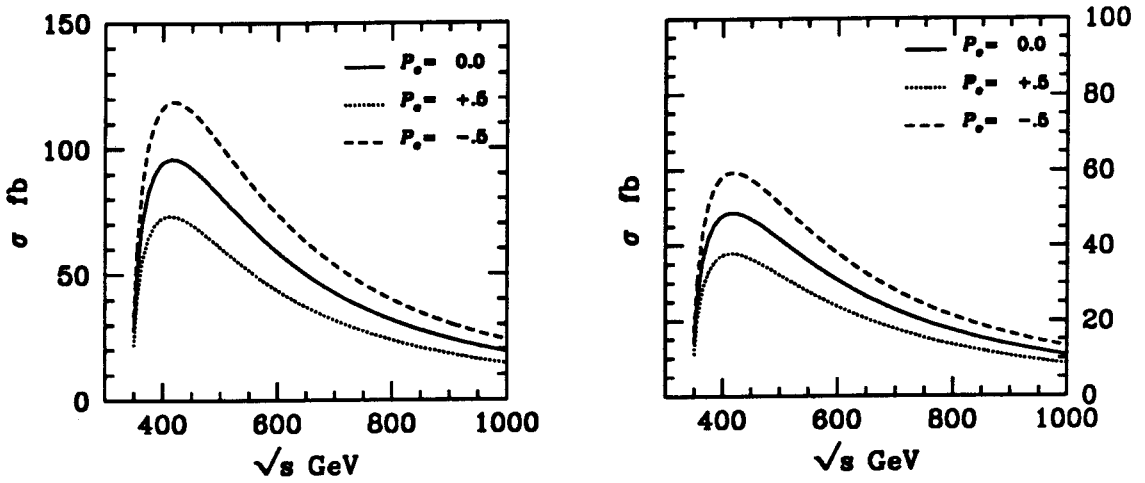


Figure 3.1: $e^+e^- \rightarrow t\bar{t}$ cross section is plotted against the c.m. energy for different beam polarizations. Top quark mass is taken to be 174 GeV. Figure on the left is with a cut-off of 10° in the leptonic polar angle whereas the other figure is for a 60° cut-off.

The number of events for various θ_0 and for beam polarizations $P_e = 0, \pm 0.5$ are listed in Table 3.1.

Dependence of the asymmetries on the c.m. energy is shown by the plots in Figure 3.2.

We have two asymmetries, viz., the A_{ch} and A_{fb} at different beam polarizations. In each case we have derived simultaneous 90% C.L. limits on $|\text{Im}c_d^\gamma|$ and $|\text{Im}c_d^Z|$ that could be put in an experiment at a future linear collider with $\sqrt{s} = 500$ GeV and an integrated luminosity of 10 fb^{-1} . The procedure to get the allowed region in the $|\text{Im}c_d^\gamma| - |\text{Im}c_d^Z|$ plane is described in Chapter 2. In the unpolarized case, each of A_{ch} and A_{fb} gives a band of allowed values in the $|\text{Im}c_d^\gamma| - |\text{Im}c_d^Z|$ plane. If both A_{ch} and A_{fb} are looked for in an experiment, the intersection region of the corresponding bands determines the best 90% CL limits which can be put simultaneously on $|\text{Im}c_d^\gamma|$ and $|\text{Im}c_d^Z|$. The best results are obtained for $\theta_0 = 35^\circ$ and are shown in Figure 3.4 for two values of the top quark mass, $m_t = 174$ GeV, and $m_t = 200$ GeV.

	$m_t = 174 \text{ GeV}$			$m_t = 200 \text{ GeV}$		
θ_0	$P_e = -0.5$	$P_e = 0$	$P_e = +0.5$	$P_e = -0.5$	$P_e = 0$	$P_e = +0.5$
0°	1003	845	687	862	723	585
10°	988	832	675	849	712	576
35°	826	689	553	711	593	475
60°	507	419	330	438	362	286

Table 3.1: Number of events at different cut-off angles for different beam polarization. Two top quark masses are considered and an integrated luminosity of 10 fb^{-1} is assumed.

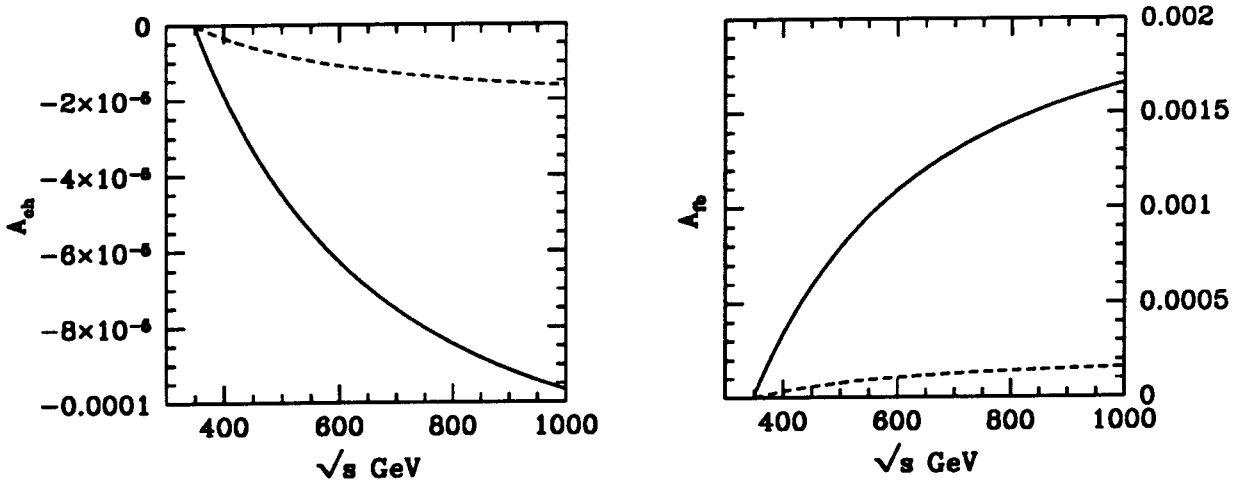


Figure 3.2: Charge asymmetry, A_{ch} (left) and the charge asymmetry combined with forward-backward asymmetry, A_{fb} (right) are plotted against the c.m. energy for a top quark mass of 174 GeV . Solid and dashed lines correspond to the cases with $\text{Im} c_d^\gamma = 0.005$ and $\text{Im} c_d^Z = 0.005$ respectively while the other DFF is kept to be zero. Beam polarization is taken to be zero.

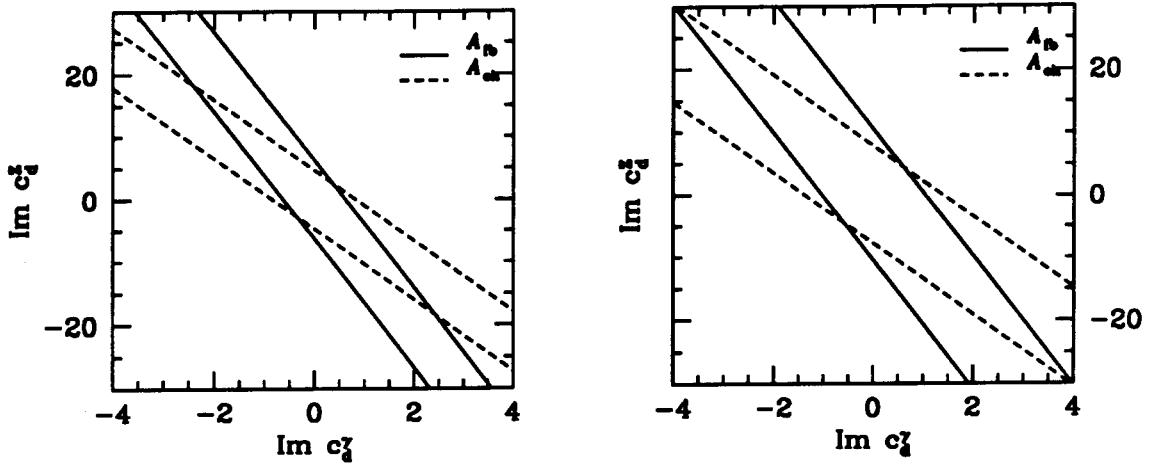


Figure 3.3: Allowed region in the $|Imc_d^\gamma| - |Imc_d^Z|$ plane for top quark masses 174 GeV (left) and 200 GeV (right) obtained from A_{ch} and A_{fb} using unpolarized beams. An integrated luminosity of 10 fb^{-1} and a c.m. of energy of 500 GeV are assumed. The cut-off angle is 35° . Solid line corresponds to unpolarized case and dash and dash-dot lines correspond to $P_e = \pm 0.5$.

We see from Figure 3.3 that the 90% C.L. limits that could be put on $|Imc_d^\gamma|$ and $|Imc_d^Z|$ simultaneously are, respectively, 2.4 and 17, for $m_t = 174 \text{ GeV}$. The same limits are 4.0 and 28 for $m_t = 200 \text{ GeV}$.

In the case of e^- beam with longitudinal polarization, $P_e = \pm 0.5$, we have obtained 90% C.L. limits which can be achieved. In this case, the use of $P_e = +0.5$ and $P_e = -0.5$ is sufficient to constrain Imc_d^γ and Imc_d^Z simultaneously even though only one asymmetry (either A_{ch} or A_{fb}) is determined. The 90% C.L. bands corresponding to $P_e = \pm 0.5$ are shown in Figures 3.4 and 3.5 for A_{ch} with $\theta_0 = 60^\circ$, and for A_{fb} with $\theta_0 = 10^\circ$, respectively. Again, these values of θ_0 are chosen to maximize the sensitivity.

It can be seen from these figures that the simultaneous limits expected to be obtained on Imc_d^γ and Imc_d^Z are, respectively, about 0.45 and 1.5 for $m_t = 174 \text{ GeV}$ from both the types of asymmetries. These limits are about 0.78 and 2.5 for $m_t = 200 \text{ GeV}$. We see thus that the use of polarization leads to an improvement by a

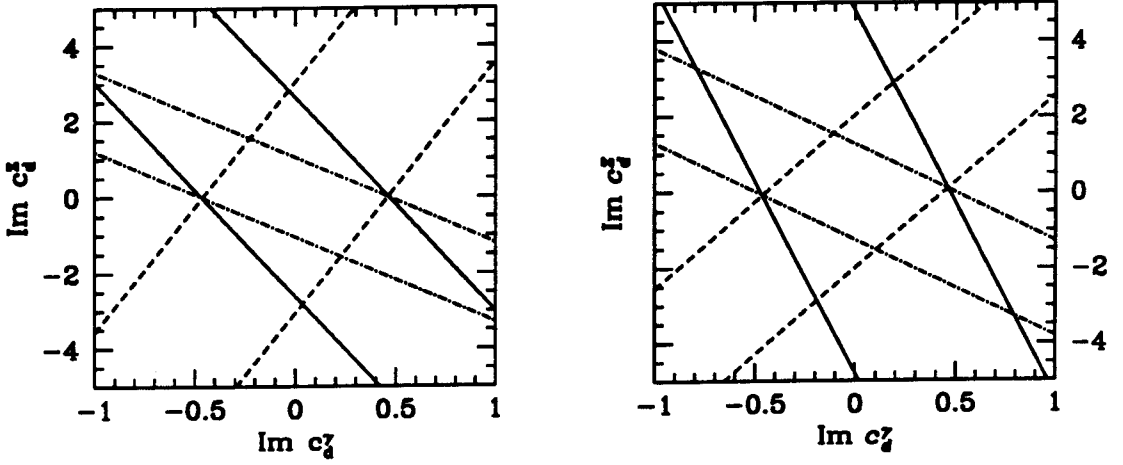


Figure 3.4: Allowed region in $|\text{Im } c_d^\gamma| - |\text{Im } c_d^Z|$ plane obtained from A_{ch} (left) at a cut-off of 60° and A_{ch}^{fb} (right) at a cut-off of 10° using polarized beams. Top quark mass of 174 GeV is considered, and an integrated luminosity of 10 fb^{-1} and a c.m. energy of 500 GeV are assumed.

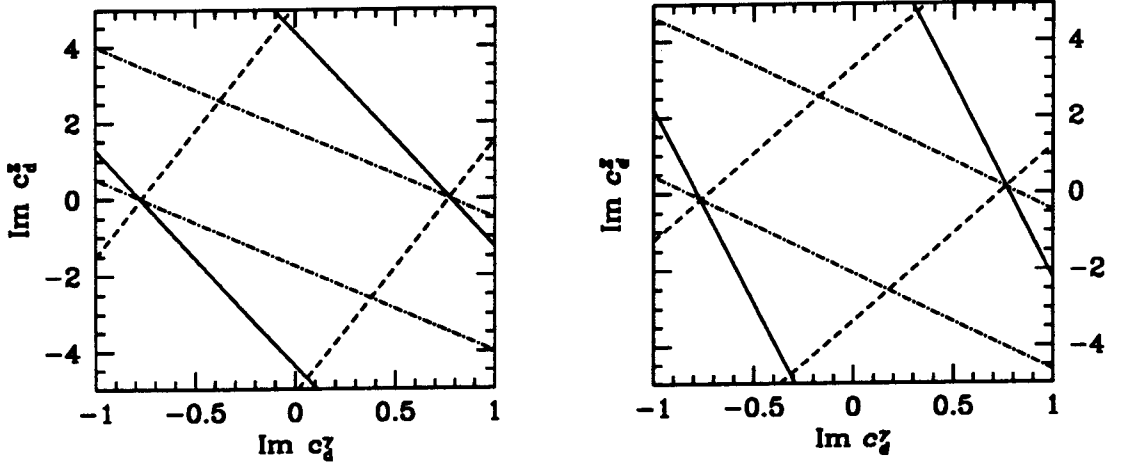


Figure 3.5: Similar to Figure 3.4. Top quark mass is taken to be 200 GeV.

factor of about 5 in the sensitivity to the measurement of $\text{Im}c_d^\gamma$, and by a factor of at least 10 in the case of $\text{Im}c_d^Z$. Moreover, with polarization, either of A_{fb} and A_{ch} , with a suitably chosen cut-off, suffices to get the same improvement in sensitivity.

Apart from simultaneous limits on $\text{Im}c_d^{\gamma,Z}$, we have also found out the sensitivities of one of $\text{Im}c_d^{\gamma,Z}$, assuming the other to be zero, using the CP -odd combination of angular distributions $\frac{d\sigma^+}{d\cos\theta}(\theta_l) - \frac{d\sigma^-}{d\cos\theta}(\pi - \theta_l)$ coming from Equation 3.2. We assume that the data is collected over bins in θ_l , and add the 90% CL limits obtained from individual bins in inverse quadrature. We find that the best individual limits are respectively 0.12 and 0.28 for $\text{Im}c_d^\gamma$ and $\text{Im}c_d^Z$, both in the case of $P_e = -0.5$, for $m_t = 174$ GeV. The corresponding limits for $m_t = 200$ GeV are 0.18 and 0.43. As expected, these limits are better than simultaneous ones. Even here, there is an improvement due to polarization, but it is not as dramatic as in the case of simultaneous limits.

Our limits on $\text{Im}c_d^{\gamma,Z}$ are summarized in Table 3.2.

To conclude, we have obtained expressions for certain simple CP -violating angular asymmetries in the production and subsequent decay of t in the presence of electric and weak dipole form factors of the top quark. These asymmetries are specially chosen so that they do not require the reconstruction of the t or \bar{t} directions or energies. We have also included the effect of longitudinal electron beam polarization. We have analyzed these asymmetries to obtain simultaneous 90% CL limits on the imaginary parts of the electric and weak dipole couplings which would be possible at future linear e^+e^- collider operating at $\sqrt{s} = 500$ GeV and with a luminosity of 10 fb^{-1} . Figs. 2-4 show the allowed regions in the $\text{Im}c_d^\gamma$ - $\text{Im}c_d^Z$ plane at the 90% C.L. Table 3.2 summarizes the 90% C.L. limits on $\text{Im}c_d^{\gamma,Z}$ in various cases.

Case	$m_t = 174 \text{ GeV}$		$m_t = 200 \text{ GeV}$	
	$ \text{Im}c_d^\gamma $	$ \text{Im}c_d^Z $	$ \text{Im}c_d^\gamma $	$ \text{Im}c_d^Z $
(a) unpolarized	2.4	17	4.0	28
(b) polarized($P_e = 0, \pm 0.5$)	0.45	1.5	0.78	2.5
(c) angular distribution:	$P_e = +0.5$	0.13	0.74	0.21
	$P_e = 0.0$	0.13	0.81	0.20
	$P_e = -0.5$	0.12	0.28	0.18

Table 3.2: Limits on dipole couplings obtainable from different asymmetries. In case (a) limits are obtained from \mathcal{A}_{ch} and \mathcal{A}_{fb} using unpolarized beams (Figure 3.3), and in case (b) from either of \mathcal{A}_{ch} (Figure 3.4(a) and 3.5(a)) and \mathcal{A}_{fb} (Figures 3.4(b) and 3.4(b)) with polarizations $P_e = 0, \pm 0.5$. Charge-asymmetric angular distribution is used in case (c) where 0 and ± 0.5 polarizations are considered separately. All the limits are at 90% CL.

Our general conclusion is that the sensitivity to the measurement of dipole couplings is improved considerably if the electron beam is polarized as in the case of asymmetries described in Chapter 2.

As mentioned earlier, since we consider only the electron beam to be polarized, the asymmetries considered here can have backgrounds from order- α collinear initial-state photon emission. This background is calculated in the next chapter.

Chapter 4

Effects Due to Helicity-Flip Initial State Radiation

The CP -odd asymmetries discussed in chapter 2 and 3 signal CP violation when the electron and positron are unpolarized because the initial state is a CP eigenstate. On the other hand, if e^+ and e^- are longitudinally polarized, and the polarizations are not equal and opposite, then the initial state is not a CP eigenstate and hence the non-vanishing of those asymmetries need not necessarily signal CP violation. This may lead to a CP conserving background contribution to the asymmetries.

At zeroth order in α no such background comes into the picture because only e^+ and e^- with opposite helicities couple with the photon or Z boson in the limit $m_e \rightarrow 0$. Hence the initial state in the process $e^+e^- \rightarrow t\bar{t}$ is always a CP eigenstate in this limit, regardless of the polarization. But this is not true at order α . Lee and Nauenberg [42] have shown that the probability for a helicity-flip collinear photon emission from an electron (or positron) is non-zero. In such a situation we can have an $e_L\bar{e}_L$ or $e_R\bar{e}_R$ initial state emitting a helicity-flip collinear photon to become $e_R\bar{e}_L$

or $e_L\bar{e}_R$ before fusing together to produce $t\bar{t}$ pairs. Evidently, the initial state is not an eigenstate of CP unless there is an equal number of $e_L\bar{e}_L$ and $e_R\bar{e}_R$ pairs in it. In simple terms this means that the initial state will not be a CP eigenstate if the electron and positron beam polarizations are not equal and opposite. In practice polarized positrons are difficult to generate. The type of colliders that we have been discussing are with a polarized electron beam and unpolarized positron beam. Therefore it is required to calculate the background to the asymmetries due to the reasons discussed above.

The photon-emission process is of order α and hence we expect the background to be small in general. Among the asymmetries discussed in the earlier chapters, the up-down asymmetry A_{ud} and the up-down asymmetry combined with the forward-backward asymmetry A_{ud}^{fb} discussed in Chapter 2 are T -odd. In the absence of CP violation, non-vanishing T -odd observable requires absorptive part of the amplitude. But the process we are considering is a tree level process and hence does not have an absorptive part. Thus A_{ud} and A_{ud}^{fb} do not have a background from helicity-flip collinear photon process. The other two asymmetries described in Chapter 2, the left-right asymmetry, A_{lr} , and the left-right asymmetry combined with the forward-backward asymmetry, A_{lr}^{fb} , are T even and hence may have a background due to the helicity-flip collinear photon emission process. Similarly, the charge asymmetry A_{ch} and charge asymmetry combined with the forward-backward asymmetry, A_{fb} in Chapter 3 are T even and will have a background. In this chapter we shall calculate background to the charge asymmetry and the charge asymmetry combined with the leptonic forward-backward asymmetry described in Chapter 3. Our result is that the background is small compared to the statistical fluctuation for the expected luminosity and can be neglected. Background to A_{lr} and A_{lr}^{fb} have not been calculated here as it requires a more complicated integra-

tion. We expect it to be negligible, however, as in the present case.

A similar calculation for momentum correlations in the processes $e^+e^- \rightarrow \tau^+\tau^-$ and $e^+e^- \rightarrow t\bar{t}$ was reported by Ananthanarayan and Rindani [41].

4.1 Calculation of the Background Contribution

The charge asymmetry as defined in Equation 3.3 is the asymmetry in the rate of production of the leptons and antileptons, or in other words, it is the total leptonic charge in the $t\bar{t}$ production and their subsequent semileptonic decay. In this section we shall calculate explicitly the background to this leptonic charge asymmetry arising within SM due to the helicity-flip collinear photon emission from the initial-state electron or positron. Since we are interested in the background from SM we set dipole couplings to zero. In our calculations we make use of the method discussed by Falk and Sehgal [43]. Analogous to the Weizsäcker-Williams spectrum in case of helicity non-flip process

$$e_\lambda^+ e_{-\lambda}^- \rightarrow e_\lambda^+ e_{-\lambda}^- \gamma \rightarrow f\bar{f}(\gamma)$$

an equivalent-particle distribution is considered in the case of helicity-flip process

$$e_\lambda^+ e_\lambda^- \rightarrow e_\lambda^+ e_{-\lambda}^- \gamma \rightarrow f\bar{f}(\gamma). \quad (4.1)$$

The cross section for the helicity-flip process in this case is given in terms of the cross section for the process $e^+e^- \rightarrow f\bar{f}$ without photon emission, $\sigma_0(\hat{s})$, by

$$\frac{d\sigma_{hf}(s)}{dz} = \frac{\alpha}{2\pi}(1-z)\sigma_0(\hat{s}). \quad (4.2)$$

σ_0 is a function of the c.m. energy (\hat{s}) of the $f\bar{f}$ system, written in terms of the c.m. energy (s) of the e^+e^- system as $\hat{s} = zs$, where z is the fraction of momentum carried by the electron or the positron after photon emission. Equation 4.2 is valid in the case of either electron or positron emitting the collinear photon.

The angular distribution of the process without photon emission is given by

$$\begin{aligned}
\frac{d\sigma_0^\pm}{d\cos\theta_l} = & \frac{3\pi\alpha^2}{32\hat{s}} B_l B_{\bar{l}} \left\{ 4A_0^\pm - 2A_1^\pm \left(\frac{1-\beta^2}{\beta^2} \log \frac{1+\beta}{1-\beta} - \frac{2}{\beta} \right) \cos\theta_l \right. \\
& + 2A_2^\pm \left(\frac{1-\beta^2}{\beta^3} \log \frac{1+\beta}{1-\beta} (1-3\cos^2\theta_l) \right. \\
& \left. \left. - \frac{2}{\beta^2} (1-3\cos^2\theta_l - \beta^2 + 2\beta^2 \cos^2\theta_l) \right) \right. \\
& + 2B_1^\pm \frac{1-\beta^2}{\beta^2} \left(\frac{1}{\beta} \log \frac{1-\beta}{1-\beta} - 2 \right) \cos\theta_l \\
& + B_2^\pm \frac{1}{\beta^3} \left(\frac{\beta^2-2}{\beta} \log \frac{1+\beta}{1-\beta} + 6 \right) (1-3\cos^2\theta_l) \\
& + 2C_0^\pm \frac{1-\beta^2}{\beta^2} \left(\frac{1}{\beta} \log \frac{1+\beta}{1-\beta} - 2 \right) \cos\theta_l \\
& \left. - C_1^\pm \frac{1}{\beta^3} \left(\frac{3(1-\beta^2)}{\beta} \log \frac{1+\beta}{1-\beta} - 2(3-2\beta^2) \right) (1-3\cos^2\theta_l) \right\}, \quad (4.3) \\
= & T_0^\pm + T_1^\pm \cos\theta_l + T_2^\pm \cos^2\theta_l \quad (4.4)
\end{aligned}$$

Here \pm refers to whether the electron (-) or positron (+) emits the collinear photon. Equation 4.3 is similar to Equation 3.3 but now with A_i , B_i and C_i as given in Section B.2. T_i^\pm are given by

$$T_i^\pm = T_i^{(1)} (1 + P_e P_{\bar{e}}) \pm T_i^{(2)} (P_e + P_{\bar{e}}), \quad (4.5)$$

We shall see later that only the terms proportional to $(P_e + P_{\bar{e}})$ are relevant in this discussion. (This is expected since the effect of helicity-flip process will average out if we have equal and opposite polarization or no polarization). Expressions for $T_i^{(2)}$ are given in Section B.3. Here θ_l and ϕ_l are the polar and azimuthal angles of the lepton three momentum.

The antilepton angular distribution is given by

$$\frac{d\bar{\sigma}_0^\pm}{d \cos \theta_l} = \bar{T}_0^\pm + \bar{T}_1^\pm \cos \theta_l + \bar{T}_2^\pm \cos^2 \theta_l. \quad (4.6)$$

We have the following relations between the T_i and \bar{T}_i :

$$\bar{T}_0^\pm = T_0^\pm, \quad \bar{T}_1^\pm = -T_1^\pm, \quad \text{and} \quad \bar{T}_2^\pm = T_2^\pm.$$

The lab frame is the c.m. frame of e^+ and e^- to start with. However, after initial state radiation, the e^+e^- are no longer in their c.m. frame. Expression for $d\sigma_0^\pm/d \cos \theta_l$ in the lab frame is obtained by boosting $(d\sigma_0^\pm/d \cos \theta_l)^{(c.m.)}$ along the negative/positive z axis. The boost variable is $\beta_z = \frac{1-z}{1+z}$, where z is the momentum fraction carried by the fermion after photon emission.

In the c.m. frame with CP -even cuts the charge asymmetry is zero, since we have set CP -odd dipole couplings to zero. The boost taking the c.m. frame to the lab frame redefines the cuts giving rise to a non-zero asymmetry. We calculate the asymmetry in the following way. The charge asymmetry as defined by Equation 3.3 in the present case becomes

$$A_{ch} = \frac{\alpha}{2\pi} \int_{4m_l^2/s}^1 A_{ch}(z) (1-z) dz, \quad (4.7)$$

with

$$A_{ch}(z) = [A_{ch}^+(z) + A_{ch}^-(z)], \quad (4.8)$$

where \pm denotes the case where photon is emitted from the positron or electron and

$$A_{ch}^{\pm}(z) = \int_{\theta_0}^{\pi-\theta_0} \frac{1}{2\sigma} \left[\frac{d\sigma_0^{\pm}}{d\theta_l}(\theta_l) - \frac{d\bar{\sigma}_0^{\pm}}{d\theta_l}(\pi - \theta_l) \right] d\theta_l$$

Here $\frac{d\sigma^{\pm}}{d\theta_l}$ and $\frac{d\bar{\sigma}^{\pm}}{d\theta_l}$ are in the lab frame and the cuts on the angle are CP -even. This is equivalent to A_{ch}^{\pm} obtained in terms of $\frac{d\sigma^{\pm}}{d\theta_l}$ and $\frac{d\bar{\sigma}^{\pm}}{d\theta_l}$ in the c.m. frame with appropriate cuts on the angles. With the change of variable from θ_l to $\cos \theta_l$ and realising that the c.m. frame is reached by a boost by β_z from the lab frame, the lower and the upper limits of integration are modified to

$$f^{\pm}(\theta_0) = \frac{\cos \theta_0^{cm} \pm \beta_z}{1 \pm \beta_z \cos \theta_0^{cm}}$$

and

$$\begin{aligned} g^{\pm}(\theta_0) &= \frac{\cos(\pi - \theta_0^{cm}) \pm \beta_z}{1 \pm \beta_z \cos(\pi - \theta_0^{cm})} \\ &= \frac{-\cos \theta_0^{cm} \pm \beta_z}{1 \mp \beta_z \cos \theta_0^{cm}} \end{aligned}$$

respectively. Here again \pm denotes the case where photon is emitted by positron or electron. Notice that $f^-(\theta_0) = -g^+(\theta_0)$ and $g^-(\theta_0) = -f^+(\theta_0)$. Also we have

$$f^+(\pi - \theta_0) = \frac{-\cos \theta_0^{cm} + \beta_z}{1 - \beta_z \cos \theta_0^{cm}} = g^+(\theta_0)$$

and

$$g^+(\pi - \theta_0) = \frac{\cos \theta_0^{cm} + \beta_z}{1 + \beta_z \cos \theta_0^{cm}} = f^+(\theta_0).$$

We define $f = f^+(\theta_0)$ and $g = g^+(\pi - \theta_0)$ for convenience in notation.

Now

$$\begin{aligned} A_{ch}^+(z) &= \frac{1}{2\sigma} \int_{f^+(\theta_0)}^{g^+(\theta_0)} \left[\frac{d\sigma_0^+}{d \cos \theta_l}(\theta_l) - \frac{d\bar{\sigma}_0^+}{d \cos \theta_l}(\pi - \theta_l) \right] d \cos \theta_l \\ &= \frac{1}{2\sigma} \left\{ \int_{f^+(\theta_0)}^{g^+(\theta_0)} \frac{d\sigma_0^+}{d \cos \theta_l}(\theta_l) d \cos \theta_l - \int_{f^+(\pi - \theta_0)}^{g^-(\pi - \theta_0)} \frac{d\bar{\sigma}_0^+}{d \cos \theta_l}(\theta_l) d \cos(\pi - \theta_l) \right\} \\ &= \frac{1}{2\sigma} \int_f^g \left[\frac{d\sigma_0^+}{d \cos \theta_l}(\theta_l) - \frac{d\bar{\sigma}_0^+}{d \cos \theta_l}(\theta_l) \right] d \cos \theta_l \end{aligned} \quad (4.9)$$

Here a change of variable, $\theta_l \rightarrow \pi - \theta_l$ is made in the second step. From Equation 4.3 we get

$$A_{ch}^+(z) = \frac{1}{2\sigma} T_1^+(g^2 - f^2) \quad (4.10)$$

Similarly for electron emitting collinear photon we get

$$\begin{aligned} A_{ch}^-(z) &= \frac{1}{2\sigma} \int_{-g}^{-f} \left[\frac{d\sigma_0^+}{d \cos \theta_l}(\theta_l) - \frac{d\bar{\sigma}_0^+}{d \cos \theta_l}(\theta_l) \right] d \cos \theta_l \\ &= \frac{1}{2\sigma} T_1^+(f^2 - g^2) \end{aligned} \quad (4.11)$$

Substituting for $A_{ch}^+(z)$ and $A_{ch}^-(z)$ in Equation 4.8 we get the expression for A_{ch} as

$$A_{ch}(z) = \frac{1}{2\sigma} 4 T_1^{(2)} \beta_z (1 - \beta_z^2) \left[\frac{\sin \theta_0 \cos \theta_0}{(1 - \beta_z^2 \cos^2 \theta_0)^2} \right] (P_e + P_{\bar{e}}). \quad (4.12)$$

In a similar way we calculate the charge and forward-backward asymmetry asymmetry defined as

$$A_{fb} = \frac{\alpha}{2\pi} \int_{\frac{4m_i^2}{s}}^1 A_{fb}(z)(1-z)dz, \quad (4.13)$$

with

$$A_{fb}(z) = A_{fb}^+(z) + A_{fb}^-(z) \quad (4.14)$$

where

$$\begin{aligned} A_{fb}^\pm(z) = & \int_{\theta_0}^{\frac{\pi}{2}} \frac{1}{2\sigma} \left[\frac{d\sigma^\pm}{d\theta_l}(\theta_l) - \frac{d\bar{\sigma}^\pm}{d\theta_l}(\pi - \theta_l) \right] d\theta_l \\ & - \int_{\frac{\pi}{2}}^{\pi - \theta_0} \frac{1}{2\sigma} \left[\frac{d\sigma^\pm}{d\theta_l}(\theta_l) - \frac{d\bar{\sigma}^\pm}{d\theta_l}(\pi - \theta_l) \right] d\theta_l. \end{aligned} \quad (4.15)$$

Following the same arguments used for deriving the expression for A_{ch} we get the expression for A_{fb} in terms of the variables in the c.m. frame as

$$\begin{aligned} A_{fb}(z) = & \frac{1}{2\sigma} \left[\frac{4(1 - \beta_z^2) \cos \theta_0}{3(1 - \beta_z^2 \cos^2 \theta_0)^3} \right] \\ & \times \left[3T_0^{(2)}(1 - \beta_z^2 \cos^2 \theta_0)^2 + T_2^{(2)}(3\beta_z^2 \sin^4 \theta_0 + (1 - \beta_z^2)^2 \cos^2 \theta_0) \right] \\ & \times (P_e + P_{\bar{e}}). \end{aligned} \quad (4.16)$$

All integrations so far are done analytically. The z integration has to be done numerically. In the following section we shall present the numerical results.

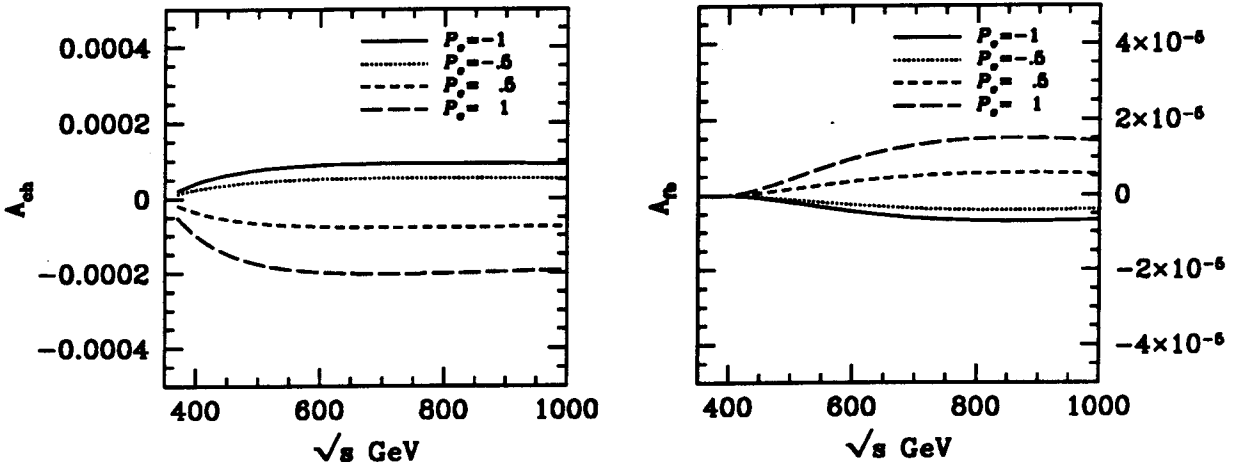


Figure 4.1: Leptonic charge asymmetry (left) and the combined asymmetry (right) are plotted against the s.m. energy for different electron beam polarizations. In all cases unpolarized positron beam is considered. Top quark mass is taken to be 174 GeV and a cut-off angle of 10° is considered.

4.2 Numerical Results

The background to the leptonic charge asymmetry and the charge asymmetry combined with the forward-backward asymmetry due to the helicity-flip initial state radiation are calculated. The asymmetries obtained are plotted in Figure 4.1 for different electron beam polarizations. In practice, production of polarized positron beam is difficult and hence we have considered only unpolarized positron beams. A cut-off of 10° is taken in our calculations.

The asymmetries given in Figure 4.1 are negligible compared to the statistical fluctuation, $1/\sqrt{N}$ plotted in Figure 4.2. Here we have assumed an integrated luminosity of 10 fb^{-1} . All the calculations are done at a top quark mass of 174 GeV.

It is clear from the figures that, as expected, the background is negligible compared to the statistical fluctuation. A similar calculation of the backgrounds to other asymmetries could be done. We expect them to be small compared to statis-

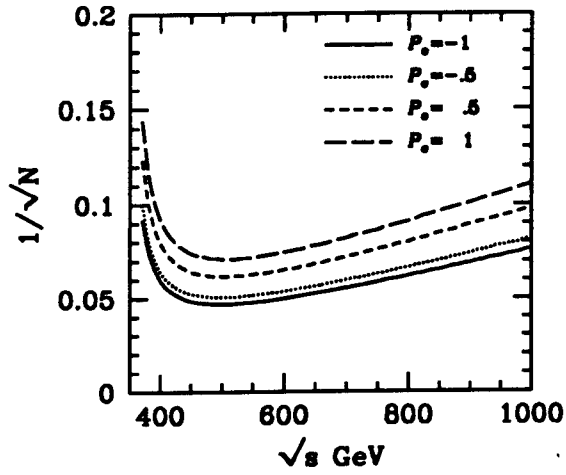


Figure 4.2: Variation of $1/\sqrt{N}$ with the c.m. energy. An integrated luminosity of 10 fb^{-1} is assumed and the cut-off angle is taken to be 10° .

tical fluctuations, and have not attempted to calculate in this thesis because of the complicated nature of calculations.

Chapter 5

CP-Violating Asymmetries in

$$\gamma\gamma \rightarrow t\bar{t}$$

So far we have been discussing *CP* violation in the top-antitop quark pair production in e^+e^- colliders, where we constructed *CP*-odd asymmetries involving final state momenta. These asymmetries, if observed, will tell what the values of the electric and the weak dipole form factors of the top quark are and, if not observed, will help in putting limits on them. The next generation of e^+e^- colliders must be linear colliders for synchrotron radiation makes it difficult for a circular collider to increase its beam energy beyond a certain value. High-energy photon beams could be produced using such linear colliders together with the already available laser technology [4]. This could be done by back-scattering of an intense laser beam off a high-energy electron beam. These photon beams can then be made to collide with either an electron beam or another photon beam. Such photon linear colliders are being discussed extensively in the literature [44 - 49] and are expected to be built in the future. Advantages of such a collider, from the physics point of view, include clean signals for Higgs production, SUSY particle detection, study of SM triple-gauge-boson couplings, etc.

The topic of CP violation in $\gamma\gamma \rightarrow t\bar{t}$ has also elicited some interest recently. Anlauf *et al.* [47, 48] have discussed CP violation in a Higgs mediated $\gamma\gamma \rightarrow t\bar{t}$ process where they study triple product correlations as well as asymmetries. Choi and Hagiwara [49], and Baek *et al.* [46] have studied top quark EDFF in $\gamma\gamma \rightarrow t\bar{t}$ with linearly polarized photon beams.

In this chapter we shall discuss some of the possible CP -violating effects in the top-antitop pair production by constructing asymmetries out of the momenta of the top (antitop) quark decay products in a $\gamma\gamma$ collider.

The next section will briefly describe the main features of a $\gamma\gamma$ collider and the following section will discuss CP violation in $\gamma\gamma \rightarrow t\bar{t}$ in the presence of top diopole moment. In the last section we shall discuss the numerical results and conclusions.

5.1 Features of a $\gamma\gamma$ Collider

In a $\gamma\gamma$ collider, high-energy photons would be produced by Compton backscattering of intense low-energy laser beams off high energy electrons [4]. The energy spectrum of a compton scattered photon is given by

$$\begin{aligned} \frac{1}{\sigma_c} \frac{d\sigma_c}{dy} &= f(x, y) \\ &= \frac{2\pi\alpha^2}{\sigma_c x m_e^2} \left[\frac{1}{1-y} + 1 - y - 4r(1-x) - 2\lambda_e \lambda_l r x (2r-1)(2-y) \right]. \end{aligned} \quad (5.1)$$

Here

$$x = \frac{4E_b\omega_0}{m_e^2} = 15.3 \left(\frac{E_b}{\text{TeV}} \right) \left(\frac{\omega_0}{\text{eV}} \right), \quad (5.2)$$

where E_b is the electron beam energy and ω_0 is the energy of the laser beam. y is given in terms of the energy of the scattered photon, ω ($\leq E_b \frac{x}{1+x}$), as

$$y = \frac{\omega}{E_b}$$

and

$$r = \frac{y}{x(1-y)} \leq 1.$$

λ_e and λ_l are the initial electron and laser photon helicities respectively. Energy distribution in terms of the variable y is related to that in terms of ω by

$$f(\omega) = \frac{1}{\sigma_c} \frac{d\sigma_c}{d\omega} = \frac{1}{E_b} f(x, y). \quad (5.3)$$

Total cross section, σ_c is given by

$$\sigma_c = \sigma_c^{np} + 2\lambda_e \lambda_l \sigma_1,$$

with

$$\sigma_c^{np} = \frac{2\pi\alpha^2}{xm_e^2} \left[\left(1 - \frac{4}{x} - \frac{8}{x^2}\right) \log(x+1) + \frac{1}{2} + \frac{8}{x} - \frac{1}{2(x+1)^2} \right]$$

and

$$\sigma_1 = \frac{2\pi\alpha^2}{xm_e^2} \left[\left(1 + \frac{2}{x}\right) \log(x+1) - \frac{5}{2} + \frac{1}{1+x} - \frac{1}{2(x+1)^2} \right].$$

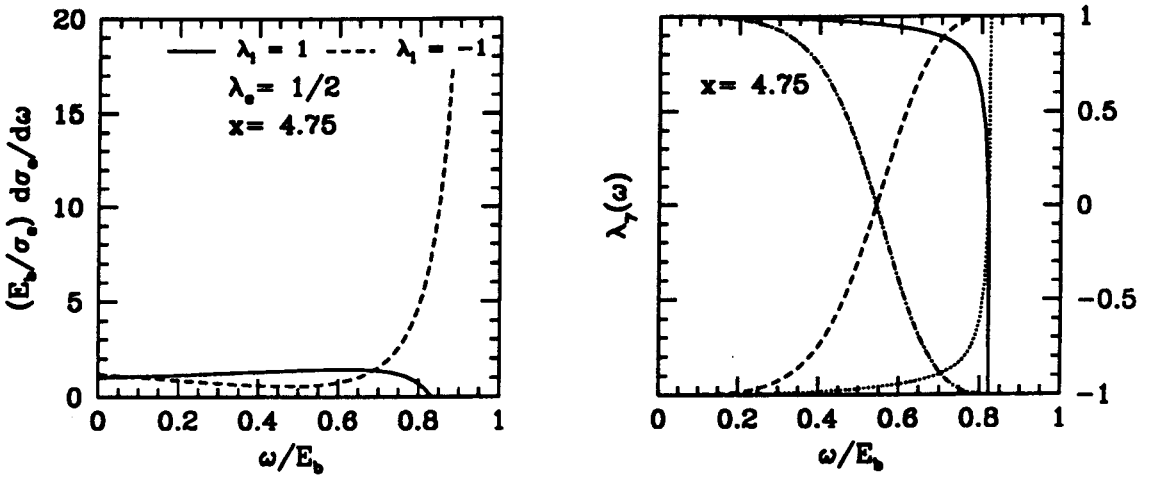


Figure 5.1: Figure on the left shows the energy distribution of Compton scattering for different helicity combinations of the initial electron beam and the laser beam. In the figure on the right side the scattered photon helicity is plotted against the energy of the scattered photon for different helicity combinations of the laser beam and the initial electron beam. Solid and dotted lines correspond to $2\lambda_e\lambda_l = 1$ with $\lambda_e = 1/2$ and $\lambda_e = -1/2$ respectively while dash line and dash-dot line correspond to $2\lambda_e\lambda_l = -1$ with $\lambda_e = 1/2$ and $\lambda_e = -1/2$ respectively.

Here σ_e^{np} is the unpolarized cross section. The energy spectrum $f(x, y)$ is plotted against y in Figure 5.1. [4].

It is clear from the figure that when $\lambda_e\lambda_l < 0$, there are more number of hard photons than soft photons, while for $\lambda_e\lambda_l > 0$ the number of hard photons are less than the number of soft photons. Also in the case of $\lambda_e\lambda_l < 0$ the spectrum peaks at higher energies resulting in nearly monochromatic beams.

Polarized photon beams are more appropriate for CP violation studies. Dependence of the helicity of the Compton scattered photon on the energy of the photon is discussed in [4] and is given by

$$\lambda_\gamma(\omega) = \frac{\lambda_l (1 - 2r) (1 - y + \frac{1}{1-y}) + 2\lambda_e r x [1 + (1 - y) (1 - 2r)^2]}{1 - y + \frac{1}{1-y} - 4r(1 - r) - 2\lambda_e \lambda_l r x (2r - 1) (2 - y)}. \quad (5.4)$$

At $2\lambda_e\lambda_l = -1$, hard photons will have $\lambda = \lambda_e$ (See Figure 5.1). As already mentioned the number of hard photon is much higher than the soft ones at $2\lambda_e\lambda_l = -1$.

Another important aspect of a collider is its luminosity. The luminosity distribution of a $\gamma\gamma$ collider depends on different factors like the conversion distance, *i.e.*, the distance from the scattering point to the interaction point, energy distribution of the beams, etc. Assuming a Gaussian profile for the electron beam with azimuthal symmetry, the luminosity distribution of a $\gamma\gamma$ collider is given in terms of the photon energy distribution by [4]

$$\frac{1}{L_{ee}} \frac{dL_{\gamma\gamma}}{d\omega_1 d\omega_2} = f_1(\omega_1) f_2(\omega_2) I_0 \left(\frac{d_1 d_2}{\sigma_1^2 + \sigma_2^2} \right) e^{-\frac{d_1 d_2}{2(\sigma_1^2 + \sigma_2^2)}}. \quad (5.5)$$

Here $f_1(\omega_1)$ and $f_2(\omega_2)$ are the energy distributions of the two photon beams (see Equation 5.3). I_0 is the zeroth order modified Bessel function with $d_i = z_i \theta_{\gamma i}$, where z_i is the conversion distance and $\theta_{\gamma i}$ is the scattering angle of the photon beam and σ_i is the half width of the Gaussian profile. L_{ee} is the geometrical luminosity of the original electron-electron collider. Making a variable change from ω_1 and ω_2 to η and W , where $\eta = \tan^{-1} \left(\frac{\omega_1 - \omega_2}{\omega_1 + \omega_2} \right)$ is the $\gamma\gamma$ rapidity and $W = 2\sqrt{\omega_1 \omega_2}$ is the $\gamma\gamma$ invariant mass, we get the luminosity distribution as

$$\frac{1}{L_{ee}} \frac{dL_{\gamma\gamma}}{dW d\eta} = \frac{W}{2} f_1 \left(\frac{W e^\eta}{2} \right) f_2 \left(\frac{W e^{-\eta}}{2} \right) I_0 \left(\frac{d_1 d_2}{\sigma_1^2 + \sigma_2^2} \right) e^{-\frac{d_1 d_2}{2(\sigma_1^2 + \sigma_2^2)}}. \quad (5.6)$$

Taking the conversion distance to be zero for simplicity, the expression for the luminosity distribution becomes

$$\frac{1}{L_{ee}} \frac{dL_{\gamma\gamma}}{dW d\eta} = \frac{W}{2} f_1 \left(\frac{W e^\eta}{2} \right) f_2 \left(\frac{W e^{-\eta}}{2} \right). \quad (5.7)$$

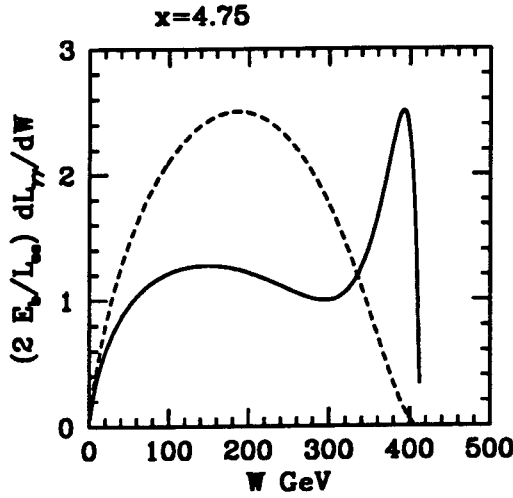


Figure 5.2: Luminosity distributions is plotted against the $\gamma\gamma$ invariant mass, $W = 2\sqrt{\omega_1\omega_2}$. Initial electron beam energy, E_b is taken to be 250 GeV and a laser beam of energy 1.24 eV is assumed. Solid line is for $2\lambda_e\lambda_l = -1$ while dotted curve is for $2\lambda_e\lambda_l = 1$. The curve is for zero conversion distance.

Figure 5.2 gives luminosity distribution after rapidity is integrated out. Luminosity peaks at higher values of invariant mass in case of $2\lambda_e\lambda_l = -1$ and the peak value could be as high as 90% of L_{ee} , while for $2\lambda_e\lambda_l = 1$ the spectrum is almost a Gaussian peaking at low energies.

For large values of L_{ee} , which are possible to achieve, we expect large $t\bar{t}$ production in a $\gamma\gamma$ collider. In the next section we shall discuss some of the CP -violating effects which could be tested in these colliders.

5.2 Charge Asymmetries in $\gamma\gamma \rightarrow t\bar{t}$

In this section we shall discuss some of the asymmetries defined in the earlier chapters, in the context of a $\gamma\gamma$ collider with features described in the previous section. Rest of this section will discuss the charge asymmetry arising due to the top quark dipole moment in $\gamma\gamma \rightarrow t\bar{t}$ process with subsequent decay of t and \bar{t} .

Charge asymmetry as defined in Chapter 3 is the total leptonic charge asymmetry in the process with $t\bar{t}$ decaying semileptonically.

As in the earlier cases, here again, considering on-shell production of $t\bar{t}$ pairs, the production and the decay parts of the amplitude can be separated (see Section 2.2). The production helicity amplitudes are calculated using a method developed by Vega and Wudka [44] as discussed below.

This method makes use of the identity introduced by Michel and Bouchiat [45], viz.,

$$u(p, \lambda') \bar{u}(p, \lambda) = \frac{1}{2}(\not{p} + m)(\delta_{\lambda\lambda'} + \sum_i \gamma_5 \eta^i \sigma_{\lambda\lambda'}^i). \quad (5.8)$$

Here the σ^i are the three Pauli matrices and η^i are the spin vectors corresponding to the four-momentum p , defined such that

$$\begin{aligned} \eta_i \cdot \eta_j &= -\delta_{ij} \\ \eta_i \cdot p &= 0. \end{aligned} \quad (5.9)$$

In the case where $\lambda' = \lambda$ expression (5.8) reduces to the usual projection operator for a state of momentum p and helicity λ . For

$$p = |\vec{p}| \left(\frac{E}{|\vec{p}|}; \sin \theta \cos \phi, \sin \theta \sin \phi, \cos \theta \right),$$

a standard representation of the η_i is given by

$$\eta_1^\mu = (0; \cos \theta \cos \phi, \cos \theta \sin \phi, -\sin \theta)$$

$$\begin{aligned}
\eta_2^\mu &= (0; -\sin \phi, \cos \phi, 0) \\
\eta_3^\mu &= \left(\frac{|\vec{p}|}{m}; \frac{E}{m} \frac{\vec{p}}{|\vec{p}|} \right),
\end{aligned} \tag{5.10}$$

where $\eta_k^\mu = (0; \delta_k^i)$ for the case when $|\vec{p}| = 0$.

For spinors with different momenta, this gives

$$\begin{aligned}
u(p', \lambda) \otimes \bar{u}(p, \lambda) &= -\lambda \frac{1}{2} \gamma_0 (\not{p}' + m) \gamma_5 \not{\eta}^\lambda e^{i\lambda\phi} \\
u(p', \lambda) \otimes \bar{u}(p, -\lambda) &= -\lambda \frac{1}{2} \gamma_0 (\not{p}' + m) (1 - \lambda \gamma_5 \not{\eta}^3) e^{i\lambda\phi},
\end{aligned} \tag{5.11}$$

where $\eta^\lambda = \eta_1 - i\lambda \eta_2$. Here we have assumed that the masses of the spinors are the same and also $\vec{p}' = -\vec{p}$.

This method is made use of in calculating the amplitude of the process $\gamma\gamma \rightarrow t\bar{t}$ with the effective $t\bar{t}\gamma$ coupling,

$$\Gamma_\mu^j = c_v^j \gamma_\mu + c_a^j \gamma_\mu \gamma_5 + \frac{c_d^j}{2m_t} i\sigma_{\mu\nu} \gamma_5 (p_t + p_{\bar{t}})^\nu, \quad j = \gamma, Z$$

arising from the Lagrangian given by Equation 1.7.

There are two diagrams, one corresponding to the t -channel process and the other for the cross channel process, which are shown in Figure 5.3.

The production helicity amplitude $M(\lambda_{\gamma_1}, \lambda_{\gamma_2}, \lambda_t, \lambda_{\bar{t}})$ is given in terms of the amplitudes corresponding to the two diagrams in Figure 5.3 by

$$M(\lambda_{\gamma_1}, \lambda_{\gamma_2}, \lambda_t, \lambda_{\bar{t}}) = M_1(\lambda_{\gamma_1}, \lambda_{\gamma_2}, \lambda_t, \lambda_{\bar{t}}) + M_2(\lambda_{\gamma_1}, \lambda_{\gamma_2}, \lambda_t, \lambda_{\bar{t}})$$

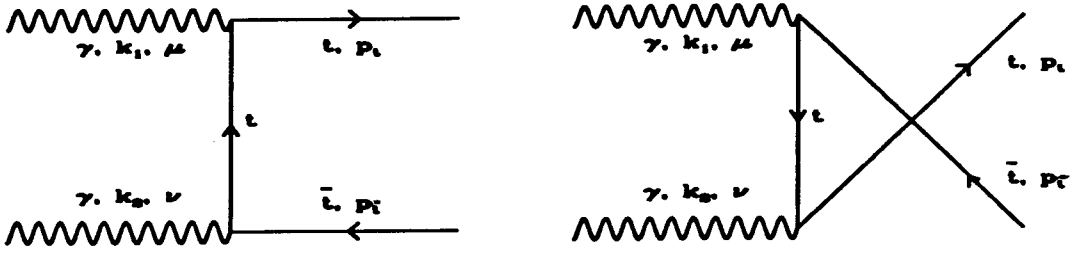


Figure 5.3: The two Feynman diagrams for the $\gamma\gamma \rightarrow t\bar{t}$ process.

$$\begin{aligned}
 &= \frac{ie^2 Q_t^2}{2E_t^2(1 - \beta^2 \cos^2 \theta)} \epsilon_{1\mu}(\lambda_{\gamma_1}) \epsilon_{2\nu}(\lambda_{\gamma_2}) \\
 &\quad \times [T_1^{\mu\nu} (1 + \beta \cos \theta) + T_2^{\mu\nu} (1 - \beta \cos \theta)], \quad (5.12)
 \end{aligned}$$

where

$$T_1^{\mu\nu}(\lambda_{\gamma_1}, \lambda_{\gamma_2}, \lambda_t, \lambda_{\bar{t}}) = \bar{u}(p_t, \lambda_t) \Gamma^\mu \frac{(\not{p}_t - \not{k}_1 + m)}{(p_t - k_1)^2 - m^2} \Gamma^\nu v(p_{\bar{t}}, \lambda_{\bar{t}})$$

and

$$T_2^{\mu\nu}(\lambda_{\gamma_1}, \lambda_{\gamma_2}, \lambda_t, \lambda_{\bar{t}}) = \bar{u}(p_t, \lambda_t) \Gamma^\mu \frac{(\not{p}_t - \not{k}_2 + m)}{(p_t - k_2)^2 - m^2} \Gamma^\nu v(p_{\bar{t}}, \lambda_{\bar{t}}).$$

θ_t is the scattering angle in the c.m. frame of $t\bar{t}$. Using the relation

$$v(\vec{p}, \lambda) = (-)^{\frac{\lambda}{2} - \frac{1}{2}} \gamma^5 u(\vec{p}, \lambda)$$

we obtain

$$T_1^{\mu\nu} = \text{Tr} \left\{ (-)^{\frac{\lambda_{\bar{t}}}{2} - \frac{1}{2}} \gamma^5 u(\vec{p}, \lambda_{\bar{t}}) \bar{u}(p, \lambda_t) [\Gamma^\mu (\not{p}_t - \not{k}_1 + m) \Gamma^\nu] \right\}$$

and

$$T_2^{\mu\nu} = \text{Tr} \left\{ (-)^{\frac{\lambda_t}{2} - \frac{1}{2}} \gamma^5 u(\bar{p}, \lambda_t) \bar{u}(p, \lambda_t) [\Gamma^\nu (\not{p}_t - \not{k}_2 + m) \Gamma^\mu] \right\}.$$

Making use of Equation 5.11 and choosing the polarization vectors

$$\epsilon^\mu(\lambda_{\gamma_1}) = \frac{1}{\sqrt{2}}(0; 1, i \lambda_{\gamma_1}, 0)$$

and

$$\epsilon^\mu(\lambda_{\gamma_2}) = \frac{1}{\sqrt{2}}(0; 1, -i \lambda_{\gamma_2}, 0),$$

we get the helicity amplitudes as

$$\begin{aligned} M(\lambda_\gamma, \lambda_\gamma, \lambda_t, \lambda_t) &= -\frac{4m_t e^2 Q_t^2}{\sqrt{s}(1 - \beta_t^2 \cos^2 \theta_t)} \left\{ (\lambda_\gamma + \lambda_t \beta_t) \right. \\ &\quad \left. -i d_t 2m_t \left[2 + \frac{s}{4m_t^2} \beta_t (\beta_t - \lambda_t \lambda_\gamma) \sin^2 \theta_t \right] \right. \\ &\quad \left. + d_t^2 \frac{s \lambda_\gamma}{2} \left[\frac{4m_t^2}{s} + \beta_t (\beta_t - \lambda_\gamma \lambda_t) \sin^2 \theta_t \right] \right\} \\ M(\lambda_\gamma, \lambda_\gamma, \lambda_t, -\lambda_t) &= -\frac{4m_t e^2 Q_t^2}{(1 - \beta_t^2 \cos^2 \theta_t)} \\ &\quad \times \beta_t \sin \theta_t \cos \theta_t \left[\lambda_\gamma i d_t - m_t d_t^2 \right] \\ M(\lambda_\gamma, -\lambda_\gamma, \lambda_t, \lambda_t) &= \frac{4m_t e^2 Q_t^2}{\sqrt{s}(1 - \beta_t^2 \cos^2 \theta_t)} \\ &\quad \times \left[\lambda_t \beta_t + i d_t \frac{s}{2m_t} \beta_t^2 - d_t^2 \frac{s}{2} \lambda_t \beta_t \right] \sin^2 \theta_t \\ M(\lambda_\gamma, -\lambda_\gamma, \lambda_t, -\lambda_t) &= \frac{2\beta_t e^2 Q_t^2}{(1 - \beta_t^2 \cos^2 \theta_t)} \sin \theta_t \left\{ (\lambda_\gamma \lambda_t + \cos \theta_t) \right. \\ &\quad \left. - d_t^2 \frac{s}{2} \left[\frac{4m_t^2}{s} \cos \theta_t + \lambda_\gamma \lambda_t (1 - \beta_t^2 \cos^2 \theta_t) \right] \right\}. \quad (5.13) \end{aligned}$$

These expressions agree with those in [46].

The number of events for the process $\gamma\gamma \rightarrow X$, in terms of the luminosity distribution (Equation 5.7) and the Stokes parameters of the two photon beams, ξ_i and $\bar{\xi}_i$, is given by Ginzburg *et al.* [4] as

$$dN_{\gamma\gamma \rightarrow X} = dL_{\gamma\gamma} \left(d\sigma_{00} + \Lambda d\tau + \xi_2 \bar{\xi}_2 d\tau_{22} + \xi_2 d\sigma_{20} + \bar{\xi}_2 d\sigma_{02} \right). \quad (5.14)$$

If the photon beam is circularly polarized, and if there is no transverse electron polarization and linear laser beam polarization, then ξ_2 corresponds to the helicity of the photon beam. At zero conversion distance dN becomes

$$dN_{\gamma\gamma \rightarrow X} = dL_{\gamma\gamma} \left(d\sigma_{00} + \xi_2 \bar{\xi}_2 d\tau_{22} + \xi_2 d\sigma_{20} + \bar{\xi}_2 d\sigma_{02} \right). \quad (5.15)$$

Expressions for $d\sigma_{ij}$ and ξ_2 are given in Section B.4. The density matrix elements of the production process corresponding to different $d\sigma_{ij}$, in case of t decaying leptonically with \bar{t} decaying hadronically (ρ^+) and *vice versa* (ρ^-), are given in Appendix B, Section B.5. Only terms upto order d_t are kept assuming higher order terms are negligible.

Expressions for the decay amplitudes are given by Equations 2.13 and 2.14. Using all these we get the following differential cross sections (see Equation 2.17).

$$\begin{aligned} \frac{d\sigma_{ij}^\pm}{d \cos \theta_t dE_l d \cos \theta_l d\phi_l} &= \frac{3\alpha^2 \beta}{16x_w^2 \sqrt{s}} \frac{E_l}{\Gamma_t \Gamma_W m_W} \left(\frac{1}{1 - \beta \cos \theta_u} - \frac{4E_l}{\sqrt{s}(1 - \beta^2)} \right) \\ &\times \left\{ \left[\rho_{ij}^\pm(++) + \rho_{ij}^\pm(--) \right] (1 - \beta \cos \theta_u) \right. \\ &+ \left[\rho_{ij}^\pm(++) - \rho_{ij}^\pm(--) \right] (\cos \theta_u - \beta) \\ &\left. + 2 \operatorname{Re} \left(\rho_{ij}^\pm(+-) \right) (1 - \beta^2) \right\} \end{aligned}$$

$$\begin{aligned} & \times \sin \theta_t \sin \theta_l (\cos \theta_t \cos \phi_l - \sin \theta_t \cot \theta_l) \\ & + 2 \operatorname{Im} \left(\rho_{ij}^{\pm} (+-) \right) (1 - \beta^2) \sin \theta_t \sin \theta_l \sin \phi_l \} . \end{aligned} \quad (5.16)$$

This cross section is integrated over the luminosity spectrum (Equation 5.7) to get the number of events. *i.e.*,

$$dN = \int \frac{dL_{\gamma\gamma}}{dW} d\sigma(W) dW,$$

where $W = \sqrt{s}$ is the invariant mass of the two photon state.

Charge asymmetry, as defined in Equation 3.3, is redefined in the present case to take care of the luminosity distribution to be

$$\begin{aligned} A_{ch} = & \frac{1}{2N} \left\{ \int \frac{dL_{\gamma\gamma}}{d\omega_1 d\omega_2} d\omega_1 d\omega_2 \int_{-1}^1 d \cos \theta_t \right. \\ & \times \left. \int_{\theta_0}^{\pi-\theta_0} d\theta_l \left[\frac{d\sigma^-}{d \cos \theta_t d\theta_l}(\theta_l) - \frac{d\sigma^+}{d \cos \theta_t d\theta_l}(\pi - \theta_l) \right] \right\} \end{aligned} \quad (5.17)$$

Here luminosity distribution in terms of ω_1 and ω_2 is taken, rather than that in terms of W and η , anticipating the ease in doing the computation.

Expression for the angular distribution given by Equation 5.16 is in the c.m. frame whereas the expression for A_{ch} above (Equation 5.17) is in the lab frame. Changing the variable of integration to $\cos \theta_l$ and realising that the lab frame is obtained by boosting the c.m. frame by $\beta_\gamma = \frac{\omega_1 - \omega_2}{\omega_1 + \omega_2}$, we get the lower and the upper limits of integration as

$$f(\theta_0) = \frac{\cos \theta_0^{cm} + \beta_\gamma}{1 + \beta_\gamma \cos \theta_0^{cm}}$$

and

$$\begin{aligned} g(\theta_0) &= \frac{\cos(\pi - \theta_0^{cm}) + \beta_\gamma}{1 + \beta_t \cos(P_\gamma - \theta_0^{cm})} \\ &= \frac{-\cos \theta_0^{cm} + \beta_\gamma}{1 - \beta_\gamma \cos \theta_0^{cm}}. \end{aligned}$$

Making use of the fact that

$$f(\pi - \theta_0) = \frac{-\cos \theta_0^{cm} + \beta_\gamma}{1 - \beta_\gamma \cos \theta_0^{cm}} = g(\theta_0)$$

and

$$g(\pi - \theta_0) = \frac{\cos \theta_0^{cm} + \beta_\gamma}{1 + \beta_\gamma \cos \theta_0^{cm}} = f(\theta_0)$$

we get the final expression for A_{ch} as (refer Equation 4.9)

$$\begin{aligned} A_{ch} &= \frac{1}{2N} \left\{ \int \frac{dL_{\gamma\gamma}}{d\omega_1 d\omega_2} d\omega_1 d\omega_2 \int_{-1}^1 d\cos \theta_t \right. \\ &\quad \times \left. \int_{f(\theta_0)}^{g(\theta_0)} d\cos \theta_l \left[\frac{d\sigma^-}{d\cos \theta_t d\cos \theta_l}(\theta_l) - \frac{d\sigma^+}{d\cos \theta_t d\cos \theta_l}(\theta_l) \right] \right\} \quad (5.18) \end{aligned}$$

where the differential cross section is in the c.m. frame. A similar expression holds for A_{fb} .

$$\begin{aligned} A_{fb} &= \frac{1}{2N} \int \frac{dL_{\gamma\gamma}}{d\omega_1 d\omega_2} d\omega_1 d\omega_2 \int_{-1}^1 d\cos \theta_t \\ &\quad \times \left\{ \int_{f(\theta_0)}^{\beta_\gamma} d\cos \theta_l \left[\frac{d\sigma^-}{d\cos \theta_t d\cos \theta_l}(\theta_l) - \frac{d\sigma^+}{d\cos \theta_t d\cos \theta_l}(\theta_l) \right] \right. \\ &\quad \left. + \int_{\beta_\gamma}^{g(\theta_0)} d\cos \theta_l \left[\frac{d\sigma^-}{d\cos \theta_t d\cos \theta_l}(\theta_l) - \frac{d\sigma^+}{d\cos \theta_t d\cos \theta_l}(\theta_l) \right] \right\}. \quad (5.19) \end{aligned}$$

These asymmetries are used to fix the DFF's using

$$A_{ch}(c_d^\gamma, c_d^Z) = \frac{1.65}{2\sqrt{N}}$$

as described in Section 1.6. The following section discusses the results we obtained.

5.3 Results

Charge asymmetry and forward-backward asymmetry combined with charge asymmetry are studied for different initial beam helicities. Also, fixing a particular helicity combination, asymmetries are studied at different electron beam energies and for different laser beam energies. In doing so, the value of x is kept constant. Variation of asymmetries with x , fixing variables like the helicities and cut-off angle is also considered. Asymmetries are also studied at different cut-off angles with beam energy and other parameters kept constant. All the calculations are done assuming a geometrical integrated luminosity of 20 fb^{-1} for the electron-electron collider. We shall discuss the results in the following.

Table 5.1 displays asymmetries obtained for different helicity combinations. There is no combined asymmetry when both $\lambda_e^1 = \lambda_e^2$ and $\lambda_l^1 = \lambda_l^2$. This is expected as the forward and backward directions cannot be distinguished in this case because the two colliding photons are identical. In SM electromagnetic interactions respect parity and hence the cross section is symmetric under $\lambda_e^i \leftrightarrow -\lambda_e^i$. Thus the total number of events, which gets contribution only from SM, remains the same under this transformation.

The best limit obtained is $2.3 \times 10^{-17} \text{ e cm}$ coming from A_{fb} with initial beam

				Asymmetries		Limits on Im d_t from		
λ_e^1	λ_e^2	λ_t^1	λ_t^2	N	A_{ch}	A_{fb}	$ A_{ch} $	$ A_{fb} $
(in $10^{-16} e cm$)								
-5	-5	-1	-1	76	-.019	0	2.76	
-5	-5	1	-1	252	-.025	-.129	1.19	.23
-5	-5	-1	1	252	-.025	.129	1.19	.23
-5	-5	1	1	631	-.035	0	.54	
.5	-5	-1	-1	73	-.024	.013	2.31	4.25
.5	-5	1	-1	32	-.021	-.080	3.89	1.03
.5	-5	-1	1	163	-.021	.033	1.73	1.12
.5	-5	1	1	73	-.024	.013	2.31	4.25
-5	.5	-1	-1	73	-.024	-.013	2.31	4.25
-5	.5	1	-1	163	-.021	-.033	1.73	1.12
-5	.5	-1	1	32	-.021	.080	3.89	1.03
-5	.5	1	1	73	-.024	-.013	2.31	4.25
.5	.5	-1	-1	631	-.035	0	.54	
.5	.5	1	-1	252	-.025	-.129	1.19	.23
.5	.5	-1	1	252	-.025	.129	1.19	.23
.5	.5	1	1	76	-.019	0	2.76	
Unpolarized				194	-.028	0	1.19	

Table 5.1: Asymmetries and corresponding 90% C.L. limits obtained on the DFF's for various combinations of initial beam helicities. Top quark mass is kept at $m_t = 174$ GeV and an initial electron beam of energy $E_b = 250$ GeV and a laser beam of energy $w_0 = 1.24$ eV are considered. The cut-off angle take is $\theta_0 = 30^\circ$. N is the total number of events. Asymmetries are for $\text{Im } d_t = \frac{e}{2m_t}$.

E_b GeV	N	Asymmetries		Limits from	
		A_{ch}	A_{fb}	$ A_{ch} $ (in $10^{-16} e cm$)	$ A_{fb} $
250	252	-.025	.129	1.191	.229
500	1441	-.167	.420	.074	.029
750	1210	-.223	.347	.060	.039
1000	996	-.227	.244	.065	.061

Table 5.2: Variation of DFF limits obtained at different beam energies keeping x value at 4.75 (by choosing suitable laser beam energy in each case). Top quark mass of 174 GeV is considered and the cut-off angle is taken to be 30° . Asymmetries are for $\text{Im } d_t = \frac{e}{2m_t}$. Helicities of the initial electron and laser beams are $\lambda_e^1 = -.5$, $\lambda_e^2 = -.5$, $\lambda_l^1 = -1$ and $\lambda_l^2 = 1$.

helicities satisfying $\lambda_e^1 = \lambda_e^2$ and $\lambda_l^1 = -\lambda_l^2$. Limit from A_{ch} in this case is $1.19 \times 10^{-16} e cm$. We consider this helicity combination for further analysis. It may be noted, however, that with unpolarized electron beams and laser beams we can measure only the charge asymmetry. Limit obtained on the DFF in the unpolarized case is $1.19 \times 10^{-16} e cm$. Forward-backward combined asymmetry is zero in this case.

Table 5.2 lists the limits for different electron beam energies. The table shows that the limits are better around a beam energy of 500 GeV in the case of combined asymmetry and at around 750 GeV in the case of charge asymmetry. The limit obtained at this value is almost 20 times better than the limit at 250 GeV in the case of charge asymmetry while in the case of combined asymmetry it is a factor of almost 8.

Cut-off angle is varied to study the variation of limits on DFF's. The result is

θ_0 deg.	N	Asymmetries		Limits from	
		A_{ch}	A_{fb}	$ A_{ch} $ (in 10^{-16} e cm)	$ A_{fb} $
0	290	.000	.149		.185
10	286	-.003	.146	9.234	.189
20	273	-.012	.140	2.444	.203
30	251	-.025	.128	1.197	.230
40	221	-.041	.113	.774	.277
50	186	-.057	.095	.599	.362
60	144	-.073	.074	.534	.529
70	98	-.086	.050	.551	.937
80	50	-.094	.026	.706	2.595

Table 5.3: Limits on EDFF of the top quark from the charge asymmetry and the combined asymmetry for different cut-off angles. Helicities of the initial electron and laser beams are $\lambda_e^1 = -.5$, $\lambda_e^2 = -.5$, $\lambda_l^1 = -1$ and $\lambda_l^2 = 1$. A top quark mass of 174 GeV and an electron beam energy of 250 GeV are used. Laser beam energy is taken to be 1.24 eV, which corresponds to $x = 4.75$. Asymmetries are at $\text{Im } d_t = \frac{e}{2m_t}$.

tabulated in Table 5.3. Charge asymmetry, which is the total leptonic charge in the semi-leptonic decay of $t\bar{t}$ is zero when there is no cut-off. Charge asymmetry is found to give best limits on the dipole form factors around a cut-off of 60° whereas the combined asymmetry is better at lower cut-offs.

For a fixed beam energy and at a fixed cut-off angle, variation of DFF limits with x is studied in Table 5.4. From the table it is clear that the limits are better at higher x values¹

To conclude, we find that for an electron beam energy of 250 GeV, and for a suitable

¹For $x > 4.83$ e^+e^- production due to the collision of high energy photon beam with laser beam is considerable [4]. This introduces additional e^+e^- beam backgrounds as well as degrading the photon spectrum.

x	N	Asymmetries		Limits from	
		A_{ch}	A_{fb}	$ A_{ch} $	$ A_{fb} $
				(in 10^{-16} e cm)	
2.60	1.1	-.0039	.0343	112.81	12.83
3.20	28.8	-.0111	.0717	7.85	1.22
4.74	250.8	-.2468	.128	1.20	.23

Table 5.4: DFF's calculated at different x values for a fixed beam energy, $E_b = 250$ GeV at a cut-off angle of 30° . Top quark mass is taken to be 174 GeV and the helicities of the initial beams are $\lambda_e^1 = -.5$, $\lambda_{e\gamma}^2 = -.5$, $\lambda_l^1 = -1$ and $\lambda_l^2 = 1$.

choice of longitudinal polarizations of the laser photons and electron beams, and assuming a geometrical luminosity of 20 fb^{-1} for the electron beam, it is possible to obtain limits on the imaginary part of the top EDFF of the order of 10^{-17} e cm . An order of magnitude improvement is possible if the beam energy is increased to 500 GeV. In that case the sensitivity would be comparable to that obtained in $e^+e^- \rightarrow t\bar{t}$ with $\sqrt{s} = 500 \text{ GeV}$.

For comparison, we mention the result of Choi and Hagiwara [49]. They have obtained limits on the real part of the dipole moments of the top quark from a number asymmetry and with linearly polarized photons, to be of the order of 10^{-18} e cm for a beam energy of 250 GeV.

Chapter 6

CP-violating Effective Vertex in a Leptoquark Model

In the previous chapters we have discussed asymmetries arising due to the electric and the weak dipole form factors of the top quark. We used an effective Lagrangian, which has a top quark dipole coupling in addition to the usual SM couplings, the presence of which violates *CP*. Various *CP*-odd asymmetries were constructed, the non-zero value of which would signal *CP* violation. These asymmetries may be used to get information on dipole form factors (DFF). The two processes we have considered were $e^+e^- \rightarrow t\bar{t}$ and $\gamma\gamma \rightarrow t\bar{t}$ with subsequent decay of $t\bar{t}$ into the semileptonic channel.

The dipole coupling term in the effective Lagrangian could arise from one of various possible sources. In this chapter we shall consider a scenario where *CP* violation originates from the fundamental couplings in a specific model. DFF's of top quark and τ lepton have been calculated in several models [18, 29, 30, 50]. In most cases the values obtained are an order below the observable level in the next generation colliders. We discuss DFF's of top quark and τ lepton arising due to

the one-loop correction to the $t\bar{t}\gamma(Z)$ vertex in the presence of a leptoquark. Leptoquarks are particles carrying simultaneously lepton and baryon number which couple leptons with quarks. In general the coupling can be complex, which may act as a source of CP violation. A large number of extensions of SM including grand unified theories, technicolour models, superstring inspired models and composite models predict the existence of colour triplet leptoquarks. Without reference to specific models, the masses and couplings of leptoquarks can be constrained using low-energy experiments [51]. These experiments test predictions of leptoquark interactions for atomic parity violation, meson decay, flavour-changing neutral currents and meson-antimeson mixing.

There have been several direct searches for leptoquarks at high energy accelerators. At the Large Electron-Positron collider (LEP) at CERN, a lower bound of 45-73 GeV for the mass of leptoquarks was put [52]. The limit coming from $p\bar{p}$ colliders is 175 GeV from D0 [53] and 131-133 GeV from CDF [54] on the mass of a scalar leptoquark decaying into an electron-jet pair. On the mass of third generation scalar leptoquark decaying into $b\tau$ CDF [54] has given a bound of 99 GeV and a bound of 80 GeV was obtained by D0 [53] for the leptoquark decaying into $b\nu_\tau$. The excess of large- Q^2 events found at the DESY collider HERA in e^+p scattering [55] could be explained using leptoquarks [56]. The earlier lower bound obtained by HERA is between 92 and 184 GeV [57]. Bounds possible at future pp , ep , e^+e^- , $e\gamma$ and $\gamma\gamma$ experiments has been a topic of serious study.

Indirect bounds on masses and couplings can be obtained from the results of low-energy experiments [51]. However, these constraints are strong only for leptoquarks that couple to quarks and leptons of the first and second generations.

While there are strong constraints on masses of leptoquarks which also couple

to pairs of quarks, thus violating baryon number as well as lepton number, the constraints on the couplings and masses of leptoquarks which do not couple to two quarks are weaker. Moreover, these constraints are strongest for the first and second generations, and considerably weaker for leptoquarks coupling only to the third generation of quarks and leptons.

Strong constraints on leptoquarks which couple to leptons and quarks of the third generation have been obtained from their contributions to the radiative corrections to Z properties [58, 59, 60]. The authors of [58] have studied vertex corrections to the leptonic partial widths of the Z induced by leptoquark loops and obtained stringent constraints on leptoquark masses and couplings. The authors of [59, 60] performed a global fit to the LEP data including contributions from a scalar leptoquark loop. They also arrive at stringent constraints on leptoquark masses and couplings.

In this chapter we consider third generation leptoquarks coupling with top quark and tau lepton within the context of $SU(2)_L \times U(1)_Y \times SU(3)_C$ gauge theory to calculate EDFF and WDFP of the top quark and the tau lepton. We also use the present experimental limits on the DFF values of the tau lepton to obtain bounds on the masses and couplings of the leptoquarks. Recently, other papers [61, 62] on DFF in third-generation leptoquark models have also appeared. We discuss their results in the last section.

We describe in the next section couplings of scalar leptoquarks with various transformation properties under $SU(2)_L \times U(1) \times SU(3)_C$. In Section 6.2 we obtain expressions for the imaginary parts of the EDFF's and WDFP's of τ and t arising from these leptoquark couplings, and write dispersion relations for obtaining the corresponding real parts. In Section 6.3 we present numerical results and conclu-

sions.

6.1 Scalar Leptoquark Couplings in $SU(2)_L \times U(1) \times SU(3)_C$ Theory

We will describe in this section leptoquark couplings in an $SU(2)_L \times U(1) \times SU(3)_C$ gauge theory, assuming that baryon-number violating couplings to diquarks are somehow forbidden, as required by strong bounds on proton decay searches. In that case, the only possible leptoquark representations which could have couplings to the standard-model representations of quarks and leptons are as shown in Table 6.1, together with their quantum numbers [63].

The most general Lagrangian containing all possible forms of couplings of scalar leptoquarks to a lepton and quark pair is given by

$$\mathcal{L}_{eff} = \mathcal{L}_{F=2} + \mathcal{L}_{F=0}, \quad (6.1)$$

where

$$\mathcal{L}_{F=2} = (g_{1L} \bar{q}_R^c i\tau_2 l_L + g_{1R} \bar{u}_L^c e_R) S_1 + \tilde{g}_{1R} \bar{d}_L^c e_R \tilde{S}_1 + g_{3L} \bar{q}_R^c i\tau_2 \vec{l}_L \cdot \vec{S}_3 + h.c., \quad (6.2)$$

$$\mathcal{L}_{F=0} = h_{2L} \bar{u}_R R_2^T i\tau_2 l_L + h_{2R} \bar{q}_L e_R R_2 + \tilde{h}_{2L} \bar{d}_R \tilde{R}_2^T i\tau_2 l_L + h.c., \quad (6.3)$$

The two pieces correspond to the fermion number $F = 0$ for the leptoquarks R_2 and \tilde{R}_2 , and $F = -2$ for S_1 , \tilde{S}_1 and S_3 . Colour indices are suppressed in writing Equation 6.1. The $SU(2)_L \times U(1) \times SU(3)_c$ quantum numbers and electric charges are of the various leptoquarks are given in Table 6.1.

	$SU(2)_L$	$U(1)$	$SU(3)_c$	Q
S_1	1	$\frac{1}{3}$	3^*	$\frac{1}{3}$
\tilde{S}_1	1	$\frac{4}{3}$	3^*	$\frac{4}{3}$
S_3	3	$\frac{1}{3}$	3^*	$\frac{4}{3}, \frac{1}{3}, -\frac{2}{3}$
R_2	2	$\frac{2}{6}$	3	$\frac{5}{3}, \frac{2}{3}$
\tilde{R}_2	2	$\frac{1}{6}$	3	$\frac{2}{3}, -\frac{1}{3}$

Table 6.1: $SU(2)_L$, $U(1)$, $SU(3)_c$ and electric charge assignments of the various leptoquarks

Of the various couplings occurring in Equation 6.1, those of \tilde{S}_1 and \tilde{R}_2 do not contribute to τ and t DFF's in the limit of massless neutrinos and b quark, and so we will not consider these.

The low-energy constraints arising from decays of pseudoscalar mesons are very stringent, unless the leptoquark couplings to the light quarks are chiral. Hence many authors assume couplings in Equation 6.1 to be either left handed or right handed. However, we are going to consider only the third generation leptoquarks on whose couplings there are no limits from meson decays. So we need not assume their couplings to be chiral. More importantly, we need both left- and right-handed couplings to be present for the EDFF and WDFF to be nonzero. If, however, the third generation leptoquarks mix substantially with those of the first and second generations, the low-energy constraints would apply more or less unchanged. We will therefore assume mixing to be absent.

While only one of the components of each leptoquark multiplets would contribute to the form factors we calculate, it is important to note that the constraints we will use on the leptoquark couplings and masses were derived assuming that leptoquarks within a multiplet are degenerate.

The couplings of leptoquarks to a single γ or Z is given by

$$\mathcal{L}_{\gamma,Z} = -ie \sum_i \phi_i^\dagger \overleftrightarrow{\partial}_\mu \phi_i \left[Q_i A^\mu - \frac{T_{3L} - Q_i s_W^2}{s_W c_W} Z^\mu \right], \quad (6.4)$$

where ϕ_i are the various scalar fields, T_{3i} and Q_i are the respective values of the third component of weak isospin and electric charge, and $c_W = \cos \theta_W$, $s_W = \sin \theta_W$, θ_W being the weak mixing angle.

We use the couplings written down in Equations 6.2, 6.3 and 6.4 to obtain expressions for the EDFF and WDF of τ and t at the one-loop level in the next section.

6.2 Expressions for Electric and Weak Dipole Form Factors

Using the Lagrangian described in the last section we shall look at the one-loop corrections to the $t\bar{t}\gamma(Z)$ vertex. We use Cutkosky rules [64] to calculate the imaginary part of the DFF and from this the real part is obtained using a dispersion relation.

6.2.1 EDFF and WDF of the Top Quark

At one-loop level the diagrams responsible for the correction to the $t\bar{t}\gamma(Z)$ coupling due to the leptoquark are given in Figure 6.1. We use the symbol ϕ for the generic leptoquark.

The lepton could be ν_τ instead of τ interacting with a leptoquark of different T_3 and Q values. However, as we shall see, the contribution to the CP -violating DFF's

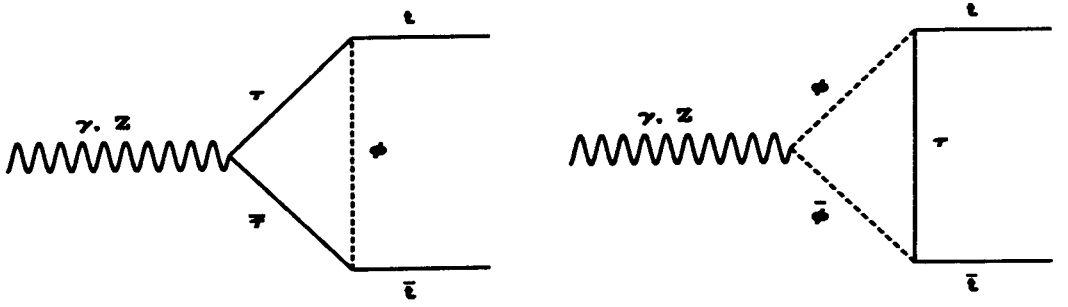


Figure 6.1: Feynman diagrams corresponding to one-loop correction to the $t\bar{t}\gamma(Z)$ vertex in the presence of a third generation leptoquark.

turns out to be proportional to the mass of the virtual lepton because of chirality flip in scalar couplings. In the limit of small ν_τ mass, only the τ contribution is present.

We use Cutkosky rule to calculate the absorptive part of the process. This means considering intermediate particles to be on shell and hence the conditions on the γ/Z boson momentum for diagram in Figure 6.1 are $q^2 > 4m_\tau^2$ and $q^2 > 4m_\phi^2$ in case of τ pair production and leptoquark pair production respectively, where m_ϕ is the leptoquark mass. We calculate the vertex contribution coming from these two diagrams. Appendix C shows how, after doing the loop integration, the comparison with the effective vertex is made and the expression for dipole form factor is obtained in terms of the parameters (masses and couplings) of the theory.

Using the couplings given in Equations 6.2 and 6.3 we obtain the imaginary part of the top quark EDFF and WDFF as

$$\begin{aligned}
 \text{Im } d_t^{\gamma}(s) &= -\frac{eg_\phi^2}{2\pi s} m_\tau \text{Im}(a^*b) \left\{ -F_1^t(s) + Q F_2^t(s) \right\}, \\
 \text{Im } d_t^Z(s) &= -\frac{eg_\phi^2}{2\pi s \sin \theta_W \cos \theta_W} m_\tau \text{Im}(a^*b) \\
 &\quad \times \left\{ \frac{1}{2} \left(-\frac{1}{2} + 2 \sin^2 \theta_W \right) F_1^t(s) + (T_3 - Q \sin^2 \theta_W) F_2^t(s) \right\}, \quad (6.5)
 \end{aligned}$$

where

$$F_1^t(s) = \frac{1}{\beta_t^2} \left\{ \beta_\tau + \frac{1}{s\beta_t} (m_t^2 + m_\phi^2 - m_\tau^2) \log \left(\frac{1 + \beta_t}{1 - \beta_t} \right) \right. \\ \left. \times \left[\frac{2(m_t^2 + m_\tau^2 - m_\phi^2) - s(1 - \beta_t\beta_\tau)}{2(m_t^2 + m_\tau^2 - m_\phi^2) - s(1 + \beta_t\beta_\tau)} \right] \right\} \theta(s - 4m_t^2), \quad (6.6)$$

and

$$F_2^t(s) = \frac{1}{2\beta_t^2} \left\{ \beta_\phi - \frac{1}{s\beta_t} (m_t^2 + m_\phi^2 - m_\tau^2 - \frac{s}{2}) \log \left(\frac{1 + \beta_t}{1 - \beta_t} \right) \right. \\ \left. \times \left[\frac{2(m_t^2 + m_\tau^2 - m_\phi^2) - s(1 - \beta_t\beta_\phi)}{2(m_t^2 + m_\tau^2 - m_\phi^2) - s(1 + \beta_t\beta_\phi)} \right] \right\} \theta(s - 4m_\phi^2). \quad (6.7)$$

In the above equation, T_3 and Q refer respectively to the third component of isospin and charge of the leptoquark ϕ , g_ϕ is the absolute value of the coupling constant, assuming $|g_L| = |g_R|$ (and $|h_{2L}| = |h_{2R}|$) occurring in 6.2 and 6.3, and a and b are phase factors of the corresponding vector and axial vector couplings (see Appendix C). β_t , β_τ and β_ϕ refer to the velocities of t , τ and ϕ ,

$$\beta_{t,\tau,\phi} = \sqrt{1 - \frac{4m_{t,\tau,\phi}^2}{s}}. \quad (6.8)$$

The expression in Equation 6.6 is valid for $s > 4m_t^2$. $F_1^t(s)$ for $2m_\tau < \sqrt{s} < 2m_t$ is given by the analytic continuation of Equation 6.6.

$$F_1^t(s) = \frac{1}{\beta_t^2} \left\{ \beta_\tau + \frac{2}{s\sqrt{-\beta_t^2}} (m_t^2 + m_\phi^2 - m_\tau^2) \right. \\ \left. \times \tan^{-1} \left[\frac{\sqrt{-\beta_t^2} \beta_\tau s}{2(m_t^2 + m_\tau^2 - m_\phi^2) - s} \right] \right\} \theta(s - 4m_\tau^2) \theta(4m_t^2 - s) \quad (6.9)$$

The real parts of the form factors are obtained using an unsubtracted dispersion relation

$$\text{Re } d_t^{\gamma, Z}(s) = \frac{P}{\pi} \int_{4m_\tau^2}^{\infty} \frac{\text{Im } d_t^{\gamma, Z}(s')}{s' - s} ds', \quad (6.10)$$

where P denotes the principal part of the integral.

It can be seen that the dispersion integrals are convergent and do not need any subtraction. This is to be expected since the dipole form factors, which correspond to dimension 5 operators, should be finite in a renormalizable theory.

6.2.2 EDFF and WDF of the τ Lepton

The EDFF and WDF of the tau lepton also arise in the same leptoquark theory from exactly analogous diagrams as in Figure 6.1, with the roles of t and τ interchanged. Proceeding exactly as in the previous section, we obtain expressions for the imaginary parts of the tau lepton EDFF and WDF, neglecting the b mass.

$$\begin{aligned} \text{Im } d_\tau^\gamma(s) &= \frac{eg_\phi^2}{2\pi s} m_t \text{Im}(a^* b) \left\{ \frac{2}{3} F_1^\tau(s) + Q F_2^\tau(s) \right\}, \\ \text{Im } d_\tau^Z(s) &= -\frac{eg_\phi^2}{2\pi s \sin \theta_W \cos \theta_W} m_t \text{Im}(a^* b) \\ &\quad \times \left\{ \frac{1}{2} \left(\frac{1}{2} - \frac{4}{3} \sin^2 \theta_W \right) F_1^\tau(s) + (T_3 - Q \sin^2 \theta_W) F_2^\tau(s) \right\}, \end{aligned} \quad (6.11)$$

where

$$F_1^\tau(s) = \frac{1}{\beta_\tau^2} \left\{ \beta_t + \frac{1}{s\beta_\tau} (m_\tau^2 + m_\phi^2 - m_t^2) \log \left(\frac{1 + \beta_t}{1 - \beta_t} \right) \right\}$$

$$\times \left[\frac{2(m_\tau^2 + m_t^2 - m_\phi^2) - s(1 - \beta_t \beta_\tau)}{2(m_\tau^2 + m_t^2 - m_\phi^2) - s(1 + \beta_t \beta_\tau)} \right] \Big\} \theta(s - 4m_t^2), \quad (6.12)$$

and

$$\begin{aligned} F_2^\tau(s) = & \frac{1}{2\beta_\tau t^2} \left\{ \beta_\phi - \frac{1}{s\beta_\tau} (m_\tau^2 + m_\phi^2 - m_t^2 - \frac{s}{2}) \log \left(\frac{1 + \beta_t}{1 - \beta_t} \right) \right. \\ & \times \left. \left[\frac{2(m_\tau^2 - m_t^2 - m_\phi^2) - s(1 - \beta_t \beta_\phi)}{2(m_\tau^2 - m_t^2 - m_\phi^2) - s(1 + \beta_t \beta_\phi)} \right] \right\} \theta(s - 4m_\phi^2). \end{aligned} \quad (6.13)$$

Since both m_t and m_ϕ are larger than m_τ , there is no domain where an analytic continuation is needed.

As before, the real parts of the form factors are given by the unsubtracted dispersion relations:

$$\text{Re } d_{\tau}^{\gamma, Z}(s) = \frac{P}{\pi} \int_{4m_\tau^2}^{\infty} \frac{\text{Im } d_{\tau}^{\gamma, Z}(s')}{s' - s} ds'. \quad (6.14)$$

In the next section we will evaluate the real and imaginary parts of the t and τ form factors numerically for different choices of masses and couplings of the leptoquarks. Using the experimental limits on the tau lepton DFF's we obtain bounds on the masses and couplings of the leptoquarks. This is also discussed in the next section.

6.3 Discussion of Numerical Results

We use here the expressions given in the previous section to get numerical values for the various form factors. While we have analytic expressions for the imaginary

parts, the real parts, given by the dispersion integrals, have been evaluated by numerical integration.

To investigate how large the form factors can be consistent with LEP constraints, we have plotted in Figure 6.2 the τ form factors as functions of \sqrt{s} . We have chosen $m_t = 180$ GeV and a maximal value $\text{Im}(a^*b) = 1/2$. We have considered three different leptoquark masses, viz., 200 GeV, 250 GeV and 500 GeV. g_ϕ is chosen to be 1.

In all cases dipole form factors are larger for higher leptoquark masses upto around c.m. energy of 500 GeV. At higher energies dependence on the mass becomes weaker than that at lower energies. Among the leptoquarks belonging to the three representations considered, R_2 (see Table 6.1 for quantum numbers) gives the largest form factors. The leptoquarks S_3 (isospin triplet) and S_1 (isospin singlet) give the same values for DFF's except for the sign. Hence, results of only R_2 and S_3 are displayed here. Figure 6.3 shows the dependence of real part of the τ DFF's on the c.m. energy. We are working at a top quark mass of 180 GeV and hence there is a peak at 360 GeV. A similar, but not so prominent, behaviour is seen at the leptoquark threshold also.

In the case of top quarks the behaviour is similar to that of the tau lepton DFF's. Figure 6.4 shows the variation of the top quark DFF with c.m. energy.

Note that Figures corresponding to top quark imaginary and real parts of EDFF, and real part of WDFF are plotted at in two parts, with different scales for the y axis in the two parts. Behaviour is similar to that in tau lepton case with peaks at τ and leptoquark resonances.

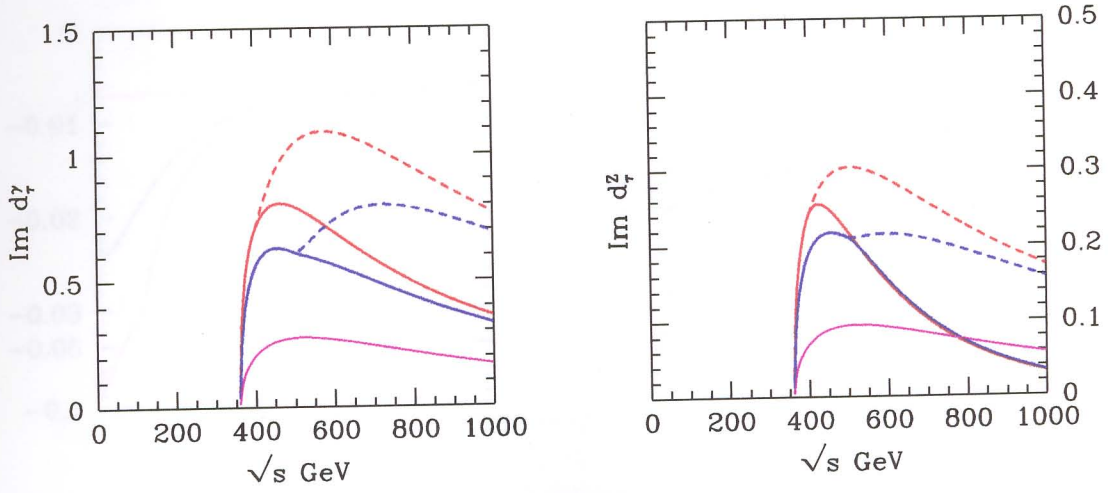


Figure 6.2: Imaginary part of electric (left) and weak (right) dipole form factors of τ in units of $10^{-18} e cm$ as a function of c.m. energy \sqrt{s} . Red, blue and magenta correspond to leptoquark masses of 200 GeV, 250 GeV and 500 GeV respectively and the solid line is with isospin doublet leptoquark while the dashed line is with isospin triplet leptoquark. g_ϕ is chosen to be 1.

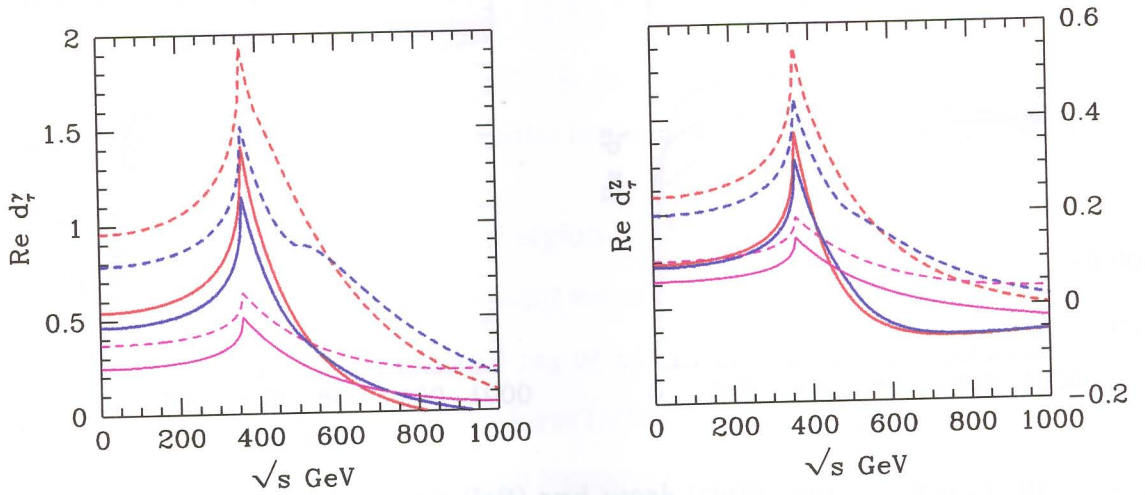


Figure 6.3: Real part of the electric (left) and weak (right) dipole form factors of τ in units of $10^{-18} e cm$ as a function of c.m. energy \sqrt{s} . Colour indices are the same as those in Figure 6.2.

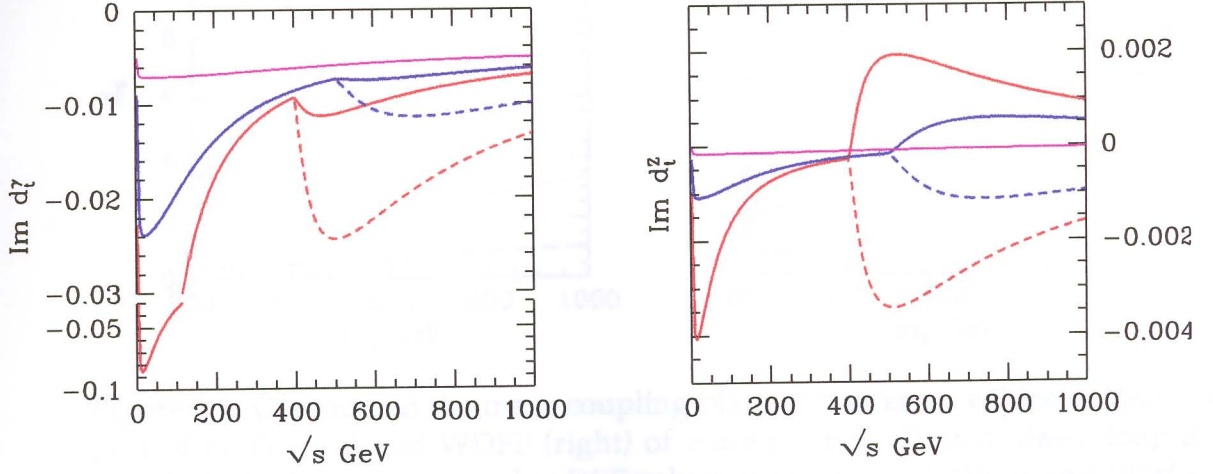


Figure 6.4: Imaginary part of electric (left) and weak (right) dipole form factors of top quark in units of 10^{-18} e cm as a function of c.m. energy, \sqrt{s} . Red, blue and magenta correspond to leptoquark masses of 200 GeV, 250 GeV and 500 GeV respectively and the solid line is with R_2 while the dashed line is with S_3 .

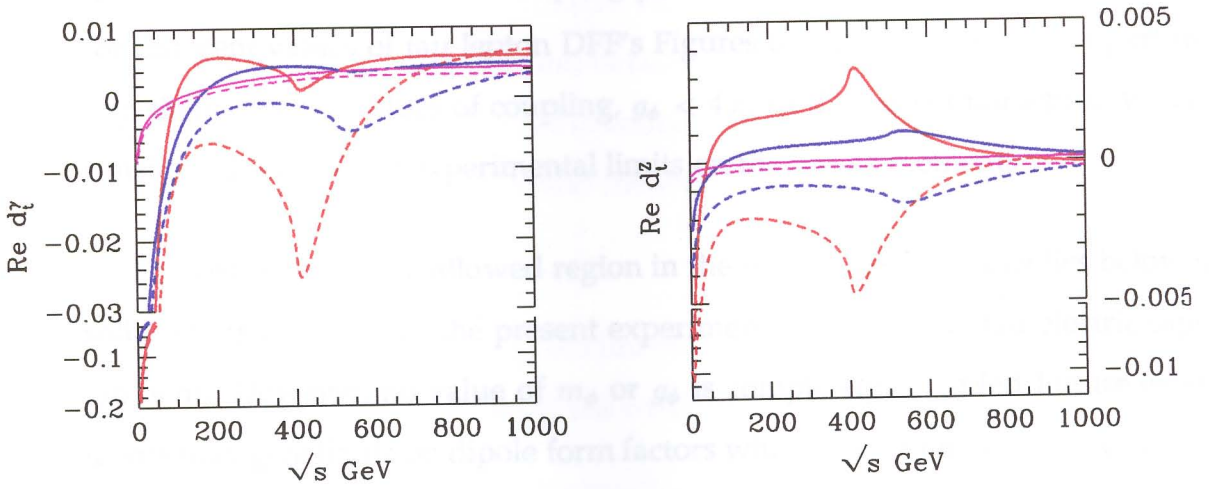


Figure 6.5: Real part of electric (left) and weak (right) dipole form factors of top quark in units of 10^{-18} e cm as a function of c.m. energy, \sqrt{s} . Red, blue and magenta correspond to leptoquark masses of 200 GeV, 250 GeV and 500 GeV respectively and the solid line is with R_2 while the dashed line is with S_3 .

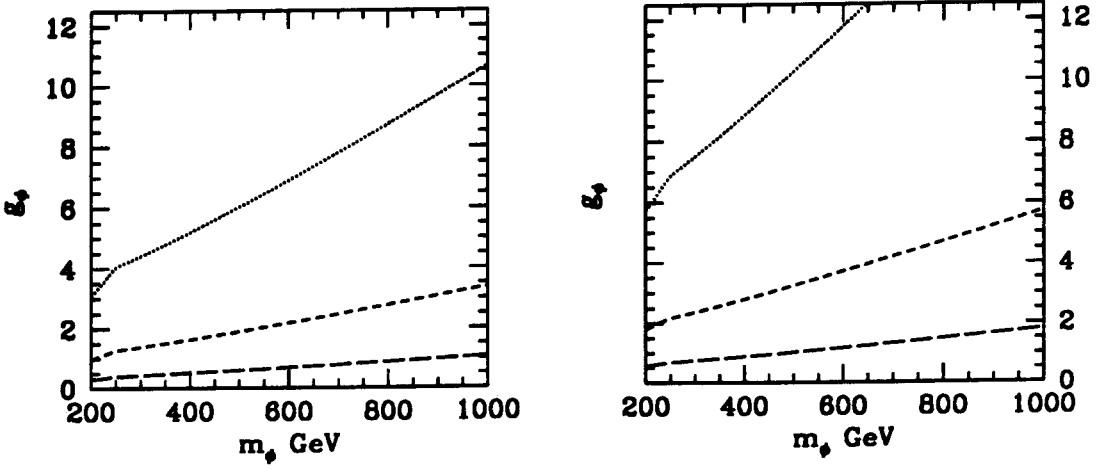


Figure 6.6: Contours in the mass-coupling plane for different values of imaginary part of EDFF (left) and WDFF (right) of τ are plotted. Dotted, dash, long dash and dash-dot lines correspond to DFF values of 10^{-17} , 10^{-18} , 10^{-19} and 10^{-20} $e\text{ cm}$ respectively. A c.m. energy of 500 GeV is assumed.

At a fixed c.m. energy the form factors are functions of two parameters – the mass and coupling of the leptoquark considered. From an assumed value of the form factor it is possible to get relation between mass and coupling of the leptoquark. Contours in the mass-coupling plane for the doublet leptoquark are given for different values of tau lepton DFF's Figures 6.6 and 6.7. Validity of perturbation theory allows values of coupling, $g_\phi < 4\pi$. In the case of tau lepton we have considered the present experimental limits on the dipole moments

Figure 6.7 shows the allowed region in the $m_\phi - g_\phi$ plane which lies below the solid line if we consider the present experimental limit on the tau electric dipole moment. However, no value of m_ϕ or g_ϕ is completely excluded. Future experiments may give limits on dipole form factors which will put more stringent upper bounds on the coupling for a fixed leptoquark mass and for a fixed coupling lower bounds on the mass will become more stringent

As mentioned before, LEP results have been used to obtain constraints on masses

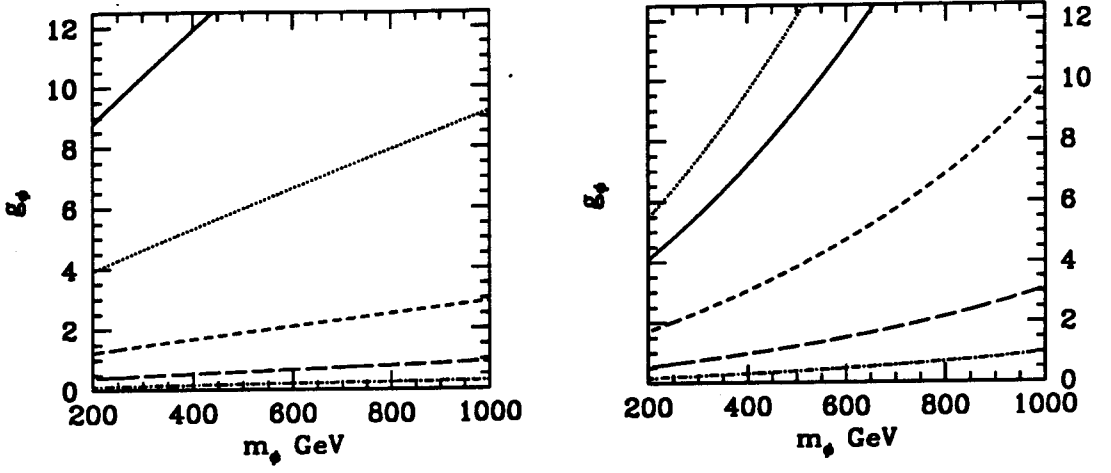


Figure 6.7: Contours in the mass-coupling plane for different values of real part of EDFF (left) and WDFF (right) of τ are plotted. Type of lines and corresponding DFF values are the same as those in Figure 6.6. The solid curve corresponds to the experimental bounds on the dipole momenta, which are $d_\tau^\gamma = 5 \times 10^{-17} \text{ e cm}$ $\text{Re } d_\tau^Z = 5.6 \times 10^{-18} \text{ e cm}$. EDFF values are at a c.m.energy of 4 GeV while WDFF values are at 91.18 GeV. Top quark mass is taken to be 180 GeV in all cases.

and couplings for third-generation leptoquarks [58, 59, 60]. We have chosen Eboli's [60] limits to compare with the constraints we get from the dipole form factors. Figure 6.8 shows contours for different values of the real part of the electric dipole form factor of τ along with the limit obtained by Eboli[60] in the $m_\phi - g_\phi$ plane. To accommodate their limits we have to restrict the electric dipole form factors of τ to be smaller than about 10^{-19} e cm and the weak dipole form factors must be smaller than about 10^{-20} e cm .

The best limits on m_ϕ and g_ϕ obtainable from the experimental limits on form factors is that from the real part of the weak dipole moment of the tau lepton.

In the case of top quark there are no experimental limits. Again, to accommodate Eboli's result we have to have electric dipole form factors of the order of 10^{-22} e cm or less and weak electric dipole form factors of the order of 10^{-23} e cm or less.

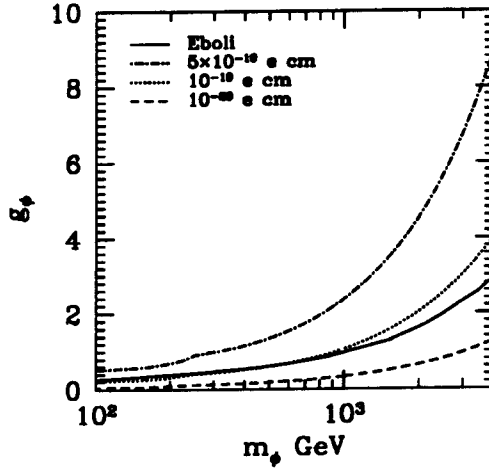


Figure 6.8: Contours in the mass-coupling plane for third generation doublet leptoquark with charge $5/3 e$. Solid line represents the limits from the one-loop calculation by Eboli[60] while the other curves correspond to different values of the real part of the electric dipole form factor of tau lepton. Top quark mass of 175 GeV is assumed and our calculations are done at a c.m. energy of 500 GeV.

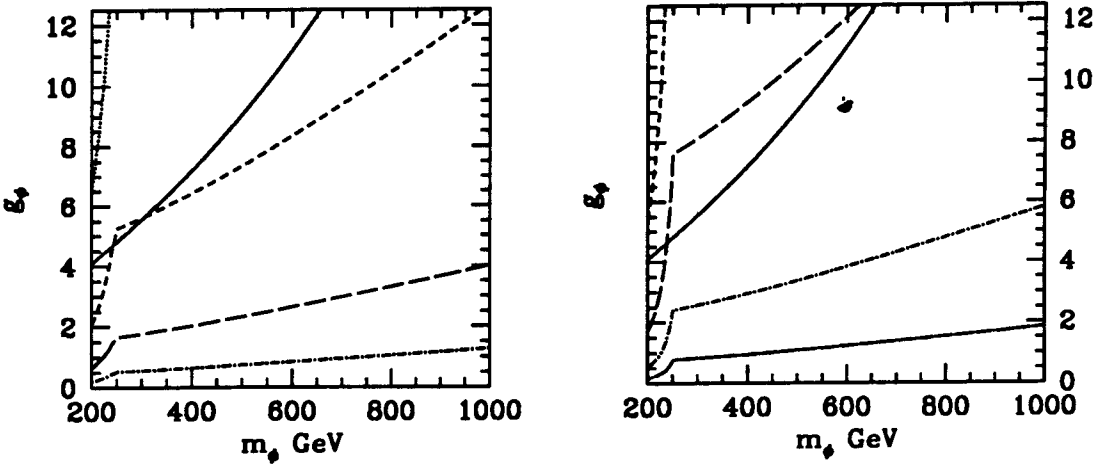


Figure 6.9: Contours in the mass-coupling plane for different values of imaginary part of EDFF (left) and WDF (right) of the top quark are plotted. Dotted, dash, long dash, dash-dot and long dash-dot lines correspond to DFF values of 10^{-18} , 10^{-19} , 10^{-20} , 10^{-21} and $10^{-22} e cm$ respectively. The solid curve corresponds to the experimental bound on the real part of the weak dipole moment of τ lepton, $5.6 \times 10^{-18} e cm$. A c.m. energy of 500 GeV and a top quark mass of 180 GeV are assumed.

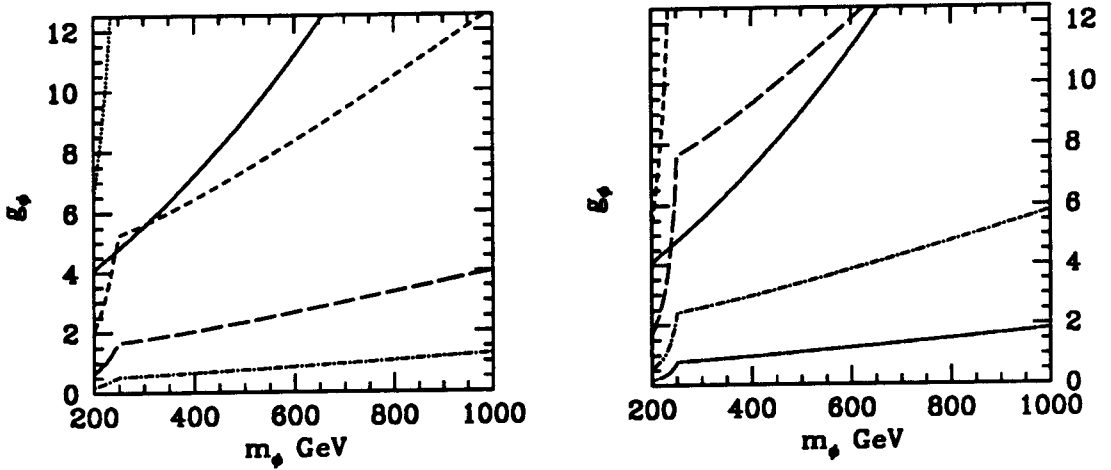


Figure 6.10: Similar to Figure 6.9 but from the real part of DFF's.

From the constraints obtained on mass and coupling from the experimental bound on the real part of the tau lepton, Figures 6.9 and 6.10 show that top quark can have values for the imaginary part of the electric dipole form factor as high as $10^{-19} e \text{ cm}$ except for a small mass range ($\sim 250 - 300 \text{ GeV}$). Imaginary part of the weak dipole form factor of top quark can be as high as $10^{-20} e \text{ cm}$ except for a mass range of around $250-700 \text{ GeV}$. We get more or less same values for the real part of both the electric and the weak dipole form factors. In case of EDFF the mass range excluded for the form factor to be $10^{-19} e \text{ cm}$ is $\sim 300 - 550 \text{ GeV}$ while no mass is excluded in case of WDFF for the same value of the form factor.

Comparing with the results obtained in Chapters 2 and 3 we may conclude the following. The asymmetries we defined there, if unobserved, would rule out top quark dipole moments of the order of $10^{-18} e \text{ cm}$. From Figures 6.9 and 6.10 we see that such a value of the dipole moment is not allowed by constraints on the mass and coupling constant values of the leptoquark coming from experimental results on τ dipole moments.

Finally, we discuss other recent work on DFF in third-generation leptoquark

models [61, 62]. Mahanta [61] has estimated the τ EDFF and has reached the conclusion that it can be as high as 10^{-19} e cm for a choice of g_ϕ and m_ϕ consistent with experimental constraints. He does not discuss the momentum dependence of DFF's. Bernreuther *et al.* [62] have obtained the form of the \sqrt{s} dependence of the DFF's of τ . Our results are in agreement with theirs as far as the order of magnitude and shape of the \sqrt{s} dependence. Our precise numbers are in slight disagreement with theirs. Neither of [61] and [62] discuss DFF's of t and τ in a concerted manner as done here.

Chapter 7

Conclusions

CP violation studies are important from the point of view of cosmology as well as for a complete understanding of particle interactions. The scope of observational effects of the violation of CP symmetry is limited within SM. The only system in which CP violation has been observed is the K -meson system. The B -meson system offers another place to study this effect in the coming years. At the same time SM, though highly successful, is not considered to be the ultimate theory. Due to various reasons, many models have been considered which lie outside the regime of SM. In the thesis we have constructed ways to observe CP violation in particle colliders taking into account effects beyond SM.

Our studies mainly concentrate on CP violation effects arising due to the top quark weak and electric dipole form factors. In the previous chapters we studied some of the CP -violating asymmetries, obtained using an effective Lagrangian with complex dipole coupling, which could be tested in the next generation linear colliders. These asymmetries were constructed out of the final state momenta. Apart from the process, $e^+e^- \rightarrow t\bar{t}$ we have looked at the top-antitop quark pair production in photon-photon collisions. Apart from the effective Lagrangian method, we have

considered a scenario were scalar leptoquarks, whose coupling with lepton and quark could be in general complex, couple with τ and t with the effect of giving a large dipole moment to these fermions at one loop order.

The main results of our studies and the conclusions drawn from them are the following. The four parameters studied are the real and the imaginary parts of the electric and the weak dipole form factors of the top quark. Different asymmetries which could be observed in the $t\bar{t}$ pair production in e^+e^- collisions are described in Chapter 2. At a c.m. energy of 500 GeV, and at an integrated luminosity of 10 fb^{-1} , our calculations show that the asymmetries will be observable if the dipole form factors are of the order of 10^{-18} e cm . This may be compared with the model predictions which are mostly two orders of magnitude lower than this value. We have considered electron beam polarization effects and found that longitudinal polarization improves the sensitivity of the experiment. Our calculations are done at 50% e^- -beam polarization with unpolarized e^+ -beam. The improvement in sensitivity with this polarization over the unpolarized case is sometimes an order of magnitude. Considering the fact that a large longitudinal polarization is likely to be available in linear colliders, we expect to obtain better sensitivity. Again, the expectation is that higher luminosity will be possible in the future colliders. This factor will improve the sensitivity further.

In Chapter 3 we have considered asymmetries which do not depend on the top quark momentum. Experimentally this is preferable as compared to the asymmetries described in Chapter 2 because the reconstruction of the top quark momentum is not required in this case and higher efficiency can be expected. Limits on dipole form factors are similar to those obtained in Chapter 2.

Possible background to the above asymmetries arising from the helicity-flip collinear

photon emission from the initial state are considered in Chapter 4. Our calculations show that in case of charge asymmetry and the forward-backward asymmetry combined with the charge asymmetry, described in Chapter 3, the background from initial state radiation is almost two orders of magnitude smaller than the statistical fluctuation at $\sqrt{s} = 500$ GeV and $\int \mathcal{L} = 10 \text{ fb}^{-1}$. The result is similar for different beam polarizations. T-odd asymmetries like the up-down asymmetry described in Chapter 2 do not have a background from this process as it requires absorptive part for non-zero background whereas the interaction is a tree-level process.

Photon Linear Colliders provide another place to look for $t\bar{t}$ production and hence CP violation effects due to top quark dipole moment. Chapter 5 of the thesis describes the charge asymmetry and the combined asymmetry in the process $\gamma\gamma \rightarrow t\bar{t}$. At an electron beam energy of 250 GeV and laser beam energy of 1.24 eV EDFF of top quark obtained is of the order of 10^{-16} e cm . Charge asymmetry measured with a cut-off angle of around 60° gives better limits than other cut-off angles. On the other hand, the combined asymmetry seems to give better limits at smaller cut-offs. Beam energy around 500 GeV gives better sensitivity for the combined asymmetry while for charge asymmetry the sensitivity peaks at a higher beam energy. The above results are with opposite helicity combination of electron beam helicities and laser beam helicities with the product of corresponding electron-beam and laser-beam helicities kept to be $-1/2$. Looking at the variation with x values, it is seen that larger x gives better limit. Our calculations are done at a geometrical luminosity of the electron-electron collider of 20 fb^{-1} . Increase in the luminosity will improve the limits.

Apart from these asymmetries obtained from an effective lagrangian study of the

processes $e^+e^- \rightarrow t\bar{t}$ and $\gamma\gamma \rightarrow t\bar{t}$, we have considered in this thesis (Chapter 6) the one loop effects on the $t\bar{t}\gamma(Z)$ vertex. For leptoquark masses of a few hundred GeV and unit coupling constant the electric dipole form factor of tau lepton (both real and imaginary parts) is found to be of the order of 10^{-18} e cm whereas the weak dipole form factors are an order smaller than this. In the case of top quark these are of the order of 10^{-20} e cm and 10^{-21} e cm respectively. To accommodate the constraints on masses and couplings of leptoquarks obtained from LEP results by Eboli [60] the EDFF of tau lepton should be of the order 10^{-19} e cm up to a mass range of up to .5 TeV and above this the EDFF should be an order or magnitude less. Mass-coupling countours are obtained for different values of the real and the imaginary parts of both EDFF and WDFF of the top quark and the tau lepton. Best limits on mass and coupling obtained is from the experimental bound on the real part of the weak dipole moment of the tau lepton.

Appendix A

A.1 QCD Lagrangian

The electroweak Lagrangian is given in Section 1.1 (Equation 1.2). Here we give Lagrangian invariant under $SU(3)_c$, which represents strong interactions.

$$\mathcal{L}_{QCD} = -\frac{1}{4} G_{\mu\nu}^a G^{a\mu\nu} + \bar{\psi}^k \not{D}^{kl} \psi^l \quad (\text{A.1})$$

where the field strength is given by

$$G_{\mu\nu}^a = \partial_\mu G_\nu^a - \partial_\nu G_\mu^a + g_{QCD} f^{abc} G_\mu^b G_\nu^c,$$

and the covariant derivative is

$$D_{kl}^\mu = \delta_{kl} \partial^\mu + i g_q T_{kl}^a G_a^\mu.$$

Here g_{QCD} is the QCD coupling constants and $a = 1, \dots, 8$ and $k, l = 1, 2, 3$.

Note that the kinetic energy term was already present in Equation 1.2. All the other terms are new.

A.2 Dirac Field Bilinears Under Space Inversion

In Section 1.2 we have defined the space inversion and the charge conjugation transformations. This Section we give the transformation properties of Dirac field

bilinears under Parity and Section A.3-A.4 give the details of the derivations and the transformation properties of the Dirac field bilinears under Charge Conjugation.

Transformation of Dirac field bilinears under space inversion are given below:

$$\begin{aligned}
 \psi_1 &\rightarrow \gamma^0 \psi_1 & (A.2) \\
 \bar{\psi}_1 &\rightarrow \bar{\psi}_1 \gamma^0 \\
 \bar{\psi}_1 \psi_2 &\rightarrow \bar{\psi}_1 \psi_2 \\
 \bar{\psi}_1 \gamma^5 \psi_2 &\rightarrow -\bar{\psi}_1 \gamma^5 \psi_2 \\
 \bar{\psi}_1 \gamma_\mu \psi_2 &\rightarrow \bar{\psi}_1 \gamma^\mu \psi_2 \\
 \bar{\psi}_1 \gamma_\mu \gamma^5 \psi_2 &\rightarrow -\bar{\psi}_1 \gamma^\mu \gamma^5 \psi_2 \\
 \bar{\psi}_1 \sigma_{\mu\nu} \psi_2 &\rightarrow \bar{\psi}_1 \sigma^{\mu\nu} \psi_2 \\
 \bar{\psi}_1 \sigma_{\mu\nu} \gamma^5 \psi_2 &\rightarrow -\bar{\psi}_1 \sigma^{\mu\nu} \gamma^5 \psi_2
 \end{aligned}$$

It is understood that the transformed fields are evaluated at $t' = t$, $\vec{x}' = -\vec{x}$.

A.3 Dirac Spinors Under Charge Conjugation

The Dirac equation for an electron and positron are respectively

$$[\gamma^\mu (i \partial_\mu + e A_\mu) - m] \psi = 0 \quad (A.3)$$

$$[\gamma^\mu (i \partial_\mu - e A_\mu) - m] \psi_C = 0 \quad (A.4)$$

Charge conjugation is defined as the transformation taking a particle to its antiparticle. Therefore ψ_C is the charge conjugated form of ψ . To obtain the exact form of ψ_C we do the following. Taking the complex conjugate of Equation A.3, we get

$$[(\gamma^\mu)^* (-i \partial_\mu - e A_\mu) - m] \psi^* = 0$$

Multiplying by $C\gamma^0$ on the left and carrying through $C\gamma^0$ to the right we get

$$[\gamma^\mu (i \partial_\mu - e A_\mu) - m] (C \gamma^0 \psi^*) = 0 \quad (\text{A.5})$$

Here C is a 4×4 matrix satisfying the condition

$$C^{-1} \gamma^\mu C = (-\gamma^\mu)^T.$$

Comparing Equation A.5 with Equation A.4 we see that

$$\psi_C = C \gamma^0 \psi^* = C \bar{\psi}^T.$$

A.4 Dirac Field Bilinears Under Charge Conjugation

Transformation of Dirac field bilinears under charge conjugation are given below:

$$\begin{aligned} \psi_1 &\rightarrow C \bar{\psi}_1^T \\ \bar{\psi}_1 &\rightarrow -\psi_1^T C^{-1} \\ \bar{\psi}_1 \psi_2 &\rightarrow \bar{\psi}_2 \psi_1 \end{aligned} \quad (\text{A.6})$$

$$\bar{\psi}_1 \gamma^5 \psi_2 \rightarrow \bar{\psi}_2 \gamma^5 \psi_1$$

$$\bar{\psi}_1 \gamma_\mu \psi_2 \rightarrow -\bar{\psi}_2 \gamma_\mu \psi_1$$

$$\bar{\psi}_1 \gamma_\mu \gamma^5 \psi_2 \rightarrow \bar{\psi}_2 \gamma_\mu \gamma^5 \psi_1$$

$$\bar{\psi}_1 \sigma_{\mu\nu} \psi_2 \rightarrow -\bar{\psi}_2 \sigma_{\mu\nu} \psi_1$$

$$\bar{\psi}_1 \sigma_{\mu\nu} \gamma^5 \psi_2 \rightarrow \bar{\psi}_2 \sigma_{\mu\nu} \gamma^5 \psi_2$$

Appendix B

Different coefficients, A , B , C and D entering in the expression for differential cross sections are given here. In terms of the production density matrix elements, these are given by

$$A = \rho(++) + \rho(--)$$

$$B = \rho(++) - \rho(--)$$

$$C = 2 \operatorname{Re} \rho(+)$$

and

$$D = 2 \operatorname{Im} \rho(+).$$

In the following expressions for A , B , C and D appearing in different chapters are given.

B.1 Expressions for A_i , B_i , C_i and D_i

Coefficients, A_i , B_i , C_i and D_i in the expression for differential cross section 2.17 and 3.2 are given below:

$$\begin{aligned} A_0 = & \left\{ 2(2 - \beta^2) \left[2c_v^2 + 2(r_L + r_R)c_v^Z + (r_L^2 + r_R^2)c_v^{Z^2} \right] \right. \\ & \left. + 2\beta^2(r_L^2 + r_R^2)c_a^{Z^2} \right\} (1 - P_e P_{\bar{e}}) \end{aligned}$$

$$\begin{aligned}
& + \left\{ 2(2 - \beta^2) \left[2(r_L - r_R)c_v^\gamma c_v^Z + (r_L^2 - r_R^2)c_v^{Z^2} \right] \right. \\
& \left. + 2\beta^2(r_L^2 - r_R^2)c_a^{Z^2} \right\} (P_{\bar{e}} - P_e), \\
A_1 &= -8\beta c_a^Z \left\{ \left[(r_L - r_R)c_v^\gamma + (r_L^2 - r_R^2)c_v^Z \right] (1 - P_e P_{\bar{e}}) \right. \\
& \left. + \left[(r_L + r_R)c_v^\gamma + (r_L^2 + r_R^2)c_v^Z \right] (P_{\bar{e}} - P_e) \right\}, \\
A_2 &= 2\beta^2 \left\{ \left[2c_v^{\gamma^2} + 2(r_L + r_R)c_v^\gamma c_v^Z + (r_L^2 + r_R^2)(c_v^{Z^2} + c_a^{Z^2}) \right] (1 - P_e P_{\bar{e}}) \right. \\
& \left. + \left[2(r_L - r_R)c_v^\gamma c_v^Z + (r_L^2 - r_R^2)(c_v^{Z^2} + c_a^{Z^2}) \right] (P_{\bar{e}} - P_e) \right\}, \\
B_0^\pm &= 4\beta \left\{ (c_v^\gamma + r_L c_v^Z) (r_L c_a^Z \mp \text{Im} c_d^\gamma \mp r_L \text{Im} c_d^Z) (1 - P_e)(1 + P_{\bar{e}}) \right. \\
& \left. + (c_v^\gamma + r_R c_v^Z) (r_R c_a^Z \mp \text{Im} c_d^\gamma \mp r_R \text{Im} c_d^Z) (1 + P_e)(1 - P_{\bar{e}}) \right\}, \\
B_1 &= -4 \left\{ \left[(c_v^\gamma + r_L c_v^Z)^2 + \beta^2 r_L^2 c_a^{Z^2} \right] (1 - P_e)(1 + P_{\bar{e}}) \right. \\
& \left. - \left[(c_v^\gamma + r_R c_v^Z)^2 + \beta^2 r_R^2 c_a^{Z^2} \right] (1 + P_e)(1 - P_{\bar{e}}) \right\}, \\
B_2^\pm &= 4\beta \left\{ (c_v^\gamma + r_L c_v^Z) (r_L c_a^Z \pm \text{Im} c_d^\gamma \pm r_L \text{Im} c_d^Z) (1 - P_e)(1 + P_{\bar{e}}) \right. \\
& \left. + (c_v^\gamma + r_R c_v^Z) (r_R c_a^Z \pm \text{Im} c_d^\gamma \pm r_R \text{Im} c_d^Z) (1 + P_e)(1 - P_{\bar{e}}) \right\}, \\
C_0^\pm &= 4 \left\{ \left[(c_v^\gamma + r_L c_v^Z)^2 \pm \beta^2 \gamma^2 c_a^Z (\text{Im} c_d^\gamma r_L + \text{Im} c_d^Z r_L^2) \right] (1 - P_e)(1 + P_{\bar{e}}) \right. \\
& \left. - \left[(c_v^\gamma + r_R c_v^Z)^2 \pm \beta^2 \gamma^2 c_a^Z (\text{Im} c_d^\gamma r_R + \text{Im} c_d^Z r_R^2) \right] (1 + P_e)(1 - P_{\bar{e}}) \right\}, \\
C_1^\pm &= -4\beta \left\{ (c_v^\gamma + r_L c_v^Z) (r_L c_a^Z \pm \gamma^2 \text{Im} c_d^\gamma \pm r_L \gamma^2 \text{Im} c_d^Z) (1 - P_e)(1 + P_{\bar{e}}) \right. \\
& \left. + (c_v^\gamma + r_R c_v^Z) (r_R c_a^Z \pm \gamma^2 \text{Im} c_d^\gamma \pm r_R \gamma^2 \text{Im} c_d^Z) (1 + P_e)(1 - P_{\bar{e}}) \right\}, \\
D_0^\pm &= \mp 4\beta \gamma^2 \left\{ (c_v^\gamma + r_L c_v^Z) (\text{Re} c_d^\gamma + r_L \text{Re} c_d^Z) (1 - P_e)(1 + P_{\bar{e}}) \right. \\
& \left. - (c_v^\gamma + r_R c_v^Z) (\text{Re} c_d^\gamma + r_R \text{Re} c_d^Z) (1 + P_e)(1 - P_{\bar{e}}) \right\}, \\
D_1^\pm &= \pm 4\beta^2 c_a^Z \left\{ r_L (\text{Re} c_d^\gamma + r_L \text{Re} c_d^Z) (1 - P_e)(1 + P_{\bar{e}}) \right. \\
& \left. + r_R (\text{Re} c_d^\gamma + r_R \text{Re} c_d^Z) (1 + P_e)(1 - P_{\bar{e}}) \right\}.
\end{aligned}$$

B.2 Expressions for A_i , etc. in Chapter 4

A_i^\pm , B_i^\pm , C_i^\pm and D_i^\pm used in Equation 4.3 are given by

$$A_i^\pm = A_i^{(1)} (1 + P_e P_{\bar{e}}) \pm A_i^{(2)} (P_e + P_{\bar{e}}), \text{ etc.},$$

where

$$A_0^{(1)} = \{2(2 - \beta^2) [2c_v^{\gamma^2} + 2(r_L + r_R)c_v^\gamma c_v^Z + (r_L^2 + r_R^2)c_v^{Z^2}] + 2\beta^2(r_L^2 + r_R^2)c_a^{Z^2}\}$$

$$A_1^{(1)} = -8\beta c_a^Z [(r_L - r_R)c_v^\gamma + (r_L^2 - r_R^2)c_v^Z]$$

$$A_2^{(1)} = 2\beta^2 [2c_v^{\gamma^2} + 2(r_L + r_R)c_v^\gamma c_v^Z + (r_L^2 + r_R^2)(c_v^{Z^2} + c_a^{Z^2})]$$

$$B_0^{(1)} = 4\beta [(r_L + r_R)c_v^\gamma c_a^Z + (r_L^2 + r_R^2)c_v^Z c_a^Z]$$

$$B_1^{(1)} = -4 [2(r_L - r_R)c_v^\gamma c_a^Z + (r_L^2 - r_R^2)(c_v^{Z^2} + \beta^2 c_a^{Z^2})]$$

$$B_2^{(1)} = 4\beta [(r_L + r_R)c_v^\gamma c_a^Z + (r_L^2 + r_R^2)c_v^Z c_a^Z]$$

$$C_0^{(1)} = 4 [(r_L - r_R)c_v^\gamma c_a^Z + (r_L^2 - r_R^2)c_v^{Z^2}]$$

$$C_1^{(1)} = -4\beta [(r_L + r_R)c_v^\gamma c_a^Z + (r_L^2 + r_R^2)c_v^Z c_a^Z]$$

$$D_0^{(1)} = 0$$

$$D_1^{(1)} = 0$$

$$A_0^{(2)} = \{2(2 - \beta^2) [2(r_L - r_R)c_v^\gamma c_v^Z + (r_L^2 - r_R^2)c_v^{Z^2}] + 2\beta^2(r_L^2 - r_R^2)c_a^{Z^2}\}$$

$$A_1^{(2)} = -8\beta c_a^Z [(r_L + r_R)c_v^\gamma + (r_L^2 + r_R^2)c_v^Z]$$

$$A_2^{(2)} = 2\beta^2 [2(r_L - r_R)c_v^\gamma c_v^Z + (r_L^2 - r_R^2)(c_v^{Z^2} + c_v^{Z^2})]$$

$$B_0^{(2)} = 4\beta [(r_L - r_R)c_v^\gamma c_a^Z + (r_L^2 - r_R^2)c_v^Z c_a^Z]$$

$$\begin{aligned}
B_1^{(2)} &= -4 \left[2c_v^{\gamma^2} + 2(r_L + r_R)c_v^{\gamma}c_a^Z + (r_L^2 + r_R^2)(c_v^{Z^2} + \beta^2 c_a^{Z^2}) \right] \\
B_2^{(2)} &= 4\beta \left[(r_L - r_R)c_v^{\gamma}c_a^Z + (r_L^2 - r_R^2)c_v^Z c_a^Z \right] \\
C_0^{(2)} &= 4 \left[(2c_v^{\gamma^2} + (r_L + r_R)c_v^{\gamma}c_a^Z + (r_L^2 + r_R^2)(c_v^{Z^2} + \beta^2 c_a^{Z^2}) \right] \\
C_1^{(2)} &= -4\beta \left[(r_L - r_R)c_v^{\gamma}c_a^Z + (r_L^2 - r_R^2)c_v^Z c_a^Z \right] \\
D_0^{(2)} &= 0 \\
D_1^{(2)} &= 0
\end{aligned}$$

B.3 T_i in Chapter 4

Expressions for T_i used in Equations 4.16 and 4.12 are given below:

$$\begin{aligned}
T_0^{(2)} &= (P_e + P_{\bar{e}}) \\
&\times \left\{ \left(\frac{6}{\beta_t^3} + \frac{3 - \beta_t^2}{\beta_t^4} \log \left(\frac{1 + \beta_t}{1 - \beta_t} \right) \right) \right. \\
&\times \left(4\beta_t c_a^Z c_v^{\gamma} (r_L - r_R) + 4\beta_t c_a^Z c_v^Z (r_L^2 - r_R^2) \right) \\
&- 8\beta_t t c_a^Z \left(\frac{2(3 - 2\beta_t^2)\gamma}{\beta_t^3} + \frac{3}{\beta_t^4 \gamma} \log \left(\frac{1 + \beta_t}{1 - \beta_t} \right) \right) \\
&\times \left(c_v^{\gamma} (r_L - r_R) + c_v^Z (r_L^2 - r_R^2) \right) \\
&+ 4\gamma^2 \left(2 \left((8t^2 + 2) c_v^{\gamma} c_v^Z (r_L - r_R) \right. \right. \\
&+ \left. \left(2\beta_t^2 c_a^{Z^2} + (8t^2 + 2) c_v^{Z^2} \right) (r_L^2 - r_R^2) \right) \\
&+ \left. \left(\frac{4}{\beta_t^2} + \frac{2}{\beta_t^3} \log \left(\frac{1 + \beta_t}{1 - \beta_t} \right) \right) (8t^2 - 2) \right. \\
&\times \left. \left. \left(2c_v^{\gamma} c_v^Z (r_L - r_R) + \left(2\beta_t^2 c_a^{Z^2} + (8t^2 - 2) c_v^{Z^2} \right) (r_L^2 - r_R^2) \right) \right\} \\
T_1^{(2)} &= (P_e + P_{\bar{e}})
\end{aligned}$$

$$\begin{aligned}
& \times \left\{ -4 \left(\frac{4\gamma^2}{\beta_t} + \frac{2}{\beta_t^2} \log \left(\frac{1+\beta_t}{1-\beta_t} \right) \right) \right. \\
& \times \left(2\beta_t c_a^Z c_v^\gamma (r_L + r_R) + 2\beta_t c_a^Z c_v^Z (r_L^2 + r_R^2) \right) \\
& + 4 \left(\frac{4}{b^2} + \frac{2}{b^3} \log \left(\frac{1+\beta_t}{1-\beta_t} \right) \right) \\
& \times \left(2c_v^{\gamma^2} + 2c_v^\gamma c_v^Z (r_L + r_R) + (\beta_t^2 c_a^{Z^2} + c_v^{Z^2}) (r_L^2 + r_R^2) \right) \\
& - 8t \left(\frac{4\gamma}{b^2} + \frac{2}{b^3} \gamma \log \left(\frac{1+\beta_t}{1-\beta_t} \right) \right) \\
& \times \left. \left(2c_v^{\gamma^2} + 2c_v^\gamma c_v^Z (r_L + r_R) + c_v^{Z^2} (r_L^2 + r_R^2) \right) \right\} \\
T_2^{(2)} &= (P_e + P_{\bar{e}}) \\
& \times \left\{ -3 \left(\frac{6}{\beta_t^3} + \frac{3-\beta_t^2}{\beta_t^4} \log \left(\frac{1+\beta_t}{1-\beta_t} \right) \right) \right. \\
& \times \left(4\beta_t c_a^Z c_v^\gamma (r_L - r_R) + 4\beta_t c_a^Z c_v^Z (r_L^2 - r_R^2) \right) \\
& + 24\beta_t t c_a^Z \left(\frac{(6-4\beta_t^2)\gamma}{\beta_t^3} + \frac{3}{\beta_t^4} \gamma \log \left(\frac{1+\beta_t}{1-\beta_t} \right) \right) \\
& \times \left(c_v^\gamma (r_L - r_R) + c_v^Z (r_L^2 - r_R^2) \right) \\
& - \left(\frac{(12-8\beta_t^2)\gamma^2}{\beta_t^2} + \frac{6}{\beta_t^3} \log \left(\frac{1+\beta_t}{1-\beta_t} \right) \right) \\
& \times \left. \left((8t^2 - 2) 2c_v^\gamma c_v^Z (r_L - r_R) - (2\beta_t^2 c_a^{Z^2} + (-8t^2 + 2) c_v^{Z^2}) (r_L^2 - r_R^2) \right) \right\}
\end{aligned}$$

B.4 Expression for $d\sigma_{ij}$ in Chapter 5

Expressions for $d\sigma_{ij}$ and ξ_2 (Equation 5.15) are given in terms of the amplitudes. Helicities of the product are summed over.

$$d\sigma_{00} = \frac{1}{4} \sum_{\lambda_\gamma, \lambda'_\gamma} |M(\lambda_\gamma, \lambda'_\gamma)|^2$$

$$\begin{aligned}
d\sigma_{22} &= \frac{1}{4} \sum_{\lambda_\gamma, \lambda'_\gamma} \lambda_\gamma \lambda'_\gamma |M(\lambda_\gamma, \lambda'_\gamma)|^2 \\
(d\sigma_{20} + d\sigma_{02}) &= \frac{1}{2} \sum_{\lambda_\gamma} \lambda_\gamma |M(\lambda_\gamma, \lambda_\gamma)|^2 \\
(d\sigma_{20} - d\sigma_{02}) &= \frac{1}{2} \sum_{\lambda_\gamma} \lambda_\gamma |M(\lambda_\gamma, -\lambda_\gamma)|^2
\end{aligned}$$

The Stokes parameters, ξ_i are given by

$$\xi_i = \frac{\Phi_i}{\Phi_0},$$

where $j = 0, 1, 2, 3$ and Φ_i is a function depending on the azimuthal angle, ϕ of the scattered photon beam when initial electron beam is taken along the z axis:

$$\Phi_j = \sum_{n=0}^4 (C_{jn} \cos n\phi + S_{jn} \sin n\phi).$$

The circular polarization of the photon, after averaging over the azimuthal angle, is

$$\langle \xi_2 \rangle = C_{20}/C_{00},$$

where

$$\begin{aligned}
C_{00} &= \frac{1}{1-y} + 1 - y - 4r(1-r) - 2\lambda_e \lambda_l r x (2r-1)(2-y) \\
C_{20} &= 2\lambda_e r x \left[1 + (1-y)(2r-1)^2 \right] - \lambda_l (2r-1) \left(\frac{1}{1-y} + 1 - y \right). \quad (\text{B.7})
\end{aligned}$$

B.5 Production Density Matrix Elements Corresponding to Different $d\sigma_{ij}$

Expressions for $\rho_{ij}(\lambda_t, \lambda_{\bar{t}})$ used in Equation 5.16 are given below.

$$\begin{aligned}\rho_{00}^+(\lambda_t, \lambda_t') &= \frac{1}{4} \sum_{\lambda_\gamma, \lambda_\gamma', \lambda_{\bar{t}}} M(\lambda_\gamma, \lambda_\gamma', \lambda_t, \lambda_{\bar{t}}) M^*(\lambda_\gamma, \lambda_\gamma', \lambda_t', \lambda_{\bar{t}}) \\ \rho_{22}^+(\lambda_t, \lambda_t') &= \frac{1}{4} \sum_{\lambda_\gamma, \lambda_{\bar{t}}} [M(\lambda_\gamma, \lambda_\gamma, \lambda_t, \lambda_{\bar{t}}) M^*(\lambda_\gamma, \lambda_\gamma, \lambda_t', \lambda_{\bar{t}}) \\ &\quad - M(\lambda_\gamma, -\lambda_\gamma, \lambda_t, \lambda_{\bar{t}}) M^*(\lambda_\gamma, -\lambda_\gamma, \lambda_t', \lambda_{\bar{t}})] \\ (\rho_{20}^+(\lambda_t, \lambda_t') + \rho_{02}^+(\lambda_t, \lambda_t')) &= \frac{1}{2} \sum_{\lambda_\gamma, \lambda_{\bar{t}}} \lambda_\gamma M(\lambda_\gamma, \lambda_\gamma, \lambda_t, \lambda_{\bar{t}}) M^*(\lambda_\gamma, \lambda_\gamma, \lambda_t', \lambda_{\bar{t}}) \\ (\rho_{20}^+(\lambda_t, \lambda_t') - \rho_{02}^+(\lambda_t, \lambda_t')) &= \frac{1}{2} \sum_{\lambda_\gamma, \lambda_{\bar{t}}} \lambda_\gamma M(\lambda_\gamma, -\lambda_\gamma, \lambda_t, \lambda_{\bar{t}}) M^*(\lambda_\gamma, -\lambda_\gamma, \lambda_t', \lambda_{\bar{t}})\end{aligned}$$

and

$$\begin{aligned}\rho_{00}^-(\lambda_{\bar{t}}, \lambda_{\bar{t}}') &= \frac{1}{4} \sum_{\lambda_\gamma, \lambda_\gamma', \lambda_t} M(\lambda_\gamma, \lambda_\gamma', \lambda_t, \lambda_{\bar{t}}) M^*(\lambda_\gamma, \lambda_\gamma', \lambda_t, \lambda_{\bar{t}}') \\ \rho_{22}^-(\lambda_{\bar{t}}, \lambda_{\bar{t}}') &= \frac{1}{4} \sum_{\lambda_\gamma, \lambda_t} [M(\lambda_\gamma, \lambda_\gamma, \lambda_t, \lambda_{\bar{t}}) M^*(\lambda_\gamma, \lambda_\gamma, \lambda_t, \lambda_{\bar{t}}') \\ &\quad - M(\lambda_\gamma, -\lambda_\gamma, \lambda_t, \lambda_{\bar{t}}) M^*(\lambda_\gamma, -\lambda_\gamma, \lambda_t, \lambda_{\bar{t}}')] \\ (\rho_{20}^-(\lambda_{\bar{t}}, \lambda_{\bar{t}}') + \rho_{02}^-(\lambda_{\bar{t}}, \lambda_{\bar{t}}')) &= \frac{1}{2} \sum_{\lambda_\gamma, \lambda_t} \lambda_\gamma M(\lambda_\gamma, \lambda_\gamma, \lambda_t, \lambda_{\bar{t}}) M^*(\lambda_\gamma, \lambda_\gamma, \lambda_t, \lambda_{\bar{t}}') \\ (\rho_{20}^-(\lambda_{\bar{t}}, \lambda_{\bar{t}}') - \rho_{02}^-(\lambda_{\bar{t}}, \lambda_{\bar{t}}')) &= \frac{1}{2} \sum_{\lambda_\gamma, \lambda_t} \lambda_\gamma M(\lambda_\gamma, -\lambda_\gamma, \lambda_t, \lambda_{\bar{t}}) M^*(\lambda_\gamma, -\lambda_\gamma, \lambda_t, \lambda_{\bar{t}}')\end{aligned}$$

Substituting the amplitudes from 5.13 we get

$$\rho_{00}^\pm(++) = \frac{1}{4} C \left\{ \frac{s}{2m_t^2} [(1 - \beta_t^4) + \beta_t^2 (1 - \beta_t^2) \sin^4 \theta_t] \right.$$

$$\begin{aligned}
& + \beta_t^2 \sin^2 \theta_t (1 + \cos^2 \theta_t)] \\
& + \frac{2s\beta_t}{m_t} \text{Im } d_t [(2 - \sin^2 \theta_t) (1 - \beta_t^2) - \beta_t^2 \sin^4 \theta_t] \Big\} \\
\rho_{00}^{\pm}(\text{--}) &= \frac{1}{4} C \left\{ \frac{s}{2m_t^2} [(1 - \beta_t^4) + \beta_t^2 (1 - \beta_t^2) \sin^4 \theta_t \right. \\
& + \beta_t^2 \sin^2 \theta_t (1 + \cos^2 \theta_t)] \\
& \left. - \frac{2s\beta_t}{m_t} \text{Im } d_t [(2 - \sin^2 \theta_t) (1 - \beta_t^2) - \beta_t^2 \sin^4 \theta_t] \right\} \\
\rho_{00}^{\pm}(+-) &= -\frac{1}{4} C \frac{\sqrt{s} 4\beta_t s}{4m_t^2} \text{Im } d_t \sin \theta \cos \theta ((1 - \beta_t^2) + \beta_t^2 \sin^2 \theta) \\
\rho_{22}^{\pm}(++) &= \frac{1}{4} C \left\{ \frac{s}{2m_t^2} [(1 - \beta_t^4) - \beta_t^2 (1 - \beta_t^2) \sin^4 \theta_t \right. \\
& - \beta_t^2 \sin^2 \theta_t (1 + \cos^2 \theta_t)] \\
& \left. + \frac{2s\beta_t}{m_t} \text{Im } d_t [(2 - \sin^2 \theta_t) (1 - \beta_t^2) + \beta_t^2 \sin^4 \theta_t] \right\} \\
\rho_{22}^{\pm}(\text{--}) &= \frac{1}{4} C \left\{ \frac{s}{2m_t^2} [(1 - \beta_t^4) - \beta_t^2 (1 - \beta_t^2) \sin^4 \theta_t \right. \\
& - \beta_t^2 \sin^2 \theta_t (1 + \cos^2 \theta_t)] \\
& \left. - \frac{2s\beta_t}{m_t} \text{Im } d_t [(2 - \sin^2 \theta_t) (1 - \beta_t^2) + \beta_t^2 \sin^4 \theta_t] \right\} \\
\rho_{22}^{\pm}(+-) &= -\frac{1}{4} C \frac{\sqrt{s} 4\beta_t s}{4m_t^2} \text{Im } d_t \sin \theta \cos \theta ((1 - \beta_t^2) - \beta_t^2 \sin^2 \theta) \\
\rho_{20}^{\pm}(++) &= \frac{1}{2} C \left\{ \left[2\beta_t \pm \frac{s\beta_t^2}{2m_t^2} \sin^2 \theta_t \cos \theta_t \right] + 8m_t \text{Im } d_t \right\} \\
\rho_{20}^{\pm}(\text{--}) &= \frac{1}{2} C \left\{ - \left[2\beta_t \pm \frac{s\beta_t^2}{2m_t^2} \sin^2 \theta_t \cos \theta_t \right] + 8m_t \text{Im } d_t \right\} \\
\rho_{20}^{\pm}(+-) &= \mp \frac{1}{2} C \sqrt{s} \left\{ \frac{\beta_t^2}{m_t} \sin^3 \theta_t \right.
\end{aligned}$$

$$\begin{aligned}
& +i \frac{s\beta_t}{2m_t^2} \text{Re } d_t \sin \theta_t \left((1 - \beta_t^2) \cos \theta_t + \beta_t^2 \sin^2 \theta_t \right) \Big\} \\
\rho_{02}^{\pm}(++) &= \frac{1}{2} C \left\{ \left[2\beta_t \mp \frac{s\beta_t^2}{2m_t^2} \sin^2 \theta_t \cos \theta_t \right] + 8m_t \text{Im } d_t \right\} \\
\rho_{02}^{\pm}(--) &= \frac{1}{2} C \left\{ - \left[2\beta_t + \frac{s\beta_t^2}{2m_t^2} \sin^2 \theta_t \cos \theta_t \right] + \frac{s}{m_t} \text{Im } d_t 2(1 - \beta_t^2) \right\} \\
\rho_{20}^{\pm}(+-) &= \pm \frac{1}{2} C \sqrt{s} \left\{ \frac{\beta_t^2}{m_t} \sin^3 \theta_t \right. \\
& \quad \left. + i \frac{s\beta_t}{2m_t^2} \text{Re } d_t \sin \theta_t \left((1 - \beta_t^2) \cos \theta_t - \beta_t^2 \sin^2 \theta_t \right) \right\}
\end{aligned}$$

Here

$$C = 16 \pi^2 Q_t^4 \alpha^2 \frac{16 m_t^2}{s (1 - \beta_t^2 \cos^2 \theta_t)^2},$$

where Q_t is the charge of the top quark. Note that we have kept only linear terms in d_t assuming that the value of dipole form factor is small and hence higher order terms can be neglected.

Appendix C

C.1 $t\bar{t}\gamma(Z)$ Vertex at One-Loop Level

The following discussion is on getting the $t\bar{t}\gamma(Z)$ vertex at one-loop level in the presence of a leptoquark (Chapter 6). Comparison is made with the effective vertex to obtain the expression for the dipole coupling.

For a Lagrangian

$$\mathcal{L} = g_\phi \bar{\tau} (a + b\gamma^5) t \phi + g_\phi \bar{t} (a^* - b^*\gamma^5) \tau \phi^\dagger,$$

with $|a|^2 + |b|^2 = 1$, the vertex factor at one loop level from the τ pair-production diagram (Figure 6.1(a)) is

$$\begin{aligned} -ie \Gamma_\gamma^{1\mu} &= \int \frac{d^4 k}{(2\pi)^4} i g_\phi (a^* - b^* \gamma^5) i \frac{\not{k} + m_\tau}{k^2 - m_\tau^2} i e \gamma^\mu \\ &\quad \times i \frac{\not{k} - \not{q} + m_\tau}{(k - q)^2 - m_\tau^2} i g (a + b \gamma^5) \frac{i}{(k - p_t)^2 - m_\phi^2} \\ \Gamma_\gamma^{1\mu} &= -i g_\phi^2 \int \frac{d^4 k}{(2\pi)^4} \times \left\{ (a^* - b^* \gamma^5) (\not{k} + m_\tau) \gamma^\mu (\not{k} - \not{q} + m_\tau) (a + b \gamma^5) \right\} / \\ &\quad \left\{ (k^2 - m_\tau^2) \left((k - q)^2 - m_\tau^2 \right) \left((k - p_t)^2 - m_\phi^2 \right) \right\} \end{aligned} \quad (C.9)$$

In terms of the couplings in Equations 6.2 and 6.3 g , a and b are given, in case of S_i type leptoquark ($i = 1, 3$), by

$$a = \frac{(g_R + g_L)}{2g_\phi}; \quad b = \frac{(g_R - g_L)}{2g_\phi} \quad (C.10)$$

and for R_2 type of leptoquark

$$a = \frac{(h_{2R} + h_{2L})}{2g_\phi}; \quad b = \frac{(h_{2R} - h_{2L})}{2g_\phi}. \quad (\text{C.11})$$

After rearranging, the numerator of Equation C.9 becomes

$$\begin{aligned} N\tau = & (2k^\mu \not{k} - \not{k} \gamma^\mu \not{q}) \left[|a|^2 + |b|^2 + 2\text{Re}(a^*b) \gamma^5 \right] \\ & + m_\tau (2k^\mu - \gamma^\mu \not{q}) \left[|a|^2 - |b|^2 + 2i\text{Im}(a^*b) \gamma^5 \right] \end{aligned}$$

We are interested in the dipole terms and hence will look at only terms proportional to γ^5 . After integration we see that there is no term proportional to $\text{Re}(a^*b) (p_t - p_{\bar{t}})^\mu \gamma^5$. The term proportional to $\text{Im}(a^*b) (p_t - p_{\bar{t}})^\mu \gamma^5$ is identified with the dipole term:

$$\begin{aligned} \Gamma_\gamma^{1\mu} |_{\text{dipoleterm}} = & \frac{g_\phi^2}{2\pi^2} m_\tau \text{Im}(a^*b) (p_t - p_{\bar{t}})^\mu \gamma^5 \\ & \times \left\{ \frac{\pi}{2s\beta_t^2} \left(\beta_\tau + \frac{1}{s\beta_t} (m_t^2 + m_\phi^2 - m_\tau^2) \log \left(\frac{1 + \beta_t}{1 - \beta_t} \right) \right. \right. \\ & \times \left. \left. \left[\frac{2(m_t^2 + m_\tau^2 - m_\phi^2) - s(1 - \beta_t\beta_\tau)}{2(m_t^2 + m_\tau^2 - m_\phi^2) - s(1 + \beta_t\beta_\tau)} \right] \right) \theta(s - 4m_\tau^2) \right\} \end{aligned}$$

From Equations C.10 and C.11 we get

$$g_\phi \text{Im}(a^*b) = \text{Im}(g_{iR}^* g_{iL}) \quad (\text{C.12})$$

for S_i leptoquark and for R_2 type of leptoquark

$$g_\phi \text{Im}(a^*b) = \text{Im}(h_{2R}^* h_{2L}). \quad (\text{C.13})$$

In a similar way we get the expression for the leptoquark pair-production diagram (Figure 6.1(b)) as

$$\begin{aligned}\Gamma_{\gamma}^{1\mu} |_{\text{dipoleterm}} &= \frac{-Q_{\phi} g_{\phi}^2}{2\pi^2} m_{\tau} \text{Im}(a^*b) (p_t - p_{\bar{t}})^{\mu} \gamma^5 \\ &\quad \left\{ \frac{1}{2s\beta_t^2} \left(\beta_{\phi} - \frac{1}{s\beta_t} (m_t^2 + m_{\phi}^2 - m_{\tau}^2 - \frac{s}{2}) \log \left(\frac{1 + \beta_t}{1 - \beta_t} \right) \right. \right. \\ &\quad \left. \left. \times \left[\frac{2(m_t^2 + m_{\tau}^2 - m_{\phi}^2) - s(1 - \beta_t\beta_{\phi})}{2(m_t^2 + m_{\tau}^2 - m_{\phi}^2) - s(1 + \beta_t\beta_{\phi})} \right] \right) \theta(s - 4m_{\phi}^2) \right\}\end{aligned}$$

The corresponding expressions for the Z couplings are

$$\Gamma_{\gamma}^{1\mu} |_{\text{dipoleterm}} = -\frac{(-1 + 2\sin^2 \theta_W)}{4\sin \theta_W \cos \theta_W} \Gamma_{\gamma}^{1\mu} (\text{Im}(a^*b))$$

and

$$\Gamma_{\gamma}^{1\mu} |_{\text{dipoleterm}} = \frac{(T_3 - Q_{\phi} \sin^2 \theta_W)}{4\sin \theta_W \cos \theta_W} \Gamma_{\gamma}^{2\mu} (\text{Im}(a^*b))$$

where T_3 is the third component of the isospin of the leptoquark considered and Q_{ϕ} , its charge. θ_W is the weak mixing angle.

Bibliography

- [1] F. Abe *et al.* (CDF Collab.), *Phys. Rev. Lett.*, **74**, (1995) 2626; S. Abachi *et al.* (D0 Collab.), *Phys. Rev. Lett.* **74**, (1995) 2632.
- [2] M. Woods, SLAC-PUB-7320, hep-ex/9611006, Talk given at 12th International Symposium on High Energy Spin Physics (SPIN 96), Amsterdam, Netherlands, 10-14 Sep 1996; SLAC-PUB-6694, Presented at 11th International Symposium on High Energy Spin Physics and the 8th International Symposium on Polarization Phenomena in Nuclear Physics (SPIN 94), Bloomington, IN, 15-22 Sep 1994.
- [3] CERN Courier, January/February 1994, p9.
- [4] I. F. Ginzburg *et al*, *Nucl. Inst. Meth.*, **205** (1983) 47; I. F. Ginzburg *et al*, *Nucl. Inst. Meth.*, **219** (1984) 5; V. Telnov, *Nucl. Inst. Meth.*, **A 355** (1995) 3.
- [5] T. Lee and C. Yang, *Phys. Rev.* **102** (1956) 290.
- [6] C. S. Wu *et al.*, *Phys. Rev.* **105** (1957) 1413
- [7] J. H. Christenson, J. W. Cronin, V. L. Fitch and R. Turlay, *Phys. Rev. Lett.* **13** (1964) 138.
- [8] R.M. Barnett *et al.*, Review of Particle Properties, *Phys. Rev. D* **54** (1996) 1.
- [9] OPAL Collab. CERN-PPE/96-184, To appear in *Z. Phys.*, C.

- [10] E. P. Shabalin, *Sov. J. Nucl. Phys.* **28** (1978) 75; *ibid*, **31** (1980) 864; *ibid*, **33** (1980) 228.
- [11] L. Wolfenstein, *Phys. Rev. Lett.* **13** (1964) 562.
- [12] J. Prentki and M. Veltman, *Phys. Lett.* **15** (1965) 88.
- [13] T.T. Wu and C.N. Yang, *Phys. Rev. Lett.* **13** (1964) 380.
- [14] M. Kobayashi and T. Maskawa, *Prog. Theor. Phys.* **49** (1973) 652.
- [15] S. Weinberg, *Phys. Rev. Lett.* **37** (1976) 657.
- [16] R. N. Mohapatra and J. C. Pati, *Phys. Rev.* **D11** (1975) 566.
- [17] N. G. Deshpande and Xiao- Gang He, *Phys. Rev.*, **D 49** (1994) 4812.
- [18] W. Bernreuther, P. Overman, *Z. Phys.*, **C 61** (1994) 599; W. Bernreuther and A. Brandenburg, *Phys. Lett.*, **B 314** (1993) 104; W. Bernreuther and A. Brandenburg, *Phys. Rev. D* **49** (1994) 4481 D. Chang, Wai-Yee Keung and I. Phillips, CERN-TH.6658/92, hep-ph/9209267; A. Soni, R.M. Xu, *Phys.Rev.Lett.* **69** (1992) 33; A. Pilaftsis and M. Nowakowski, *Int. J. Mod. Phys. A* **94** 1097; D. Atwood and A. Soni, JLAB-TH-96-14, hep-ph/9607481; Ashok Das, Chung Kao, *Phys.Lett.*, **B372** (1996) 106; T. Hasuike, *et al.*, TOKUSHIMA-96-04, hep-ph/9611304; B. Grzadkowski and Z. Hioki, *Phys.Lett.*, **B 391** (1997) 172.
- [19] M. Masip and A. Rasin, *Nucl. Phys.* **B 460** (1996) 449; K. C. Chou and Y. L. Wu, *Nucl. Phys. Proc. Suppl.* **52 A** (1997) 159; N. Haba, *Phys. Lett.* **B 398** (1997) 305; T. Falk and K. A. Olive, *Phys. Lett.* **B 375** (1996) 196.
- [20] G. Barenboim, J. Bernabeu, M. Raidal, *Nucl. Phys.* **B 478** (1996) 527; G. Barenboim and J. Bernabeu, *Z. Phys.* **C 73** (1997) 321; G. Barenboim, J. Bernabeu,

- M. Raidal, FTUV-96-70, hep-ph/9702337; G. Barenboim *et al*, *Phys. Rev. D* **55** (1997) 4213;
- [21] I. Bigi and H. Krasemann, *Z. Phys. C* **7** (1981) 127; J. Kühn, *Acta Phys. Austr. Suppl.* **XXIV** (1982) 203; I. Bigi *et al.*, *Phys. Lett. B* **181** (1986) 157.
- [22] B. Grzadkowski, *Phys. Lett.*, **B 305** (1993) 384; B. Grzadkowski and W.-Y. Keung, *Phys. Lett. B* **316** (1993) 137; E. Christova and M. Fabbrichesi, *Phys. Lett. B* **320** (1994) 299; A. Bartl, E. Christova and W. Majerotto, *Nucl. Phys. B* **460** (1996) 235, Erratum-*ibid*, **B 465** (1996) 365; T. Arense and L. M. Sehgal, *Phys. Rev. D* **51** (1995) 3525 ; J.P.Ma and A. Brandenburg, *Z. Phys. C* **56** (1992) 97.
- [23] B. Grzadkowski and Z. Hoiki, *Nucl. Phys. B* **484** (1997) 17; *Phys. Lett. B* **391** (1997) 172.
- [24] D. Atwood and A. Soni, *Phys. Rev. D* **45** (1992) 2405; J. F. Gunion, B. Grzadkowski and X-G. He, hep-ph/9605326.
- [25] W. Bernreuther, *et al.*, *Z. Phys. C* **43** (1989) 117.
- [26] U. Baur and D. Zeppenfeld, CERN-TH.5006 (1988); A. Brandenburg and J.P. Ma, *Phys. Lett. B* **298** (1993) 211.
- [27] J.F. Donoghue and G. Valencia, *Phys. Rev. Lett.* **58**, (1987) 451; G.L. Kane, G.A. Ladinsky and C.-P. Yuan, *Phys. Rev. D* **45**, (1991) 124; T. Arens and L.M. Sehgal, *Phys. Rev. D* **50** (1994) 4372; W. Bernreuther, O. Nachtmann, P. Overmann and T. Schröder, *Nucl. Phys. B* **388** (1992) 53; B. Grzadkowski, *Phys. Lett. B* **305** (1993) 384.
- [28] J. Bernabeu, G. A Gonzalez-Sprinberg and J. Vidal, FTUV/95-15, IFIC/95-15, Proceedings of the Ringberg Workshop on Electroweak Interaction in e^+e^- Collisions, (1995) 329;

- [29] C.R. Schmidt, *Phys. Lett. B* **293** (1992) 111; C.R. Schmidt and M.E. Peskin, *Phys. Rev. Lett.* **69** (1992) 410.
- [30] D. Chang, W.-Y. Keung and I. Phillips, *Nucl. Phys. B* **408** (1993) 286; *ibid* **429** (1994) 255 (E)
- [31] Saurabh D. Rindani, *Pramana* **45 S** (1995) 263.
- [32] P. Poulose and S.D. Rindani, *Phys. Lett. B* **349** (1995) 379.
- [33] B. Ananthanarayan and S. D. Rindani, *Phys. Rev. Lett.* **73** (1994) 1215; *Phys. Rev. D* **50** (1994) 4447; *Phys.Rev. D* **51** (1995) 5996.
- [34] S. Y. Tsai, *Phys. Rev. D* **4** (1971) 2821; S. Kawasaki, T. Shirafuji and S. Y. Tsai, *Prog. Theor. Phys.* **49** (1973) 1656;
- [35] T. Arens and L. M. Sehgal, *Nucl. Phys. B* **393** (1993) 46.
- [36] R. Gastmans and T. T. Wu, *The Ubiquitous Photon: Helicity Method for QED and QCD*, Oxford Science Publications (1990), p590.
- [37] R. Kleiss and W. J. Stirling, *Nucl. Phys. B* **262** (1985) 235; *ibid B* **241** (19) 61.
- [38] Jeżabek and J.H. Kühn, *Nucl. Phys. B* **320** (1989) 20.
- [39] P. Poulose and S.D. Rindani, *Phys. Lett. B* **383** (1996) 212
- [40] P. Poulose and S.D. Rindani, *Phys. Rev. D* **54** (1996) 4326
- [41] B. Ananthanarayan and S.D. Rindani, *Phys. Rev. D* **52** (1995) 2684.
- [42] T. D. Lee and M. Nauenberg, *Phys. Rev. B* **133** (1964) 1549.
- [43] B. Falk and L. M. Sehgal, *Phys. Lett. B* **325** (1994) 509
- [44] Roberto Vega and Jose Wudka, *Phys. Rev. D* **53** (1996) 5286.

- [45] C. Bouchiat and L. Michel, *Nucl. Phys* **5**, 416 (1958).
- [46] M.S. Baek, S.Y. Choi, C.S. Kim, YUMS 97-7, SNUTP 97-035, hep-ph/9704312.
- [47] H. Anlauf, W. Bernreuther and A. Brandenburg, *Phys. Rev. D* **52** (1995) 3803.
- [48] W. Bernreuther, A. Brandenburg and P. Overmann, hep-ph/9602273, PITHA-96-02.
- [49] S.Y. Choi and K. Hagiwara, *Phys. Lett. B* **359** (1995) 369.
- [50] Anjan S. Joshipura, *Phys. Rev. D* **43** (1991) 25.
- [51] M. Hirsch, H.V. Klapdor-Kleingrothaus and S.G. Kovalenko, *Phys. Lett. B* **378** (1996) 17; U. Mahanta, *Phys. Lett. B* **337** (1994) 128; A.A. Gvozdev *et al*, hep-ph/9505229.
- [52] B. Adeva *et al.*, *Phys. Lett. B* **261** (1992) 169.
- [53] John Hobbs, Talk at XXXII Rencontres de moriond, March, 1997.
- [54] F. Abe, *et al.*, *Phys. Rev. Lett.* **78** (1997) 2906.
- [55] H1 Collab., C. Adloff *et al.*, DESY 97-024, hep-ex/9702012, *Z. Phys. C* in press; ZEUS Collab., J. Breitweg *et al.*, DESY 97-025, hep-ex/9702015, *Z. Phys. C* in press.
- [56] G. Altarelli, *et al.*, CERN-TH/97-40, hep-ph/9703276; M. A. Doncheski and S. Godfre, OCIP-C-97-02, hep-ph/9703285; J. Blumlein, *Z. Phys. C* (1997) (in the press), hep-ph/9703287; J. Kalinowski, *et al*, DESY 97-037, hep-ph/9703288; M. Suzuki, LBNL-401211, hep-ph/9703316.
- [57] Johannes Blumlein *et al.* *Mod. Phys. Lett. A* **9** (1994) 3007.

- [58] G. Bhattacharyya, J. Ellis and K. Sridhar, *Phys. Lett. B* **336** (1994) 100;
Erratum-*ibid* **B 338** (1994) 522.
- [59] J. K. Mizukoshi et al., *Nucl. Phys. B* **443** (1995) 20.
- [60] Oscar J. P. Éboli, IFUSP-P 1170, hep-ph/9508342.
- [61] Uma Mahanta, *Phys. Rev. D* **54** (1996) 3377.
- [62] W. Bernreuther, A. Brandenburg and P. Overmann, *Phys. Lett. B* **391** (1997) 413.
- [63] W. Buchmüller and D. Wyler, *Phys. Lett B* **177** (1986) 377; A. J. Davies and Xiao-Gang He, *Phys. Rev. D* **43** (1991) 225.
- [64] R. E. Cutkosky, *J. Math. Phys.* **1** (1960) 429.